TUNNELLING DENSITY OF STATES STUDIES OF THE TOPOLOGICAL KONDO EFFECT

by

ANDY OCTAVIAN LATIEF

A thesis submitted to
University of Birmingham
for the degree of
DOCTOR OF PHILOSOPHY

Theoretical Physics Group
School of Physics and Astronomy
University of Birmingham
July 2018

Abstract

Coupling Majorana fermions to metallic conduction electrons will lead to the so-called topological Kondo effect, which is an embodiment of the exotic non-local properties that Majorana fermions possess. Using its minimal setup, this thesis studies the influence of this effect on the scattering properties of conduction electrons by analysing the component of the electron tunnelling density of states (tDOS) which oscillates at twice the Fermi wavenumber k_F. We find that at zero bias this $2k_F$-tDOS displays a non-monotonic behaviour as the temperature is lowered. Starting from the exponential suppression at temperatures much larger than the characteristic Kondo temperature, the $2k_F$-tDOS may show a Kondo logarithmic peak before it crosses over to a $T^{1/3}$ decay, depending on the ratio of the junction-to-tunnelling distance at which the tDOS is being measured and the characteristic Kondo length. This then provides a way to estimate the extent of the Kondo screening cloud. At energies much below the Kondo temperature, the $2k_F$-tDOS is described by a universal scaling function indicative of strong correlations. The non-Fermi-liquid scattering occurs in this energy regime, which can be identified by the vanishing of single-particle-to-single-particle scattering at topological Kondo fixed point that in turn manifests in the complete suppression of the $2k_F$-tDOS at zero temperature and bias. Furthermore, we also have provided a practical method to use the $2k_F$-tDOS to extract information about the single-particle scattering matrix for more general quantum impurity systems.

Acknowledgements

I would like to thank my supervisor Dr. Benjamin Béri for his support and guidance and for being an inspirational example for me. I am also thankful to all faculty members in Theoretical Physics Group, as well as fellow PhD students: Greg, Arvid, Filippo, Andy C, Jon, Austin, Max, Matt R, Matt H, Ehren, Jack, and Mani.

CONTENTS

LIST OF FIGURES

CHAPTER 1

OVERVIEW

Majorana fermions have become one of the most exciting topics in condensed matter physics recently. Originally formulated as the real solutions of Dirac equation by Ettore Majorana in 1937 [1], they continue to become the centre of discussions due to their theoretical novelty and their potential for technological applications in quantum computation [2, 3, 4, 5, 6]. Perhaps the Nobel prize in 2016 being awarded to Thouless, Haldane, and Kosterlitz for their work on topological phases, the new states of matter which, among their many fascinating features, make possible the entrance of Majorana fermions into condensed matter physics [7], is the indication of this.

In contrast to the original formulation in the context of particle physics in which Majorana fermions are portrayed as elementary spin-$\frac{1}{2}$ particles that are their own antiparticles, in condensed matter systems they emerge as quasiparticles in certain superconducting systems [8, 9, 10]. Several models have been developed, ranging from certain elusive two-dimensional "chiral" superconductors which are predicted to host Majorana modes at the vortices to one-dimensional ones which should host the exotic quasiparticles at the boundaries [9]. In this thesis we will focus on one-dimensional systems, in which the pioneering model in this direction was introduced by Alexei Kitaev in 2001 [11]. His idea is that when electrons in one-dimensional lattice are coupled to their nearest neighbours through tight-binding interaction and p-wave-pairing superconductivity, there exists a region in the parameter space in which Majorana fermions will appear as

zero-energy end states [11, 9, 12]. However, from the experimental point of view, realising this superconducting pairing is a great challenge [9]. The key insight that brought Majorana fermions closer to realisation was the discovery that systems involving strong spin-orbit coupling (e.g., topological insulators [13], or even semiconductor nanowires [14, 6]) combined with s-wave superconductivity and magnetic field may lead to similar effects. Concretely, with the nanowires put on top of s-wave superconductors, the superconductivity can be induced through proximity effect [15, 16, 17] so that, in a suitable magnetic field, the effective Hamiltonian now has similar structure to that of the Kitaev model, hence Majorana fermions are predicted to appear at the wires' ends [6, 9, 12].

Several schemes to detect these Majorana fermions have also been developed, including the prediction of zero-bias conductance peak as electrons tunnel into Majoranas in a superconducting reservoir [18, 19, 20, 21, 22]. Although signatures consistent with this have been observed in experiments [23, 24, 25, 26, 27, 28], alternative explanations also exist [29, 30, 31, 32, 33]. Another method to detect Majorana fermions uses an ungrounded superconducting island with finite charging energy [34]. This device has been studied experimentally [35] and the results are in agreement with the prediction of electron teleportation signifying the non-local nature of Majorana fermions [34], although this signature is also not definitive in the sense that alternative explanations here also exist [35].

A different direction to obtain a compelling signature is to use topological Kondo effect [36, 37, 38, 39, 40, 41, 22, 42, 43, 44, 45, 46, 47, 48]. Instead of involving the degeneracy of impurity spins like the ordinary Kondo effect [49], it uses the degeneracy that arises from Majorana fermions. The effective spin that is formed by Majorana fermions, which plays the role of impurity spin, and the one that is formed by conduction electrons, which are coupled to the Majoranas through tunnelling, are non-local in character, hence the Kondo effect that occurs due to this effective spin-spin interaction provides a framework to demonstrate the non-locality of Majorana fermions [36].

This exotic effect adds new flavours to the already rich literature of Kondo physics:

at low energies, it displays a non-Fermi-liquid behaviour, where the Majorana impurity spin is overscreened by the effective spin of single-channel conduction electrons [36]. Therefore, unlike the multi-channel case [50, 51, 52, 53, 54], here there is no competition between several electron channels to screen the impurity spin, which makes the resulting overscreened Kondo effect stable at low energies [36]. These electrons form the so-called Kondo screening cloud [55, 56, 57, 58, 59, 60, 61, 62] to screen the impurity spin perfectly, as in the case of perfectly-screened, single-channel, Kondo effect [50], or with net spin, as in the case of overscreened Kondo effect [63]. This Kondo cloud has not been detected yet in experiments [59, 60, 62]. Our discussion in this thesis centres around a possible mechanism to estimate the size of the Kondo cloud by focussing on the local electron tunnelling density of states that can be measured using scanning tunnelling microscopy. This quantity also gives us insights about single-particle-to-single-particle scattering in the topological Kondo effect that can be checked in experiments.

The organisation of this thesis is as follows: In Chapter 2, we will present a review of Majorana fermions in condensed matter systems. The Kitaev model will be discussed, which is followed by a discussion on an alternative model that can be realised in the laboratory. This chapter is finally concluded by a brief review of an exotic property of Majorana fermions, namely non-Abelian exchange statistics [64, 3, 4]. In Chapter 3, an introduction to Kondo effect is presented. This, combined with Majorana fermions, is the main ingredient to understand the topological Kondo effect, which will be reviewed in Chapter 4. Finally, the study of the tunnelling density of states in the topological Kondo device is presented in Chapter 5, which contains original calculations. The conclusions of the thesis are presented in Chapter 6.

CHAPTER 2

MAJORANA FERMIONS

2.1 Introduction

The Majorana fermion concept was originally introduced as a real solution of the Dirac equation [1],

$$(i\gamma^\mu \partial_\mu - m)\psi(x) = 0. \tag{2.1}$$

This is a relativistic equation for a spin-$\frac{1}{2}$ particle with mass m described by the wave-function $\psi(x)$, with $x = (t, \boldsymbol{x})$ a four-vector [65]. The matrices $\{\gamma^\mu\}$, which are at least 4×4 in size and with index μ running from 0 to 3, have to satisfy

$$\{\gamma^\mu, \gamma^\nu\} = 2g^{\mu\nu} I, \tag{2.2}$$

$$\gamma^0 \gamma^\mu \gamma^0 = (\gamma^\mu)^\dagger. \tag{2.3}$$

Here, $g^{\mu\nu} = \mathrm{diag}(1, -1, -1, -1)$ and I is an identity matrix of the same size as γ^μ [65]. There are infinitely many possibilities for matrices that satisfy both of the conditions above [66]. The common choice, which is called the Dirac-Pauli representation, is given

by

$$\gamma^0 = \begin{pmatrix} I_2 & 0 \\ 0 & I_2 \end{pmatrix}, \tag{2.4}$$

$$\gamma^i = \begin{pmatrix} 0 & \sigma^i \\ -\sigma^i & 0 \end{pmatrix}, \tag{2.5}$$

where I_2 is a 2×2 matrix and σ^i are Pauli matrices.

However, there is also another representation known as the Majorana representation [66]. In this representation, the γ matrices have the form

$$\gamma^0 = \begin{pmatrix} 0 & \sigma^2 \\ \sigma^2 & 0 \end{pmatrix}, \tag{2.6}$$

$$\gamma^1 = \begin{pmatrix} i\sigma^1 & 0 \\ 0 & i\sigma^1 \end{pmatrix}, \tag{2.7}$$

$$\gamma^2 = \begin{pmatrix} 0 & \sigma^2 \\ -\sigma^2 & 0 \end{pmatrix}, \tag{2.8}$$

$$\gamma^3 = \begin{pmatrix} i\sigma^3 & 0 \\ 0 & i\sigma^3 \end{pmatrix}. \tag{2.9}$$

These matrices satisfy Eqs. (2.2) and (2.3), hence Dirac equation written using them also describes a spin-$\frac{1}{2}$ particle. However, because all the γ matrices here have purely imaginary components, the solution of the Dirac equation in this representation, which is called the Majorana fermion, is real: $\psi^* = \psi$. Since the transformation between a particle and its antiparticle involves complex conjugation of the field, the Majorana fermion can be seen as a special solution of the Dirac equation in which it is its own antiparticle [66].

After quantising the Dirac equation, the Majorana fermion annihilation operator can

be written as

$$\hat{\psi}(x) = \int \frac{d^3p}{(2\pi)^3} \frac{1}{\sqrt{2E_{\boldsymbol{p}}}} \sum_s \left[\hat{a}_{\boldsymbol{p},s} u_s(p) e^{-ip\cdot x} + \hat{a}^\dagger_{\boldsymbol{p},s} u^*_s(p) e^{ip\cdot x} \right], \tag{2.10}$$

with p a four-vector momentum $p = (E_{\boldsymbol{p}}, \boldsymbol{p})$, $E_{\boldsymbol{p}} = \sqrt{\boldsymbol{p}^2 + m^2}$, and $u_s(p)$ a 4×1 spinor whose components are functions of four-momentum p [65]. One can immediately see that the second term is the Hermitian conjugate of the first one, which guarantees that $\hat{\psi}(x)$ is Hermitian. A general solution of the Dirac equation would have the second term that reads $\hat{b}^\dagger_{\boldsymbol{p},s} v_s(p) e^{ip\cdot x}$ instead, with an operator $\hat{b}_{\boldsymbol{p},s}$ and a spinor $v_s(p)$ that are totally distinct from $\hat{a}_{\boldsymbol{p},s}$ and $u_s(p)$, respectively [65].

In condensed matter systems one often encounters much simpler variants of the Majorana operator (2.10). Taking $\hat{c}$ to be a fermionic annihilation operator, we can define two Majorana operators $\hat{\gamma}_1$ and $\hat{\gamma}_2$ as

$$\hat{\gamma}_1 \equiv (\hat{c}^\dagger + \hat{c}), \tag{2.11}$$

$$\hat{\gamma}_2 \equiv i(\hat{c}^\dagger - \hat{c}). \tag{2.12}$$

It can be verified that these Majorana operators satisfy

$$\hat{\gamma}^\dagger_i = \hat{\gamma}_i, \tag{2.13}$$

for $i = 1, 2$. This relation implies that they are Hermitian operators. Furthermore, since $\hat{c}$ has to satisfy fermionic anticommutation relations $\{\hat{c}, \hat{c}^\dagger\} = 1$ and $\{\hat{c}, \hat{c}\} = \{\hat{c}^\dagger, \hat{c}^\dagger\} = 0$, the Majorana operators have to satisfy

$$\{\hat{\gamma}_i, \hat{\gamma}_j\} = 2\delta_{ij}, \tag{2.14}$$

for $i, j = 1, 2$.

Therefore, a Majorana operator should be thought as a 'half fermion' [12]. Any

fermionic operator $\hat{c}$ can be written in terms of two Majorana operators as its Hermitian and anti-Hermitian components,

$$\hat{c} = \frac{1}{2}(\hat{\gamma}_1 + i\hat{\gamma}_2). \tag{2.15}$$

This operator satisfies the usual anticommutation relations for fermions. It also has a well-defined occupation number, where its number operator is given by

$$\hat{n}_c = \hat{c}^\dagger \hat{c} = \frac{1}{2}(1 + i\hat{\gamma}_1\hat{\gamma}_2). \tag{2.16}$$

One can use the eigenvalue n_c of the number operator $\hat{n}_c$ to label the basis states $|n_c = 0, 1\rangle$ in the Hilbert space. If there are $2N$ Majorana operators, $\{\hat{\gamma}_1, \ldots, \hat{\gamma}_{2N}\}$, one then can use $|n_{c_1}, \ldots, n_{c_N}\rangle$ as the basis states [9, 12]. Adding two Majorana fermions doubles the dimension of the Hilbert space. Each Majorana fermion thus contributes a factor $\sqrt{2}$ to the Hilbert space dimension, the square root of that of an ordinary fermion. In this sense they are like "square roots" of fermions.

2.2 Majorana fermions in condensed matter systems

In the previous section we have discussed about the notion of Majorana fermions as the solutions of the Dirac equation and as quasiparticles in condensed matter systems. From now on we will focus on the latter. Although Majoranas in these systems are emergent excitations, we will refer to them as Majorana fermions and Majorana modes interchangeably. In Subsection 2.2.1 a model proposed by Alexei Kitaev in 2001 [11] is reviewed. It is a one-dimensional wire with p-wave superconductivity, in which Majorana modes appear as zero-energy states at each end of the wire. However, as this model is difficult to realise in laboratory, alternative systems that have Hamiltonian of similar structure have to be used. In Subsection 2.2.2, a semiconducting nanowire with strong spin-orbit coupling that is in contact with s-wave superconductor [23, 35, 28] is reviewed.

2.2.1 The Kitaev model

Suppose we have a one-dimensional lattice that has N sites to host fermions $\hat{c}_i$, for $1 \leq i \leq N$. The Hamiltonian of this system is given by

$$\hat{H} = -\mu \sum_{i=1}^{N} \hat{c}_i^\dagger \hat{c}_i - \frac{1}{2} \sum_{i=1}^{N-1} \left(t \hat{c}_i^\dagger \hat{c}_{i+1} + \Delta \hat{c}_i \hat{c}_{i+1} + \text{h.c.} \right). \tag{2.17}$$

Here, μ is the chemical potential, $t \geq 0$ is the hopping between nearest neighbours, and $\Delta \geq 0$ is the superconductor p-wave pairing. By expressing the Hamiltonian in momentum space we would find that, for small momenta, the pairing term depends linearly on the momentum, hence its name (see Eq. (2.27) below). This chain model [11] is considered as a toy model because it is the simplest model that can already capture the Majorana physics, but it is far from realistic [9].

For $\mu \neq 0$ and $\Delta = t = 0$, the Hamiltonian becomes

$$\hat{H} = -\mu \sum_{i=1}^{N} \hat{c}_i^\dagger \hat{c}_i, \tag{2.18}$$

which represents a system of ordinary non-interacting fermions localised at N sites (see Fig. 2.1a). However, if we set $\mu = 0$ and $\Delta = t \neq 0$ and write the Hamiltonian above in terms of Majorana operators using the prescription $\hat{c}_i = \frac{1}{2}(\hat{\gamma}_{i,1} + i\hat{\gamma}_{i,2})$, we will get

$$\hat{H} = -\frac{it}{2} \sum_{i=1}^{N-1} \hat{\gamma}_{i,1} \hat{\gamma}_{i+1,2}. \tag{2.19}$$

This Hamiltonian can be rewritten using a new fermionic operator [11, 9, 12],

$$\hat{d}_i \equiv \frac{1}{2}(\hat{\gamma}_{i+1,2} + i\hat{\gamma}_{i,1}), \tag{2.20}$$

such that we obtain

$$\hat{H} = t \sum_{i=1}^{N-1} \hat{d}_i^\dagger \hat{d}_i, \tag{2.21}$$

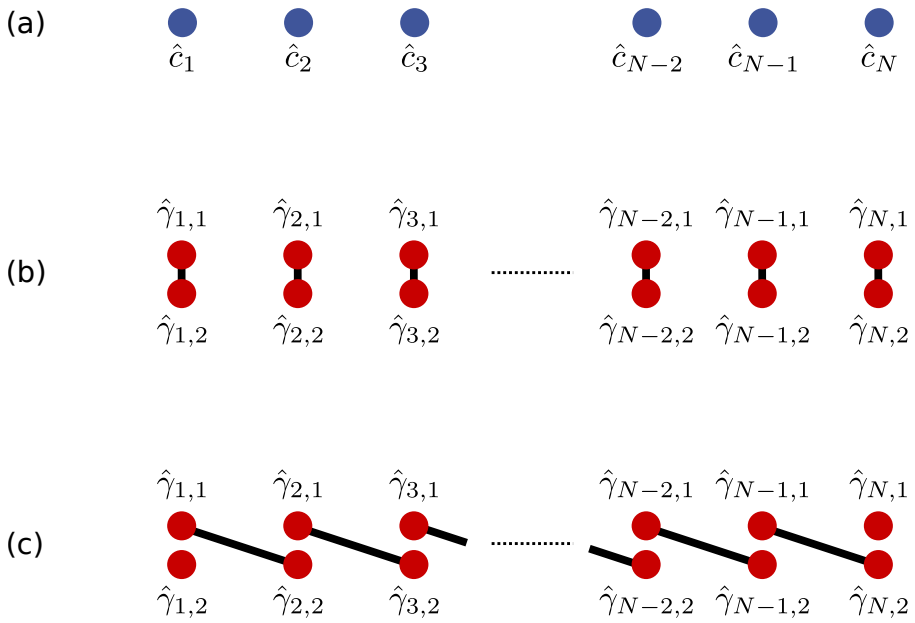

Figure 2.1: (a) One dimensional lattice with N sites hosting the fermions $\hat{c}_i$. (b) Each fermionic operator $\hat{c}_i$ is a superposition of two Majorana operators, $\hat{\gamma}_{i,1}$ and $\hat{\gamma}_{i,2}$. Here $\mu \neq 0$ and $\Delta = t = 0$, so the system is in the trivial phase. (c) When $\mu = 0$ and $\Delta = t \neq 0$, two Majorana modes from different sites combine together to form a non-local fermionic degree of freedom. This system is in the topological phase. Since the two Majorana modes in the ends of the wire do not appear in Hamiltonian, they can combine to form a highly non-local fermionic operator $\hat{f} = \frac{1}{2}(\hat{\gamma}_{1,2} + \hat{\gamma_{N,1}})$ which has zero energy. Therefore, the ground state of the Kitaev model has two-fold degeneracy, in contrast to ordinary superconductors.

where the constant term has been omitted. This Hamiltonian has a similar form to the one in Eq. (2.18). Both of them have open gap with magnitude $|\mu|$ and $2t$, respectively [9]. However, they differ in two aspects. Firstly, the fermionic operator $\hat{d}_i$ is non-local. It is generated by two Majorana fermions that are localised at different, neighbouring, sites. Secondly, there are two Majorana modes at each end of the wire, $\hat{\gamma}_{1,2}$ and $\hat{\gamma}_{N,1}$, which do not appear in the Hamiltonian above. We then can define a highly non-local fermionic operator as the following [11, 9, 12],

$$\hat{f} \equiv \frac{1}{2}(\hat{\gamma}_{1,2} + i\hat{\gamma}_{N,1}). \tag{2.22}$$

Adding and removing an electron using this fermionic operator will not change the energy

of the system, which means that the ground state is now degenerate. Therefore, the Kitaev chain model supports a twofold degenerate ground state, in contrast to ordinary superconductor whose ground state is non-degenerate [11, 9, 12]. The degeneracy that is generated by Majorana modes is a key element which will give rise to some exotic phenomena that will be discussed in this thesis.

To have a deeper understanding about the two Hamiltonians in Eqs. (2.18) and (2.21), let us go to momentum space by performing Fourier transformation,

$$\hat{c}_x = \frac{1}{\sqrt{2\pi}} \int dk\, \hat{c}_k e^{ikx}, \tag{2.23}$$

where x is now the coordinate of the lattice sites after we let $N \to \infty$. The Hamiltonian in Eq. (2.17) becomes

$$\hat{H} = -(\mu + t\cos k) \int dk\, \hat{c}_k^\dagger \hat{c}_k - \frac{\Delta}{2} \int dk\, (\hat{c}_{-k}\hat{c}_k \sin k + \text{h.c.}). \tag{2.24}$$

It is useful to define the Nambu spinor as the following [9],

$$\hat{C}_k \equiv \begin{pmatrix} \hat{c}_k \\ \hat{c}_{-k}^\dagger \end{pmatrix}. \tag{2.25}$$

Rewriting the Hamiltonian in Eq. (2.24) in terms of this Nambu spinor, one gets

$$\hat{H} = \frac{1}{2} \int dk\, \hat{C}_k^\dagger \mathcal{H}_k \hat{C}_k, \tag{2.26}$$

where we have omitted the constant term. The matrix $\mathcal{H}_k$ is given by

$$\mathcal{H}_k = \begin{pmatrix} -\mu - t\cos k & i\Delta \sin k \\ -i\Delta \sin k & \mu + t\cos k \end{pmatrix}. \tag{2.27}$$

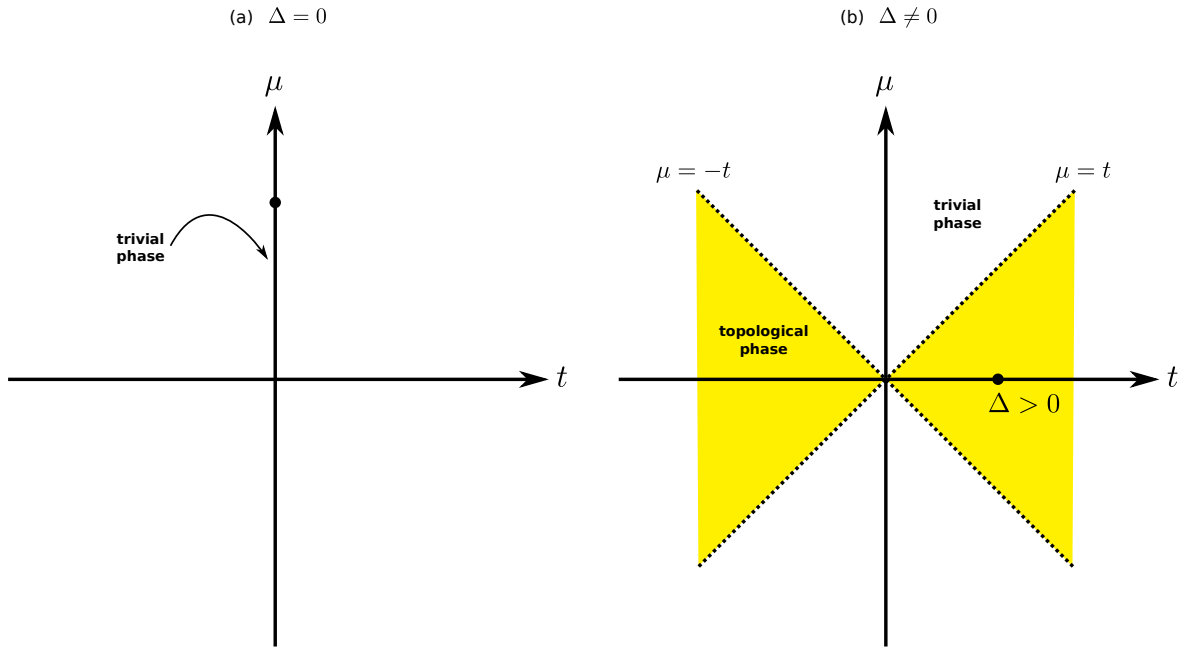

Figure 2.2: (a) Parameter space of the Kitaev model for $\Delta = 0$. The bulk gap always closes for the whole area, except at the μ-axis without the origin, in which the system is in trivial phase. (b) Parameter space of the Kitaev model for $\Delta \neq 0$. The bulk gap only closes at $\mu = \pm t$. There are two topologically distinct regions here: trivial and topological phases. The latter is represented by the point with parameter values $\{\mu = 0, t = \Delta \neq 0\}$. The system that is prepared to have parameters in this region is said to be in the topological phase. Note that one cannot move from topological phase to trivial one and vice versa without closing the bulk gap. The figure is adapted from Ref. [67].

The eigenvalues of this matrix are $\{E_k, -E_k\}$, where E_k takes the form

$$E_k = \sqrt{(\mu + t\cos k)^2 + (\Delta \sin k)^2}. \tag{2.28}$$

If we switch off the p-wave superconductivity by setting $\Delta = 0$, from Eq. (2.28) above we find that the bulk gap always closes except when $t = 0$. However, if we always turn on the p-wave superconductivity by setting $\Delta \neq 0$, the bulk gap closes only when $\mu = \pm t$. Therefore, the parameter space of the Kitaev model for $\Delta \neq 0$ can be divided into two regions, as shown in Fig. 2.2 [67]. There is a region that is represented by the parameter values $\{\mu = 0, t = \Delta \neq 0\}$. We have shown that at this particular point in the parameter space, the Hamiltonian is given by Eq. (2.21) and there exist Majorana modes at the ends of the wire. When the Kitaev model is put in the region covering this point in the

parameter space (i.e., the yellow area in Fig.2.2b), then the model is said to be in the topological phase [9, 67].

The Hamiltonian of a system that is prepared in the trivial phase cannot be continuously deformed into the one in the topological phase without closing the bulk gap [68, 69]. One can assign an integer-valued quantity called *topological invariant* to the gapped Hamiltonian such that trivial and topological phases have different values of the invariant, hence they are considered *topologically distinct* [11, 9]. In our case, for $\Delta \neq 0$, the two regions (yellow and white) in Fig. 2.2b are topologically distinct. Their Hamiltonians cannot be continuously deformed into each other without closing the gap, which happen when $\mu = \pm t$. However, the white area in Fig. 2.2b is topologically equivalent to the μ-axis in Fig. 2.2a but with the origin excluded. It is because in that figure the bulk gap always closes except when $t = 0$ (i.e., the μ-axis) as long as $\mu \neq 0$ (i.e., the origin is excluded).

This idea of assigning topological invariant to the gapped Hamiltonian stems from the field of topology in mathematics, which explores the properties of geometrical objects that do not change under continuous deformations [70]. In our context, one of the fascinating features that distinguish a topological phase from trivial one is the existence of Majorana fermions at the ends of the wire. These modes are stable under variations of parameters as long as the system is in the topological phase [9, 10]. This topological protection is due to particle-hole symmetry $\hat{P} = \begin{pmatrix} 0 & 1 \\ 1 & 0 \end{pmatrix} \hat{K}$, where $\hat{K}$ is the operator for complex conjugation and momentum inversion [12]. Under this transformation, the resulting matrix $\mathcal{H}_k$ becomes $\hat{P}\mathcal{H}_k\hat{P}^{-1} = -\mathcal{H}_k$. For every excitation $\hat{\gamma}(E)$ with energy E, there exists an excitation $\hat{\gamma}(-E)$ with energy $-E$ such that $\hat{\gamma}^\dagger(E) = \hat{\gamma}(-E)$, which then leads to symmetry of the energy spectrum around zero energy. If there is a non-degenerate excitation at $E = 0$, then it would be a Majorana, $\hat{\gamma}^\dagger = \hat{\gamma}$. However, compared to Eqs. (2.11) and (2.12), $\hat{\gamma}$ here now is an operator for an eigenstate and not just an arbitrary Hermitian combination of fermion operators. This zero-energy mode, if non-degenerate, is robust

because of spectral symmetry [71, 10]. When the gap is decreased, the decay length of Majorana wavefunctions towards the bulk of the system increases and the two Majoranas at the two ends of the wire start to overlap with each other. This results in a gradual splitting of the ground state's degeneracy away from zero energy [9]. Hence, particle-hole symmetry and bulk gap opening play key roles in protecting the Majorana fermions at zero energy.

2.2.2 1D heterostructure with Zeeman and spin-orbit couplings

The model discussed previously is far from realistic. Here we review a system that can be engineered in the laboratory and is topologically equivalent to the Kitaev wire although it has different microscopic Hamiltonian [12]. The idea uses three main ingredients: the proximity effect from s-wave superconductors, time-reversal symmetry breaking, and semiconductors with spin-orbit coupling [72, 5, 14, 6, 73].

The first ingredient is to use the proximity effect from ordinary superconductors to avoid using p-wave superconductivity that is difficult to realise in nature [9]. Instead, s-wave superconductors are used, which have pairing between electrons with different spin in the same site. This alone is not enough to achieve p-wave superconductivity that plays a central role in the Kitaev model, hence we need the second and third ingredients mentioned above. Namely, we need to apply magnetic field to break the time-reversal symmetry and to use semiconducting wire with spin-orbit coupling. Time-reversal symmetry has to be broken to prevent Kramers degeneracy, in which Majorana modes at the ends of the wire will be doubled so that each end of the wire will have two Majoranas [12]. This has to be prevented because otherwise the Majorana modes at the same end of the wire will combine together into a fermionic degree of freedom and we cannot generate the one that is non-local. Spin-orbit coupling is also necessary because the s-wave superconductivity is a pairing between electrons with two spin flavours. When the magnetic field is applied and we focus on the lower energy band which has one spin flavour, spin-orbit coupling will rotate this spin depending on the momentum. Therefore, there is a chance for the

Figure 2.3: A semiconducting wire with strong spin-orbit coupling is put on top of an s-wave superconductor such that the superconductivity in the wire can be induced through the proximity effect. A magnetic field is applied to the direction orthogonal to the wire. This system can be prepared such that it is topologically equivalent to the Kitaev model [74, 12].

s-wave pairing to work.

Hence, the Hamiltonian for our system is given by $\hat{H} = \hat{H}_0 + \hat{H}_s$, where $\hat{H}_0$ is the Hamiltonian of 1D wire with Zeeman and spin-orbit couplings and $\hat{H}_s$ is the contribution from proximity-induced s-wave pairing. The term $\hat{H}_0$ can be written as

$$\hat{H}_0 = \int d\boldsymbol{r}\, \hat{\Psi}^\dagger(\boldsymbol{r}) \mathcal{H}_0(\boldsymbol{r}) \hat{\Psi}(\boldsymbol{r}), \tag{2.29}$$

where $\hat{\Psi}(\boldsymbol{r})$ is a 2×1 matrix containing the annihilation operator $\hat{\psi}_{\sigma=\uparrow,\downarrow}(\boldsymbol{r})$ for the electron with spin σ in the wire,

$$\hat{\Psi}(\boldsymbol{r}) = \begin{pmatrix} \hat{\psi}_\uparrow(\boldsymbol{r}) \\ \hat{\psi}_\downarrow(\boldsymbol{r}) \end{pmatrix}. \tag{2.30}$$

The 2×2 matrix $\mathcal{H}_0(\boldsymbol{r})$ contains the kinetic energy for the conduction electrons in the wire, the spin-orbit interaction, and the Zeeman coupling with the magnetic field [12],

$$\mathcal{H}_0(\boldsymbol{r}) = -\frac{\boldsymbol{\nabla}^2}{2m} - \mu - i\alpha[\boldsymbol{E}(\boldsymbol{r}) \times \boldsymbol{\nabla}] \cdot \boldsymbol{\sigma} + \frac{1}{2} g\mu_B \boldsymbol{B}(\boldsymbol{r}) \cdot \boldsymbol{\sigma}. \tag{2.31}$$

Here, m is the (effective) electron mass, μ is the chemical potential, α is the spin-orbit

coupling, g is the g-factor, μ_B is the Bohr magneton, and $\boldsymbol{\sigma} = \sigma_x\hat{\boldsymbol{x}} + \sigma_y\hat{\boldsymbol{y}} + \sigma_z\hat{\boldsymbol{z}}$ is the vector of Pauli matrices. The electric and magnetic fields are denoted as $\boldsymbol{E}(\boldsymbol{r})$ and $\boldsymbol{B}(\boldsymbol{r})$, respectively. On the other hand, the term $\hat{H}_s$ in the Hamiltonian, which represents the proximity-induced s-wave pairing, can be written as [12]

$$\hat{H}_s = \int\int d\boldsymbol{r}d\boldsymbol{r}'\,\hat{\psi}_\downarrow(\boldsymbol{r})\Delta(\boldsymbol{r},\boldsymbol{r}')\hat{\psi}_\uparrow(\boldsymbol{r}') + \text{h.c.}, \tag{2.32}$$

where the pairing potential takes the form $\Delta(\boldsymbol{r}-\boldsymbol{r}') = \Delta\,\delta(\boldsymbol{r}-\boldsymbol{r}')$.

It is clear that due to the existence of the term $\hat{H}_s$, we cannot write the total Hamiltonian $\hat{H}$ in a compact notation using the spinor $\hat{\Psi}(\boldsymbol{r})$. Therefore, let us now introduce the Nambu spinor as the following,

$$\hat{\Psi}_N(\boldsymbol{r}) \equiv \begin{pmatrix} \hat{\psi}_\uparrow(\boldsymbol{r}) \\ \hat{\psi}_\downarrow(\boldsymbol{r}) \\ \hat{\psi}^\dagger_\downarrow(\boldsymbol{r}) \\ -\hat{\psi}^\dagger_\uparrow(\boldsymbol{r}) \end{pmatrix} = \begin{pmatrix} \hat{\Psi}(\boldsymbol{r}) \\ (i\sigma_y)\left[\hat{\Psi}^\dagger(\boldsymbol{r})\right]^T \end{pmatrix}. \tag{2.33}$$

Using this spinor, we can write the Hamiltonian $\hat{H} = \hat{H}_0 + \hat{H}_s$ compactly up to a constant as

$$\hat{H} = \frac{1}{2}\int\int d\boldsymbol{r}d\boldsymbol{r}'\,\hat{\Psi}_N(\boldsymbol{r})\mathcal{H}(\boldsymbol{r},\boldsymbol{r}')\hat{\Psi}_N(\boldsymbol{r}'), \tag{2.34}$$

$$\mathcal{H}(\boldsymbol{r},\boldsymbol{r}') = \begin{pmatrix} \mathcal{H}_0(\boldsymbol{r})\delta(\boldsymbol{r}-\boldsymbol{r}') & \Delta^*(\boldsymbol{r},\boldsymbol{r}')\cdot\boldsymbol{I}_{2\times2} \\ \Delta(\boldsymbol{r},\boldsymbol{r}')\cdot\boldsymbol{I}_{2\times2} & -\sigma_y\mathcal{H}_0^*(\boldsymbol{r})\sigma_y\delta(\boldsymbol{r}-\boldsymbol{r}') \end{pmatrix}. \tag{2.35}$$

where $\boldsymbol{I}_{2\times2}$ is a 2×2 identity matrix.

Now we are going to study the energy spectrum of the Hamiltonian in Eq. (2.34) above. We put the wire along the x-axis, so that $\boldsymbol{\nabla} = \hat{\boldsymbol{x}}\partial_x$. Since the spin-orbit coupling involves a cross product between the electric field and the momentum along the wire, we can focus only on the component of the electric field that is orthogonal to the wire.

Therefore, the resulting spin-orbit field is also orthogonal to the wire; we choose it to be along the y-direction. It means that we have to set $\boldsymbol{E} = E\hat{\boldsymbol{z}}$. In what follows, we focus on the case where the magnetic field is orthogonal to the spin-orbit field, $\boldsymbol{B} = B\hat{\boldsymbol{z}}$.

The matrix $\mathcal{H}_0(x)$ now becomes

$$\mathcal{H}_0(x) = \begin{pmatrix} -\frac{\partial_x^2}{2m} - \mu + \frac{1}{2}g\mu_B B & -\alpha E\partial_x \\ \alpha E\partial_x & -\frac{\partial_x^2}{2m} - \mu - \frac{1}{2}g\mu_B B \end{pmatrix}. \tag{2.36}$$

In this setup, $\mathcal{H}_0(x)$ is real. We will also set $\Delta(x, x')$ to be real and homogeneous, $\Delta(x, x') = \Delta\,\delta(x - x')$. This pairing potential only couples the electrons in the same site, hence an s-wave superconductivity.

After Fourier transforming the operators $\hat{\psi}_\sigma(x)$, we obtain the following Hamiltonian,

$$\hat{H} = \frac{1}{2}\int dk\, \hat{\Psi}_N^\dagger(k)\mathcal{H}(k)\hat{\Psi}_N(k), \tag{2.37}$$

$$\mathcal{H}(k) = \begin{pmatrix} K_+(k) & -i\alpha_0 k & \Delta & 0 \\ i\alpha_0 k & K_-(k) & 0 & \Delta \\ \Delta & 0 & -K_-(-k) & i\alpha_0 k \\ 0 & \Delta & -i\alpha_0 k & -K_+(-k) \end{pmatrix}, \tag{2.38}$$

where $K_\pm(k) \equiv \frac{k^2}{2m} - \mu \pm B_0$, $B_0 \equiv 2g\mu_B B$, $\alpha_0 \equiv \alpha E$, and $\hat{\Psi}_N(k)$ is the Nambu spinor in momentum space, which now takes the form

$$\hat{\Psi}_N(k) \equiv \begin{pmatrix} \hat{\psi}_\uparrow(k) \\ \hat{\psi}_\downarrow(k) \\ \hat{\psi}_\downarrow^\dagger(-k) \\ -\hat{\psi}_\uparrow^\dagger(-k) \end{pmatrix} = \begin{pmatrix} \hat{\Psi}(k) \\ (i\sigma_y)\left[\hat{\Psi}^\dagger(-k)\right]^T \end{pmatrix}. \tag{2.39}$$

Note that the momentum inversion in the second half of the Nambu spinor, which is expected since the second half is the time reversal of the first half, is all important. The

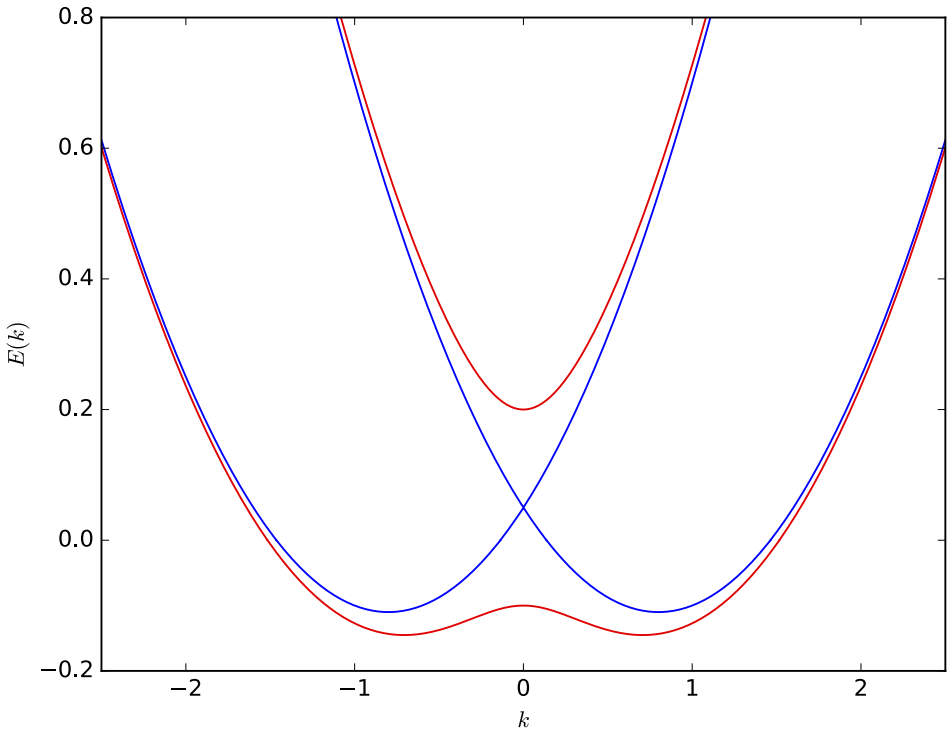

Figure 2.4: The energy spectrum of the heterostructure of semiconducting nanowire with Zeeman and spin-orbit couplings for $\Delta = 0$. The blue curves are the spectrum for $B_0 = 0$, while the red ones are for $B_0 \neq 0$. Note that the spin-orbit coupling splits the energy band into left and right valleys, while the magnetic field creates an energy gap between upper band and lower band. When the superconducting pairing Δ is switched on, the lower band has a Hamiltonian that is topologically equivalent to the one for Kitaev model. This figure is adapted from Ref. [74].

eigenvalues of this Hamiltonian are given by

$$E(k) = \pm\frac{1}{2}\sqrt{h^2(k) + (\alpha_0 k)^2 + B_0^2 + \Delta^2 \pm 2\sqrt{h^2(k)(\alpha_0 k)^2 + h^2(k)B_0^2 + B_0^2\Delta^2}}, \quad (2.40)$$

with $h(k) \equiv \frac{k^2}{2m} - \mu$.

The energy spectrum of this system, without the superconductor present, is plotted in Fig. 2.4. The blue curves are the spectrum when $B_0 = 0$. The spin-orbit interaction splits the energy curve into two, according to the spin orientation of the electrons in the y-direction. Notice that we cannot put the chemical potential μ such that the system is effectively spinless. However, when the magnetic field B_0 is switched on, the spectrum,

shown in this case by the red curves, has a gap. If we put the chemical potential μ inside this gap, the lower band only has one spin flavour, so it is effectively spinless. Therefore, if we turn on the s-wave pairing Δ, the lower band will be topologically equivalent to the one for the Kitaev model [12].

2.3 Non-Abelian exchange statistics and topological quantum computation

To demonstrate the non-Abelian exchange statistics of Majorana fermions [64, 3, 4], we are going to consider a network of one-dimensional wires that form a series of T-junctions as in Fig. 2.5 [74]. Parts of these wires are set in the topological phase, so that Majorana modes are localised at their ends. Two Majoranas can be exchanged by moving one of them into the T-junction first then moving the other. The order in which this process is carried out will affect whether the exchange is clockwise or counterclockwise. The clockwise exchange of two Majorana fermions $\hat{\gamma}_1$ and $\hat{\gamma}_2$ will have the effect [12]

$$\hat{\gamma}_1 \rightarrow -\hat{\gamma}_2, \tag{2.41}$$

$$\hat{\gamma}_2 \rightarrow \hat{\gamma}_1. \tag{2.42}$$

This transformation can be represented by a unitary operator that is called the braid operator [64, 74],

$$\hat{U} \equiv \frac{1}{\sqrt{2}}(1 + \hat{\gamma}_1\hat{\gamma}_2). \tag{2.43}$$

If there are only two Majorana fermions $\hat{\gamma}_1$ and $\hat{\gamma}_2$ in the system, we can form a fermionic degree of freedom $\hat{c} = \frac{1}{2}(\hat{\gamma}_1 + i\hat{\gamma}_2)$. Therefore, the fermionic state now can be expanded in terms of the basis $|n\rangle$, where $n = 0, 1$ is the eigenvalue of the number operator $\hat{n} = \hat{c}^\dagger\hat{c}$. The braid operator $\hat{U}$ now can be rewritten using the number operator as

$$\hat{U} = \frac{1}{\sqrt{2}}\left[1 - i(2\hat{n} - 1)\right]. \tag{2.44}$$

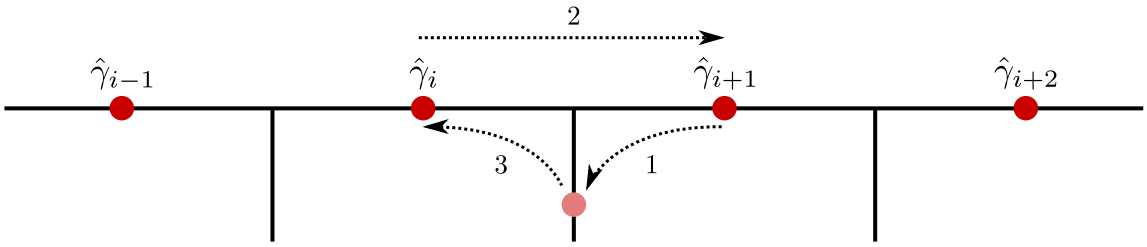

Figure 2.5: A network of one-dimensional wires hosting Majorana fermions. The T-junctions in this network enable us to perform the braiding operations on the Majorana fermions by moving one of the Majorana fermions, $\hat{\gamma}_{i+1}$ to the junction (step 1), then moving the Majorana $\hat{\gamma}_i$ to the right (step 2), followed by moving the Majorana $\hat{\gamma}_{i+1}$ back to the initial wire (step 3). Since this operation forms a clockwise exchange of Majorana fermions, the counterclockwise one can be performed by reversing the steps.

The effect of this braid operator on the basis states $\{|0\rangle, |1\rangle\}$ is to multiply the states with a complex phase of the form $e^{i\theta}$,

$$\hat{U}|0\rangle = \frac{1}{\sqrt{2}}(1+i)|0\rangle, \tag{2.45}$$

$$\hat{U}|1\rangle = \frac{1}{\sqrt{2}}(1-i)|1\rangle. \tag{2.46}$$

In contrast to the ordinary cases of braiding the bosons and fermions where the basis states are simply multiplied by ± 1, this braiding of two Majorana fermions (if they are the only Majoranas in the system) provides an example of so-called Abelian anyonic statistics [12].

However, Majorana systems are actually much more interesting than that. Suppose that our system now has four Majorana fermions $\{\hat{\gamma}_1, \hat{\gamma}_2, \hat{\gamma}_3, \hat{\gamma}_4\}$. We can choose to expand the fermionic states in terms of the basis $|n_1 n_2\rangle$, where n_1 and n_2 are eigenvalues of the number operators $\hat{n}_1 = \hat{c}_1^\dagger \hat{c}_1$ and $\hat{n}_2 = \hat{c}_2^\dagger \hat{c}_2$, with $\hat{c}_1$ and $\hat{c}_2$ are defined as

$$\hat{c}_1 \equiv \frac{1}{2}(\hat{\gamma}_1 + i\hat{\gamma}_2), \tag{2.47}$$

$$\hat{c}_2 \equiv \frac{1}{2}(\hat{\gamma}_3 + i\hat{\gamma}_4). \tag{2.48}$$

Let us define $\hat{U}_{i,i+1}$ as the braid operator when we exchange $\hat{\gamma}_i$ and $\hat{\gamma}_{i+1}$ in the clockwise

direction. As in the previous case, we can write these operators as

$$\hat{U}_{12} \equiv \frac{1}{\sqrt{2}}\left[1 - i(2\hat{n}_1 - 1)\right], \tag{2.49}$$

$$\hat{U}_{34} \equiv \frac{1}{\sqrt{2}}\left[1 - i(2\hat{n}_2 - 1)\right]. \tag{2.50}$$

The remaining braid operator is $\hat{U}_{23}$. (Other braid operators, such as $\hat{U}_{14}$, can be written using the multiplication of the previous three braid operators [12].) This operator cannot be written in a simple expression in terms of the number operator because it represents the braiding between $\hat{\gamma}_2$ and $\hat{\gamma}_3$, which form different fermionic degrees of freedom. Nevertheless, we can write it as [64]

$$\hat{U}_{23} = \frac{1}{\sqrt{2}}\left[1 + i(\hat{c}_1^\dagger - \hat{c}_1)(\hat{c}_2^\dagger + \hat{c}_2)\right] \tag{2.51}$$

because, from Eqs. (2.47) and (2.48), we have $\hat{\gamma}_2 = i(\hat{c}_1^\dagger - \hat{c}_1)$ and $\hat{\gamma}_3 = \hat{c}_2^\dagger + \hat{c}_2$.

The effect of the braiding operators $\hat{U}_{12}$, $\hat{U}_{23}$, and $\hat{U}_{34}$ on the fermionic states can be

represented in terms of matrices as

$$\hat{U}_{12} = \begin{pmatrix} e^{\frac{i\pi}{4}} & 0 & 0 & 0 \\ 0 & e^{-\frac{i\pi}{4}} & 0 & 0 \\ 0 & 0 & e^{\frac{i\pi}{4}} & 0 \\ 0 & 0 & 0 & e^{-\frac{i\pi}{4}} \end{pmatrix}, \tag{2.52}$$

$$\hat{U}_{23} = \frac{1}{\sqrt{2}} \begin{pmatrix} 1 & 0 & 0 & i \\ 0 & 1 & i & 0 \\ 0 & i & 1 & 0 \\ i & 0 & 0 & 1 \end{pmatrix}, \tag{2.53}$$

$$\hat{U}_{34} = \begin{pmatrix} e^{\frac{i\pi}{4}} & 0 & 0 & 0 \\ 0 & e^{\frac{i\pi}{4}} & 0 & 0 \\ 0 & 0 & e^{-\frac{i\pi}{4}} & 0 \\ 0 & 0 & 0 & e^{-\frac{i\pi}{4}} \end{pmatrix}, \tag{2.54}$$

where the basis is taken to be $\{|00\rangle, |10\rangle, |01\rangle, |11\rangle\}$ [64]. Note especially that the braiding operator $\hat{U}_{23}$ is represented by a non-diagonal matrix. The effect of braiding now is not simply to multiply the states with a complex phase, but it mixes the states into the superposition of basis states. Performing two braiding processes in different order will end up in different superposition of basis states, which is exemplified by the following,

$$\hat{U}_{12}\hat{U}_{23}|00\rangle = \frac{1}{2}(1+i)|00\rangle - \frac{1}{2}(1-i)|11\rangle, \tag{2.55}$$

$$\hat{U}_{23}\hat{U}_{12}|00\rangle = \frac{1}{2}(1+i)|00\rangle + \frac{1}{2}(1+i)|11\rangle. \tag{2.56}$$

This illustrates the non-Abelian exchange statistics of Majorana fermions.

One can harness this exotic property for quantum computation technologies [2, 3, 4, 5, 6]. Using the example with four Majorana fermions above, one can prepare an information using the superposition of the basis states (where we assume that there is at least one additional fermion in the distance with occupancy such that all terms have the same

overall fermion parity),

$$|\alpha\rangle = a_{00}|00\rangle + a_{10}|10\rangle + a_{01}|01\rangle + a_{11}|11\rangle, \tag{2.57}$$

with complex-valued coefficients a_{ij}, and process this information using braiding operators (2.52)-(2.54), which correspond to $\frac{\pi}{2}$ rotations [3]. Although universal quantum computation cannot be achieved using these operations [3, 9], topological quantum computation with Majorana fermions is still of much interest because of its protection from decoherence [75, 3, 9].

CHAPTER 3

KONDO EFFECT

3.1 Introduction

The Kondo effect occurs when the spin of conduction electrons interacts with localised magnetic moments of impurity atoms in metals [49]. In 1964, Jun Kondo discovered this effect and showed that it provides an explanation for the resistivity minimum observed in some metals as temperature is decreased [76]. He described this phenomenon by using the Hamiltonian

$$\hat{H} = \hat{H}_0 + \hat{H}_K, \tag{3.1}$$

where $\hat{H}_0$ is the kinetic energy of non-interacting conduction electrons in metals and $\hat{H}_K$ is the Kondo interaction term. The kinetic term $\hat{H}_0$ takes the form

$$\hat{H}_0 = \sum_{\boldsymbol{p},\sigma} \varepsilon_{\boldsymbol{p}\sigma} \hat{c}^\dagger_{\boldsymbol{p}\sigma} \hat{c}_{\boldsymbol{p}\sigma}, \tag{3.2}$$

where $\hat{c}_{\boldsymbol{p}\sigma}$ is the annihilation operator of conduction electrons with momentum $\boldsymbol{p}$, spin σ, and dispersion relation $\varepsilon_{\boldsymbol{p}\sigma}$. The Kondo interaction term $\hat{H}_K$ is given by

$$\hat{H}_K = 2J\hat{\boldsymbol{s}} \cdot \hat{\boldsymbol{S}}, \tag{3.3}$$

where $J > 0$ is the antiferromagnetic Kondo coupling, $\hat{\boldsymbol{S}}$ is the spin operator of a localised magnetic impurity atom, and $\hat{\boldsymbol{s}}$ is the spin operator of the conduction electrons given by $\hat{\boldsymbol{s}} = \frac{1}{2}\sum_{\boldsymbol{p}\boldsymbol{p}',\sigma\sigma'} \hat{c}^{\dagger}_{\boldsymbol{p}\sigma}\boldsymbol{\sigma}_{\sigma\sigma'}\hat{c}_{\boldsymbol{p}'\sigma'}$, where $\boldsymbol{\sigma}$ is the vector of Pauli matrices.

Calculating the resistivity using perturbation theory up to second order, he proved that the Hamiltonian above contributes a term that has logarithmic behaviour. Together with the contributions from other scattering mechanisms, the total resistivity has the form [76],

$$\rho = aT^5 + c\rho_0 - c\rho_1 \log\left(T/T_K\right). \tag{3.4}$$

The first term is due to scattering from phonons, where a is a proportionality constant. The constant resistivity in the second term is due to scattering from static impurities. Here, c is the concentration of magnetic impurity atoms, while ρ_0 and ρ_1 are characteristic resistances. The last term is due to Kondo scattering, where T_K is the characteristic temperature known as Kondo temperature. As temperature is lowered, the Kondo contribution increases logarithmically, while the phonon scattering term decreases. This competition between the two terms implies the existence of resistivity minimum, hence successfully describing the phenomenon that had been observed three decades before.

However, the success of Kondo's calculation to explain the resistance minimum posed another challenging problem: the resistivity diverges when the temperature approaches T_K. In this energy regime, perturbation theory fails to work. Therefore, the Kondo model cannot be used to describe what happens to the physics of the system for temperatures below T_K [49]. This problem inspired many of the theoretical developments afterwards. Around one decade after Kondo's original calculation, in 1975 Kenneth Wilson published his work in which he used non-perturbative theory based on renormalisation group and scaling [77]. The exact solutions to the Kondo Hamiltonian in Eq. (3.1) then were obtained by Wiegmann using the Bethe ansatz [78]. In the 1990s, Affleck and Ludwig described the problem using the framework of conformal field theory (CFT) [53, 61, 79].

In this chapter we shall briefly discuss the Kondo Hamiltonian (3.1) and how it gives rise to a logarithmic term in resistivity. We then describe a perturbative renormalisation

group method that is also known as poor man's scaling [80] to give us better understanding about the Kondo effect as temperature approaches zero. The low-energy scattering behaviour is then described before we review the multi-channel Kondo effect, in which the impurity interacts with more than one channel of conduction electrons.

3.2 The Anderson Hamiltonian

We may wonder how the local magnetic moment arises in the Kondo Hamiltonian (3.3). What is the microscopic model that underlies the Kondo Hamiltonian? Anderson suggested in 1961 [81] that the magnetic impurity atom can be modelled, in its simplest form, as a degenerate one-electron state, which then can interact with the sea of conduction electrons at the Fermi level through tunnelling processes. In this section we shall discuss this Anderson Hamiltonian and how it can generate the Kondo interaction as in Eq. (3.3).

The Anderson Hamiltonian can be written as

$$\hat{H}_A = \sum_{\boldsymbol{p},\sigma} \varepsilon_{\boldsymbol{p}} \hat{c}^\dagger_{\boldsymbol{p}\sigma} \hat{c}_{\boldsymbol{p}\sigma} + \varepsilon_d(\hat{n}_\uparrow + \hat{n}_\downarrow) + U\hat{n}_\uparrow\hat{n}_\downarrow + \sum_{\boldsymbol{p},\sigma} \left(t\hat{c}^\dagger_{\boldsymbol{p}\sigma}\hat{d}_\sigma + \text{h.c.} \right). \tag{3.5}$$

The first term is the kinetic energy of conduction electrons $\hat{c}_{\boldsymbol{p}\sigma}$ with wavevector $\boldsymbol{p}$, spin σ, and dispersion relation $\varepsilon_{\boldsymbol{p}}$. The second term is the energy of the impurity level when it is occupied by a single electron, with either spin-up or spin-down. Here, $\hat{n}_\sigma \equiv \hat{d}^\dagger_\sigma \hat{d}_\sigma$ is the number operator for electrons with spin σ in the impurity level and ε_d is the energy of this level. The third term with Coulomb coupling U represents the Coulomb repulsion term when there are two electrons with opposite spins in the impurity level. The fourth term is to describe the tunnelling between the impurity and the conduction electrons, characterised by the tunnelling parameter t.

The Kondo effect occurs when the total spin of the impurity level does not add up to zero [82]. Hence, we are only interested in the energy regime where classically there is one and only one electron in the impurity level. This happens when the energy restriction

$\varepsilon_d \ll \varepsilon_F \ll \varepsilon_d + U$ is met. The first inequality ensures that the impurity level is not empty, while the second one ensures that the impurity level is not fully occupied.

Classically, because of this energy restriction, there will be no transfer of electrons between the impurity level and the Fermi sea. However, quantum mechanically, the tunnelling can occur in the form of virtual excitations in a short period of time determined by Heisenberg uncertainty. Because we are interested only in the low-energy excitations of the system, we will apply the Schrieffer-Wolff transformation [49] to obtain the effective Hamiltonian. Therefore, let us consider the following second order processes:

1. An impurity electron with spin σ' hops off the impurity level onto the Fermi sea with energy $\varepsilon_{\boldsymbol{p}'}$, then a conduction electron with spin σ and energy $\varepsilon_{\boldsymbol{p}}$ hops from the Fermi sea onto the impurity level.

2. A conduction electron with spin σ and energy $\varepsilon_{\boldsymbol{p}}$ hops onto the impurity level from the Fermi sea to join the impurity electron, then one of these two electrons in the impurity level, with spin σ', hops off the impurity level onto the Fermi sea with energy $\varepsilon_{\boldsymbol{p}'}$.

Because of the energy restriction $\varepsilon_d \ll \varepsilon_F \ll \varepsilon_d + U$, we can set $\varepsilon_{\boldsymbol{p}} \approx \varepsilon_F$ and $\varepsilon_{\boldsymbol{p}'} \approx \varepsilon_F$. The effective Hamiltonian between the initial state $|i\rangle$ and the final state $|f\rangle$, both with energy E_0, is given by

$$\langle f|\hat{H}_{\text{eff}}|i\rangle = -\sum_j \frac{\langle f|\hat{H}_{\text{tun}}|j\rangle\langle j|\hat{H}_{\text{tun}}|i\rangle}{E_j - E_0}, \tag{3.6}$$

where $|j\rangle$ is the intermediate state. The initial and final energy is $E_0 = \varepsilon_d + \varepsilon_F$. For the first process, the energy of the intermediate state is $E_1 = 2\varepsilon_F$, while for the second process, $E_2 = 2\varepsilon_d + U$. Therefore, the effective Hamiltonian takes the form,

$$\begin{aligned} \hat{H}_{\text{eff}} \;=\; & -\sum_{\boldsymbol{p},\boldsymbol{p}',\sigma,\sigma'} \frac{1}{\varepsilon_F - \varepsilon_d}(t^* \hat{d}^\dagger_{\sigma'}\hat{c}_{\boldsymbol{p}'\sigma'})(t\hat{c}^\dagger_{\boldsymbol{p}\sigma}\hat{d}_\sigma) \\ & -\sum_{\boldsymbol{p},\boldsymbol{p}',\sigma,\sigma'} \frac{1}{\varepsilon_d + U - \varepsilon_F}(t\hat{c}^\dagger_{\boldsymbol{p}'\sigma'}\hat{d}_{\sigma'})(t^* \hat{d}^\dagger_{\sigma}\hat{c}_{\boldsymbol{p}\sigma}). \end{aligned} \tag{3.7}$$

Using the anticommutation relations satisfied by the operators $\hat{c}_{\boldsymbol{p}\sigma}$ and $\hat{d}_\sigma$, one gets

$$\begin{aligned}\hat{H}_{\text{eff}} &= \sum_{\boldsymbol{p},\boldsymbol{p}',\sigma,\sigma'} \left(\frac{1}{\varepsilon_F - \varepsilon_d} + \frac{1}{\varepsilon_d + U - \varepsilon_F}\right) |t|^2 \hat{d}^\dagger_{\sigma'} \hat{d}_\sigma \hat{c}^\dagger_{\boldsymbol{p}\sigma} \hat{c}_{\boldsymbol{p}'\sigma'} \\ &\quad - \sum_{\boldsymbol{p},\boldsymbol{p}',\sigma} \frac{1}{\varepsilon_d + U - \varepsilon_F} |t|^2 \hat{c}^\dagger_{\boldsymbol{p}\sigma} \hat{c}_{\boldsymbol{p}'\sigma} - \sum_{\boldsymbol{p},\sigma} \frac{1}{\varepsilon_F - \varepsilon_d} |t|^2 \hat{d}^\dagger_\sigma \hat{d}_\sigma. \end{aligned} \tag{3.8}$$

The spin operator $\hat{\boldsymbol{s}}$ for conduction electrons and $\hat{\boldsymbol{S}}$ for impurity electrons can be defined using the operators $\hat{c}_{\boldsymbol{p}\sigma}$ and $\hat{d}_\sigma$ as

$$\hat{\boldsymbol{s}} = \sum_{\boldsymbol{p},\boldsymbol{p}',\sigma,\sigma'} \hat{c}^\dagger_{\boldsymbol{p}\sigma} \frac{\boldsymbol{\sigma}_{\sigma\sigma'}}{2} \hat{c}_{\boldsymbol{p}'\sigma'}, \tag{3.9}$$

$$\hat{\boldsymbol{S}} = \sum_{\sigma,\sigma'} \hat{d}^\dagger_\sigma \frac{\boldsymbol{\sigma}_{\sigma\sigma'}}{2} \hat{d}_{\sigma'}. \tag{3.10}$$

Since we are working in the subspace containing only one impurity electron in the initial and final states, we effectively have $\hat{d}^\dagger_\uparrow \hat{d}_\uparrow + \hat{d}^\dagger_\downarrow \hat{d}_\downarrow = 1$. Neglecting the potential scattering term and the constant term in the Hamiltonian above and defining $J \equiv \left(\frac{1}{\varepsilon_F - \varepsilon_d} + \frac{1}{\varepsilon_d + U - \varepsilon_F}\right) |t|^2$, we obtain

$$\mathcal{H}_{\text{eff}} = 2J \hat{\boldsymbol{s}} \cdot \hat{\boldsymbol{S}}, \tag{3.11}$$

which is exactly the Kondo interaction term. Together with the kinetic energy term for the conduction electrons, this is then identical to the Kondo Hamiltonian (3.3).

3.3 The resistivity minimum and poor man's scaling

Let us calculate the effect of the Kondo interaction (3.3) on the transport properties of metals. We shall calculate how the resistivity of metallic conduction electrons changes when they interact with the local moment of magnetic impurities. The resistivity is given by the Drude model expression,

$$\rho = \frac{m}{ne^2 \tau(\boldsymbol{p}_F)}, \tag{3.12}$$

where m is the effective mass of electrons and e is the electron charge. $\tau(\boldsymbol{p}_F)$ is the relaxation time evaluated at Fermi momentum $\boldsymbol{p}_F$, which for a general momentum $\boldsymbol{p}$ takes the form [49]

$$\frac{1}{\tau(\boldsymbol{p})} = 2\pi c \int \frac{d^3k'}{(2\pi)^3} |T_{\boldsymbol{p}\boldsymbol{p}'}|^2 (1 - \cos\theta')\delta(\varepsilon_{\boldsymbol{p}} - \varepsilon_{\boldsymbol{p}'}). \tag{3.13}$$

Here $T_{\boldsymbol{p}\boldsymbol{p}'}$ is the element of the $\mathcal{T}$-matrix, which, up to second order in perturbation theory, is given by

$$\hat{\mathcal{T}} = \hat{H}_K + \hat{H}_K \frac{1}{\varepsilon - \hat{H}_0} \hat{H}_K. \tag{3.14}$$

The first (second) term is viewed as the first (second) order approximation to the $\mathcal{T}$-matrix $\hat{\mathcal{T}}$.

Since similar calculations will be performed in Chapter 5, here we will jump to the results directly. The Kondo contribution to the resistivity takes the form

$$\rho = \frac{3\pi m J^2 S(S+1)c}{2e^2\varepsilon_F} \left[1 - 4J\rho_0(\varepsilon_F) \log\left(\frac{k_B T}{D}\right)\right], \tag{3.15}$$

where $\rho_0(\varepsilon_F)$ is the density of states of conduction electrons at Fermi energy and $D \gg T, \varepsilon_F$ is the energy cutoff [49]. The first order contribution is temperature independent, while the second order is logarithmic.

This result can also be understood using Anderson's poor man's scaling [80]. The strategy behind this method is to lower the energy cutoff D by integrating out the degrees of freedom that have energy ε in the range $D - \delta D < |\varepsilon| < D$. As the cutoff is lowered, the Hamiltonian evolves into the one that has lower energy scale; the precise form of the evolution is dictated by requiring that the $\mathcal{T}$-matrix near the Fermi energy remains unchanged as the Hamiltonian and the cutoff evolve. This process continues until the Hamiltonian flows, while maintaining its structure, into a fixed point. This flow is represented by the flow of the coupling constants that the Hamiltonian possesses. The motivation behind this method is that if we focus only on the low energy limit of the

system, it should not care whether we use the Hamiltonian that is formulated including high energy scales or the one that only captures the low energy degrees of freedom [63].

So, let us start with the Hamiltonian (3.3) with energy cutoff D,

$$\hat{H}_K(D) = \sum_{\boldsymbol{p},\boldsymbol{p}'} \left[J_+(D)\hat{S}^+\hat{c}^\dagger_{\boldsymbol{p}\downarrow}\hat{c}_{\boldsymbol{p}'\uparrow} + J_-(D)\hat{S}^-\hat{c}^\dagger_{\boldsymbol{p}\uparrow}\hat{c}_{\boldsymbol{p}'\downarrow} + J_z(D)\hat{S}^z\left(\hat{c}^\dagger_{\boldsymbol{p}\uparrow}\hat{c}_{\boldsymbol{p}'\uparrow} - \hat{c}^\dagger_{\boldsymbol{p}\downarrow}\hat{c}_{\boldsymbol{p}'\downarrow}\right)\right]. \tag{3.16}$$

Here we have rotated the spin operators using the transformation

$$\hat{S}^+ = \hat{S}^x + i\hat{S}^y, \tag{3.17}$$

$$\hat{S}^- = \hat{S}^x - i\hat{S}^y. \tag{3.18}$$

As the cutoff D is lowered by magnitude δD, the couplings $J_z(D)$ and $J_\pm(D)$ also change according to the following flow equations,

$$\frac{dJ_z}{dD} = -2\rho_0\frac{J_+J_-}{D}, \tag{3.19}$$

$$\frac{dJ_\pm}{dD} = -2\rho_0\frac{J_zJ_\pm}{D}, \tag{3.20}$$

where $\rho_0 \equiv \rho_0(\varepsilon_F)$ [80]. This ensures that the $\mathcal{T}$-matrix near the Fermi energy remains unchanged as we are reducing the bandwidth D. If we define dimensionless coupling constants $g_z \equiv \rho_0 J_z$ and $g_\pm \equiv \rho_0 g_z$ and rewrite the differentiation with respect to D as differentiation with respect to $\log D$, we arrive at

$$\frac{dg_z}{d(\log D)} = -2g_+g_-, \tag{3.21}$$

$$\frac{dg_\pm}{d(\log D)} = -2g_zg_\pm. \tag{3.22}$$

For isotropic couplings $g_z = g_\pm \equiv g$, the equations above read

$$\frac{dg}{d(\log D)} = -2g^2. \tag{3.23}$$

Since the RHS is always negative, it means that g is always increasing as the cutoff D is lowered. For the ferromagnetic case $g < 0$, we have $g \to 0$ as $D \to 0$. It implies that at low temperatures the impurity is decoupled from conduction electrons, hence we will ignore this trivial case in the subsequent discussions. However, for the antiferromagnetic case $g > 0$, we have $g \to \infty$ as $D \to 0$, which shows that the spins of the impurity and the conduction electrons couple strongly at low energies [49]. For conventional Kondo systems where both the impurity and the conduction electron have spin-$\frac{1}{2}$, this leads to a complete screening of the impurity spin by the conduction electrons. Hence, the ground state of the Kondo systems forms a spin singlet [83].

3.4 The multi-channel Kondo effect

The Kondo effect also occurs when there are several channels of conduction electrons interacting with the impurity. This multi-channel Kondo effect is described by the Hamiltonian [50]

$$\hat{H} = \sum_{\boldsymbol{p},\sigma} \varepsilon_{\boldsymbol{p}\sigma} \hat{c}^{\dagger}_{\boldsymbol{p}\sigma} \hat{c}_{\boldsymbol{p}\sigma} + \sum_{\mu=1}^{n} 2J_{\mu} \hat{\boldsymbol{s}}_{\mu} \cdot \hat{\boldsymbol{S}}, \tag{3.24}$$

where now the conduction electrons are given a channel index μ. The Kondo coupling constants J_{μ} between the impurity and the channel μ of conduction electrons may be different in general. The behaviour of this multi-channel Kondo model depends strongly on the values of the total number of channels n and the magnitude of the impurity spin S.

Below the Kondo temperature, these n channels of conduction electrons will screen the impurity spin S such that the resulting spin has magnitude $S - n/2$ [50]. Therefore, there are three cases that need to be considered. First is $n = 2S$. Here the conduction electrons can screen the impurity spin completely. The single-channel Kondo model that has been discussed so far in this Chapter, whose $n = 1$ and $S = 1/2$, belongs to this category. The ground state of this fully-screened Kondo model is described by local Fermi liquid theory [83]. The second case is $n < 2S$, in which the conduction electrons cannot perfectly screen

the impurity spin, such that the effective spin now becomes $S' = S - n/2$. This system is called the underscreened Kondo model [63].

An interesting case happens when $n > 2S$, which is called the overscreened Kondo model. Here, the system displays the non-Fermi-liquid behaviour [63]. In a Fermi liquid, the single-particle-to-single-particle scattering is unitary at the Fermi energy [83]. However, in a non-Fermi liquid, a single particle can scatter into a superposition of many collective modes and not only a single particle anymore [61].

An example of the overscreened Kondo model is when the spin-$\frac{1}{2}$ magnetic impurity interacts with multiple channels of conduction electrons. These channels of conduction electrons compete with each other, where the channel with strongest coupling tends to screen the impurity completely at low energies. The multi-channel Kondo effect, where all channels couple to the impurity simultaneously, is therefore unstable at low energies to channel asymmetries [50].

CHAPTER 4

TOPOLOGICAL KONDO EFFECT

4.1 The minimal setup

As shown in the previous chapter, Kondo effect occurs when conduction electrons interact with an impurity spin with degenerate levels. In Chapter 2, it also has been shown that Majorana modes in solid state systems can generate degeneracy. In this chapter we will present the idea of coupling conduction electrons with the degeneracy induced by Majorana modes. The Kondo effect that arises from this topological degeneracy is called the topological Kondo effect [36, 38].

In this chapter, closely following our preprint [84], we will focus on the minimal setup of the topological Kondo model (TKM) [36, 39]. This model consists of four Majorana fermions, three of which are coupled to three leads of conduction electrons. These four Majoranas can be hosted in two semiconducting nanowires that are put on top of a superconducting island, where three out of its four ends are connected to half-infinite leads through tunnelling junctions. These leads are metallic, while the nanowires are set in the topological phase. The Majorana modes then are generated as the zero-energy states at the ends of the wires.

We assume that the tunnelling processes only occur between conduction electrons in the ith lead and the Majorana mode $\hat{\gamma}_i$, for $1 \leq i \leq 3$. The Hamiltonian of this system is

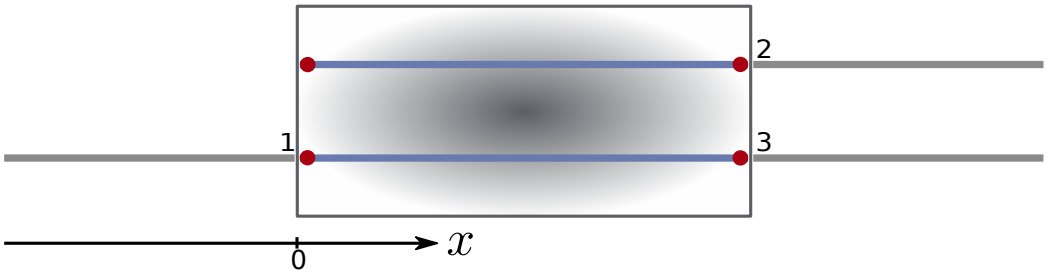

Figure 4.1: The minimal setup of the topological Kondo effect with two semiconducting wires with strong spin-orbit coupling that are put on top of a superconducting island. The wires then are coupled to the metallic leads through tunnelling. When the semiconducting wires are put in the topological phase, the Majorana fermions appear at the ends of the wires.

given by

$$\hat{H} = \hat{H}_{\text{leads}} + \hat{H}_c + \hat{H}_{\text{tun}}. \tag{4.1}$$

The first term is the Hamiltonian of the non-interacting, effectively spinless, conduction electrons in the metallic leads,

$$\hat{H}_{\text{leads}} = \sum_{i=1}^{3} \int dk\, v_F k\, \hat{a}^{\dagger}_{k,i} \hat{a}_{k,i}, \tag{4.2}$$

where v_F is Fermi velocity. Here we have linearised the conduction electron spectrum such that the momentum is linear with momentum window Λ around the Fermi wavenumber k_F. The electron operator in momentum space $\hat{a}_{p,i}(t)$ is related to the one in position space $\hat{\psi}_i(x,t)$ through the relation

$$\hat{\psi}_i(x) = \int dk\, \hat{a}_{k,i} \varphi_{k,i}(x), \tag{4.3}$$

where $x \leq 0$ is spatial coordinate in each lead. The eigenfunction $\varphi_{p,i}(x)$ of the ith lead in the absence of Majorana-lead coupling takes the form,

$$\varphi_{k,i}(x) = \frac{1}{\sqrt{2\pi}} \left[e^{ik_F x} \varphi^R_{k,i}(x) + e^{-ik_F x} \varphi^L_{k,i}(x) \right], \tag{4.4}$$

where $\varphi^R_{k,i}(x) = e^{ikx}$ and $\varphi^L_{k,i}(x) = r_i e^{-ikx}$ are the right and left movers, respectively. $r_i = e^{i\theta_i}$ is the reflection amplitude of electrons at the lead endpoint.

Working at energies much below the induced superconducting gap, the superconducting island is characterised by the charging energy E_c through the term

$$\hat{H}_c = E_c(\hat{N} - q/e)^2, \tag{4.5}$$

where $\hat{N}$ is the number operator of the electrons in the island, q is the background charge, and $-e$ is the electron charge [85]. The distance between any two Majorana modes is assumed to be large enough to ensure that the overlap of their localised wavefunctions can be ignored. In this case, the only tunnelling mechanism we consider is when the electron of lead i tunnels into the island through the Majorana $\hat{\gamma}_i$ with amplitude t_i, which is taken to be positive without loss of generality. The Hamiltonian for this is

$$\hat{H}_{\text{tun}} = e^{i\hat{\phi}/2} \sum_i t_i \hat{\gamma}_i \hat{\psi}_i(0) + \text{h.c.}, \tag{4.6}$$

where $e^{\pm i\hat{\phi}/2}$ is an operator that changes the number of electrons in the island, $N \to N \pm 1$ [36, 34].

4.2 The effective low-energy Hamiltonian

Now we are going to focus on the energy scales that are much smaller than the charging energy E_c. Therefore, the physics of the system is dominated by virtual transitions connecting the lowest energy charge state $|N_0\rangle$ to the neighbouring ones $|N_0 \pm 1\rangle$. In this Section we will perform the Schrieffer-Wolff transformation [49] to derive the effective Hamiltonian that describes the low-energy excitations of the system.

Therefore, let us consider the following second order virtual tunnelling processes:

1. An electron hops onto the island through the Majorana $\hat{\gamma}_i$, then another hops off

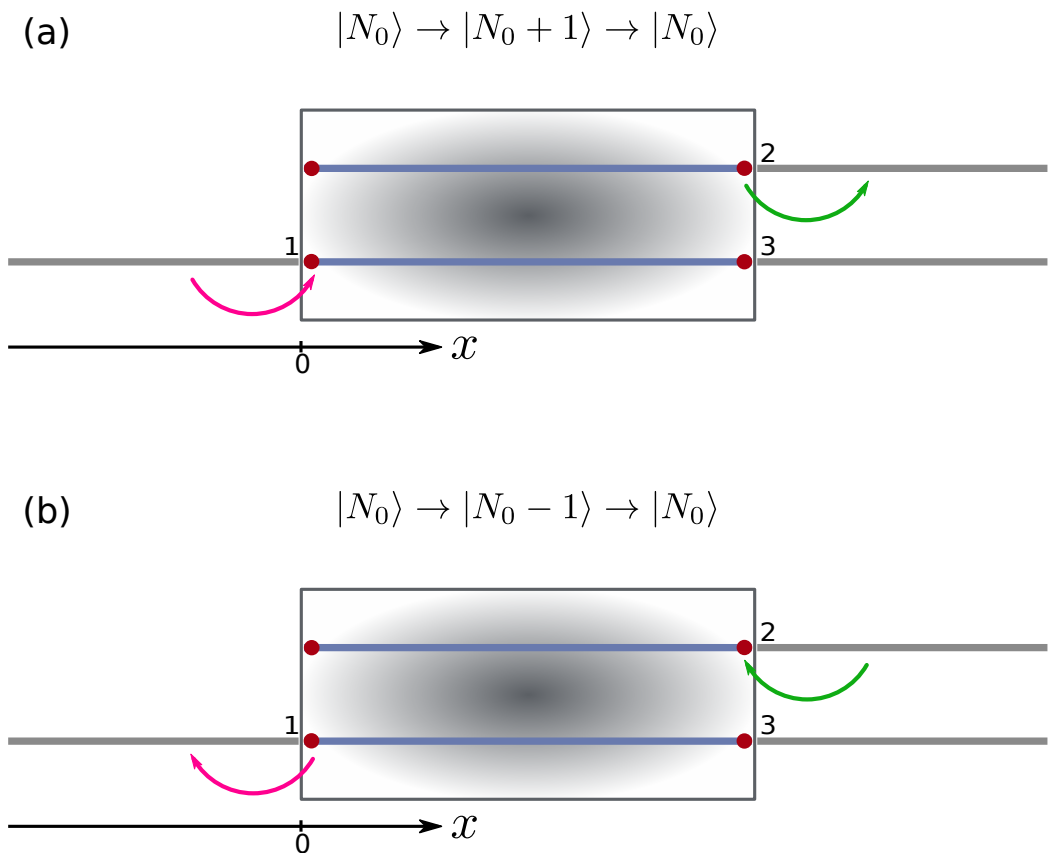

Figure 4.2: Working with energy scales much smaller than E_c, we focus on these two virtual second-order transitions when performing the Schrieffer-Wolff transformation. Note that here the purple-coded tunnelling always occurs first before the green one. (a) An electron hops onto the island through junction i (purple), then another hops off the island through junction j (green). In this process, the virtual state is $|N_0+1\rangle$. (b) An electron hops off the island through junction i (purple), then another hops onto the island through junction j (green). In this process, the virtual state is $|N_0-1\rangle$.

through the Majorana $\hat{\gamma}_j$.

2. An electron hops off the island through the Majorana $\hat{\gamma}_i$, then another hops on through the Majorana $\hat{\gamma}_j$.

Both of these processes are illustrated in Fig. 4.2. Here the purple-coded tunnelling always occurs first before the green one. In process 1, an electron hops onto the island through the junction i, such that the superconducting island changes the state from $|N_0\rangle$ to $|N_0+1\rangle$. Afterwards, an electron hops off the island through junction j, such that the island returns to the state $|N_0\rangle$. However, in process 3, the reverse process takes place.

Now the virtual tunnelling process makes the island to go from the state $|N_0\rangle$ to the virtual state $|N_0-1\rangle$ before it returns back to $|N_0\rangle$. Note that in these two processes, the index i may be the same as j or not. When an electron hops onto (off) the island through the junction i, it may hop back onto the lead (the island) through the same junction or through another junction $j \neq i$.

As before, the effective Hamiltonian between the initial state $|N_0\rangle$ and back to the final state $|N_0\rangle$, both with energy E_0, is given by

$$\langle N_0|\hat{H}_{\text{eff}}|N_0\rangle = -\sum_n \frac{\langle N_0|\hat{H}_{\text{tun}}|n\rangle\langle n|\hat{H}_{\text{tun}}|N_0\rangle}{E_n - E_0}, \tag{4.7}$$

where $|n\rangle$ is the intermediate state. The initial and final energy is $E_0 = H_c(N_0)$. For the first (second) process, the intermediate state is $|N_0 \pm 1\rangle$ with energy $H_c(N_0 \pm 1)$. Therefore, the effective Hamiltonian is given by

$$\hat{H}_{TK} = -\frac{1}{U_+}\sum_{i,j=1}^{3} t_i t_j \hat{\psi}_j^\dagger(0)\hat{\gamma}_j\hat{\gamma}_i\hat{\psi}_i(0) - \frac{1}{U_-}\sum_{i,j=1}^{3} t_i t_j \hat{\gamma}_j\hat{\psi}_j(0)\hat{\psi}_i^\dagger(0)\hat{\gamma}_i, \tag{4.8}$$

where $U_\pm \equiv H_c(N_0 \pm 1) - H_c(N_0) > 0$. Performing the anticommutation relations on the electron operator and reordering the terms, we get

$$\hat{H}_{TK} = \sum_{\substack{i,j=1 \\ i\neq j}}^{3} \lambda_{ij}^{+}\hat{\gamma}_i\hat{\gamma}_j\hat{\psi}_j^\dagger(0)\hat{\psi}_i(0) - \sum_{i=1}^{3}\lambda_{ii}^{-}\hat{\psi}_i^\dagger(0)\hat{\psi}_i(0) + \text{constant}, \tag{4.9}$$

where we have defined $\lambda_{ij}^{\pm} \equiv \left(\frac{1}{U_+} \pm \frac{1}{U_-}\right) t_i t_j$.

Tuning $\hat{H}_c$ to the middle of the Coulomb blockade valley by setting q to be an integer multiple of e, we will get $\lambda_{ii}^{-} = 0$ for any $i = 1, 2, 3$, so that the second term in the $\hat{H}_{\text{eff}}$ above vanishes. To simplify the first term, we can define

$$\hat{S}_i \equiv -\frac{i}{4}(\hat{\boldsymbol{\gamma}} \times \hat{\boldsymbol{\gamma}})_i, \tag{4.10}$$

so that $\hat{S}_1 = -\frac{i}{2}\hat{\gamma}_2\hat{\gamma}_3$, $\hat{S}_2 = -\frac{i}{2}\hat{\gamma}_3\hat{\gamma}_1$, and $\hat{S}_3 = -\frac{i}{2}\hat{\gamma}_1\hat{\gamma}_2$. These spin operators satisfy the

commutation relations $[\hat{S}_i, \hat{S}_j] = i\epsilon_{ijk}\hat{S}_k$. We can also define

$$\hat{I}_i \equiv i \sum_{j,k} \epsilon_{ikj} \hat{\psi}_j^\dagger \hat{\psi}_k, \tag{4.11}$$

so that $\hat{I}_1 = i\left(\hat{\psi}_3^\dagger\hat{\psi}_2 - \hat{\psi}_2^\dagger\hat{\psi}_3\right)$, $\hat{I}_2 = i\left(\hat{\psi}_1^\dagger\hat{\psi}_3 - \hat{\psi}_3^\dagger\hat{\psi}_1\right)$, and $\hat{I}_3 = i\left(\hat{\psi}_2^\dagger\hat{\psi}_1 - \hat{\psi}_1^\dagger\hat{\psi}_2\right)$. Similarly, these also satisfy $[\hat{I}_i, \hat{I}_j] = i\epsilon_{ijk}\hat{I}_k$. By the symmetry of indices on λ_{ij}^+, we can write

$$\hat{H}_{TK} = 2\lambda_{23}^+ \hat{I}_1\hat{S}_1 + 2\lambda_{31}^+ \hat{I}_2\hat{S}_2 + 2\lambda_{12}^+ \hat{I}_3\hat{S}_3, \tag{4.12}$$

Let us also define

$$g_i \equiv \sum_{j,k} |\epsilon_{ijk}|\lambda_{jk}^+, \tag{4.13}$$

so that $g_1 = 2\lambda_{23}^+$, $g_2 = 2\lambda_{31}^+$, and $g_3 = 2\lambda_{12}^+$. Therefore, we get

$$\hat{H}_{TK} = \sum_{i=1}^{3} g_i \hat{I}_i \hat{S}_i. \tag{4.14}$$

Together with the kinetic energy term of the lead electrons, we finally obtain the following effective Hamiltonian,

$$\hat{H} = \sum_{i=1}^{3} \int dk\, v_F k\, \hat{a}_{k,i}^\dagger \hat{a}_{k,i} + \sum_{\alpha=1}^{3} g_\alpha \hat{I}_\alpha \hat{S}_\alpha. \tag{4.15}$$

This has a similar structure to the Kondo Hamiltonian (3.1), but now the Kondo interaction takes place between effectively spin-1 conduction electrons and spin-$\frac{1}{2}$ topological qubit. Note that $\hat{I}_\alpha$ is spin-1 density because $i\epsilon_{\alpha ij}$ are generators of $SU(2)$ in the spin-1 representation. Therefore, this minimal setup of topological Kondo device is an example of overscreened, single-channel, Kondo effect [86, 36]. It displays non-Fermi-liquid low energy behaviour, but with the overscreening that is stable even at low energies, unlike the usual overscreened multi-channel case [50, 51, 52, 53].

CHAPTER 5

TUNNELLING DENSITY OF STATES IN THE TKM

In this chapter, closely along the lines of our preprint [84], and providing additional background information (e.g., details of calculations), we aim to study the oscillating (as a function of position) part of the local electron tunnelling density of states (tDOS), specifically its thermally smeared form motivated by scanning tunnelling microscopy (STM). (For works focussing on complementary non-oscillating part, see Ref. [43] and [87].) We will see that, unlike for free fermions, the amplitude of the oscillating tDOS component does not increase monotonically as temperature is lowered, but follows a form that depends on the position of the tunnelling point relative to the Kondo cloud (see Fig. 5.1). While the non-monotonic temperature dependence is already indicative of strongly correlated scattering, strikingly, we also find that at the topological Kondo fixed point, in contrast even to correlated Fermi liquids [50, 83], single-particle scattering becomes completely suppressed, and that this translates into the complete suppression of the oscillating part of the tDOS as the temperature (and bias voltage) tends to zero. Furthermore, for the minimal three-lead setup that we will focus on, the features that we predict can be turned off by decoupling any of the leads other than the one in which the tDOS is measured, which provides a direct signature of the Majorana fermion non-locality.

The tDOS, specifically its thermally smeared form, is proportional to the STM differ-

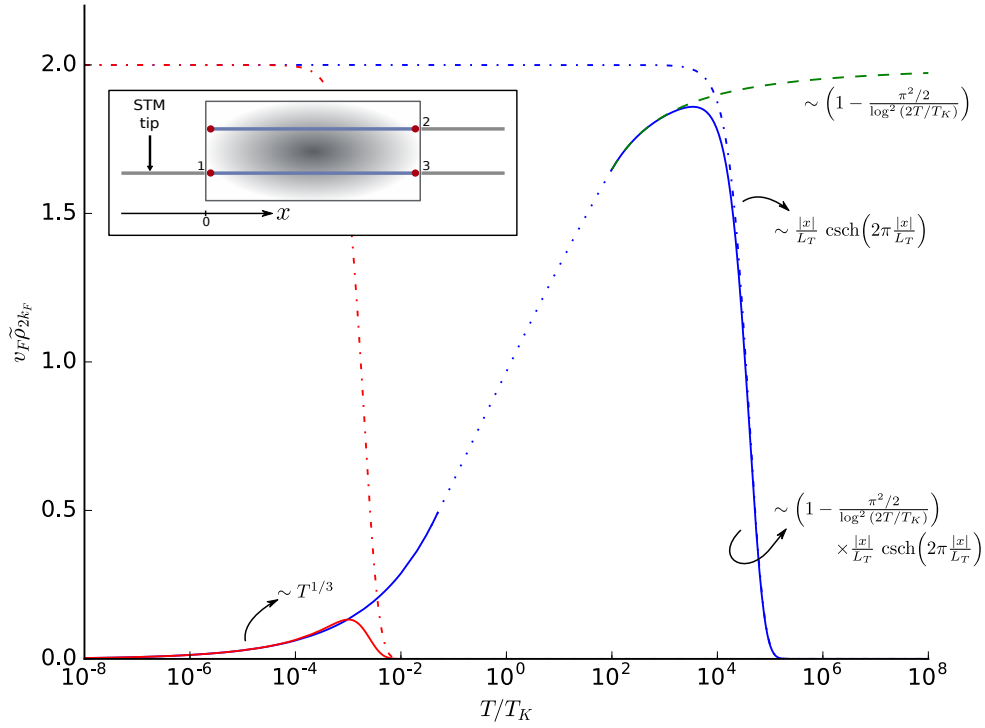

Figure 5.1: The amplitude $\widetilde{\rho}_{2k_F}$ of the oscillating component of the tDOS for zero bias, for the minimal topological Kondo setup (inset) of three Majorana modes (red dots) coupled to conduction-electron leads. The tDOS may be measured using STM. In the expression shown, v_F is Fermi velocity, T_K is Kondo temperature, and $L_K = v_F/L_K$ is $(L_T = v_F/T)$ is the Kondo length (thermal length). The solid, dashed, and dashed-dotted lines represent calculations; the dotted line extrapolates between the regions where our asymptotic approach is expected to hold. For $\widetilde{\rho}_{2k_F}(|x| \ll L_K)$ (solid and blue dots), a Kondo logarithmic peak is visible between the $T \gg T_K$ free-fermion (dash-dotted) tail and the $T \ll T_K$ power law. For $\widetilde{\rho}_{2k_F}(|x| \gg L_K)$ (solid red), the logarithmic regime is suppressed. The dashed line is $\widetilde{\rho}_{2k_F}(x = 0)$. The figure is taken from Ref. [84].

ential conductance [88] (see App. A),

$$\rho_i(x, V, T) \propto \int_{-\infty}^{\infty} d\omega \, \frac{\partial n_F(\omega - eV, T)}{\partial \omega} A_{ii}(x, \omega, T), \tag{5.1}$$

where $n_F(\omega, T) = (1 + e^{\omega/T})^{-1}$ is the Fermi function and $A_{ii}(x, \omega, T)$ is the electron spectral function. V is the applied voltage between the STM tip and the lead. Note that at zero temperature, $\rho_i(x, V, 0) \propto -A_{ii}(x, eV, 0)$.

The spectral function $A_{ij}(x, \omega, T)$ is related to the retarded Green's function $G^R_{ij}(x, y; \omega, T)$

through the relation

$$A_{ij}(x,\omega,T) = -2\,\mathrm{Im}\big[G^R_{ij}(x,x;\omega,T)\big]. \tag{5.2}$$

To calculate the retarded Green's function, we need to use the Matsubara Green's function, which is given by

$$G_{ij}(x,y;i\omega_n,T) = -\int_0^\beta d\tau\, e^{i\omega_n\tau}\left\langle \mathcal{T}_\tau\left[\hat{\psi}_i(x,\tau)\hat{\psi}^\dagger_j(y,0)\right]\right\rangle, \tag{5.3}$$

where we have used the definition [88]

$$\left\langle \hat{A}(\tau_1)\hat{B}(\tau_2)\right\rangle \equiv \frac{1}{Z}\mathrm{Tr}\left[e^{-\beta\hat{H}}\hat{A}(\tau_1)\hat{B}(\tau_2)\right] \tag{5.4}$$

for any operator $\hat{A}(\tau_1)$ and $\hat{B}(\tau_2)$, with $Z \equiv \mathrm{Tr}\left[e^{-\beta\hat{H}}\right]$ and $\beta = 1/T$. ω_n is called the Matsubara frequency, $\omega_n = (2n+1)\pi/\beta$, with integer n. $\mathcal{T}_\tau$ is a time-ordering operator, while τ is an imaginary time. To obtain the retarded Green's function from the Matsubara one, we need to perform analytic continuation from the upper half plane to the real axis, $i\omega_n \to \omega + i\eta$.

The retarded Green's function $G^R_{ij}(x,y;\omega,T)$ can be written in terms of the $\mathcal{T}$-matrix $\mathcal{T}_{ij}(\omega,T)$, which is a key object encoding Kondo correlations,

$$G^R_{ij}(x,x;\omega,T) = G^R_{0,ij}(x,x;\omega,T) + \sum_{kl} G^R_{0,ik}(x,0;\omega,T)\mathcal{T}_{kl}(\omega,T)G^R_{0,lj}(0,x;\omega,T). \tag{5.5}$$

Here $G^R_{0,ij}(x,y;\omega,T)$ is the retarded Green's function in the absence of interaction between electrons and Majoranas. This free Green's function is obtained by performing the analytic continuation of Eq. (5.3), except that the averaging is performed by using the eigenstates of the non-interacting Hamiltonian $\hat{H}_{\mathrm{leads}}$ instead (see Appendix C). It has

the form

$$G^R_{0,ij}(x,x;\omega) = -\frac{i}{v_F}\delta_{ij} - \frac{i}{v_F}\delta_{ij}e^{i2K_i(\omega,x)}, \tag{5.6}$$

$$G^R_{0,ij}(x,0;\omega) = -\frac{2i}{v_F}\cos(\theta_i/2)\delta_{ij}e^{iK_i(\omega,x)}, \tag{5.7}$$

where

$$2K_i(\omega,x) \equiv 2k_F|x| + \frac{2\omega}{v_F}|x| + \theta_i. \tag{5.8}$$

Due to the relation $\varphi^R_{k,i}(x) = r_i^*\varphi^L_{k,i}(-x)$ we have $G^R_{0,ij}(0,x;\omega) = G^R_{0,ij}(x,0;\omega)$ (see Appendix C).

Using Eq. (5.5), we can expect that the tDOS $\rho_i(x,V,T)$ of lead electrons can be decomposed into two parts: the free cloud $\rho_{0,i}(x,V,T)$, which denotes the tDOS when uncoupled from the Majoranas, and the Kondo cloud $\rho_{K,i}(x,V,T)$, which contains the message about Kondo interaction in our system.

A convenient parametrisation of the $\mathcal{T}$-matrix is

$$\mathcal{T}_{ij}(\omega,T) = -\frac{iv_F}{4\cos^2(\theta_i/2)}\delta_{ij}\xi_i(\omega,T), \qquad \theta_i \neq \pi, \tag{5.9}$$

where the δ_{ij} is because only the diagonal terms survive the average over the impurity spin inherent in the definition of the Green's function. The angle $\theta_i = \pi$ is excluded because in this case the electron operator $\hat{\psi}_i(0)$ at the Majorana-lead junction vanishes, and therefore so does the Kondo coupling.

Note that since $\mathcal{T}$ enters multiplicatively in Eq. (5.5), the spatial features for $T = 0$ are entirely due to G_0 and G_0^2. To look for spatial features informing on Kondo correlations we will therefore mostly focus on $T > 0$ and for simplicity mostly take $V \to 0$. In this zero-bias regime, the free cloud has a simple expression,

$$\rho_{0,i}(x,0,T) \propto -\frac{2}{v_F} - \frac{4\pi}{v_F}\frac{|x|}{L_T}\operatorname{cosech}\left(2\pi\frac{|x|}{L_T}\right)\cos(2k_F|x| + \theta_i), \tag{5.10}$$

where $L_T \equiv v_F/T$ is the thermal length.

As exemplified by $G^R_{0,ij}$ and $\rho_{0,i}$ above, all quantities of our interest have two contributions: a non-oscillating and a $2k_F$-oscillating component. For the rest of this work, we focus mostly on the latter because this is the piece that involves both ingoing and outgoing waves and thus encodes information about the scattering properties. [In contrast, at least for non-interacting lead electrons, the non-oscillating part is insensitive to the Kondo coupling as seen from Eqs. (5.5)-(5.7).] Denoting the oscillating components by the subscript $2k_F$, we have

$$G^R_{2k_F,ij}(x,x;\omega,T) = -\frac{i}{v_F}\delta_{ij}[1-\xi_i(\omega,T)]e^{i2K_i(\omega,x)}. \tag{5.11}$$

A key step in calculating the tDOS $\rho_i(x,V,T)$ is thus the calculation of $\xi_i(\omega,T)$. In the following, we will focus on two complementary regimes: high energies [$\max(eV,T) \gg T_K$] and low energies [$\max(eV,T) \ll T_K$], considering mostly the zero bias case. These two regimes correspond to the vicinity of two renormalisation group (RG) fixed points around which a perturbation theory can be developed: the free electron fixed point ($g_\alpha = 0$) for high energies and the topological Kondo fixed point for low energies. In the high-energy regime, the function $\xi_i(\omega,T)$ will be obtained using perturbation theory in the Kondo couplings g_i, considering terms up to third order. For low energies, we will adapt conformal field theory (CFT) results from Ref. [61] to our model.

5.1 $2k_F$-tDOS at high energies

5.1.1 Calculation of the retarded Green's function

In this regime, we will use perturbation theory to calculate the retarded Green's function in Eq. (5.5) up to third order in Kondo couplings g_α. The strategy is to start from the

Matsubara Green's function in momentum space that is given by

$$G_{ij}(k,k';\tau,T) = -\left\langle \mathcal{T}_\tau \left[\hat{a}_{k,i}(\tau)\hat{a}^\dagger_{k',j}(0) \right] \right\rangle . \tag{5.12}$$

To calculate this Green's function, we need to use the method of perturbation expansion [65, 88]. Define the operator $\hat{U}(\tau,\tau_0)$ as the following,

$$\hat{U}(\tau,\tau_0) \equiv e^{\hat{H}_0(\tau-\tau_0)} e^{-\hat{H}(\tau-\tau_0)}, \tag{5.13}$$

where the Hamiltonian $\hat{H} = \hat{H}_0 + \hat{H}_{TK}$ is as given in Eq. (4.15), where $\hat{H}_0$ now denotes the kinetic energy term of the lead electrons. Note that $\hat{U}(\tau_0,\tau_0) = 1$. Differentiating the operator $\hat{U}(\tau,\tau_0)$, one gets

$$\begin{aligned}
\frac{\partial}{\partial\tau}\hat{U}(\tau,\tau_0) &= e^{\hat{H}_0(\tau-\tau_0)}(\hat{H}_0 - \hat{H})e^{-\hat{H}(\tau-\tau_0)} \\
&= -e^{\hat{H}_0(\tau-\tau_0)}\hat{H}_{TK}e^{-\hat{H}(\tau-\tau_0)} \\
&= -\left[e^{\hat{H}_0(\tau-\tau_0)}\hat{H}_{TK}e^{-\hat{H}_0(\tau-\tau_0)}\right] e^{\hat{H}_0(\tau-\tau_0)}e^{-\hat{H}(\tau-\tau_0)} \\
&= -\hat{H}_{TK}(\tau)\hat{U}(\tau,\tau_0),
\end{aligned} \tag{5.14}$$

where $\hat{H}_{TK}(\tau) = e^{\hat{H}_0(\tau-\tau_0)}\hat{H}_{TK}e^{-\hat{H}_0(\tau-\tau_0)}$ is time evolution of the operator $\hat{H}_{TK}$ in the interaction picture. The solution for this differential equation is given by [65, 88]

$$\begin{aligned}
\hat{U}(\tau,\tau_0) &= 1 - \int_{\tau_0}^{\tau} d\tau_1\, \hat{H}_{TK}(\tau_1) + \int_{\tau_0}^{\tau} d\tau_1 \int_{\tau_0}^{\tau_1} d\tau_2\, \hat{H}_{TK}(\tau_1)\hat{H}_{TK}(\tau_2) + \cdots \\
&= 1 - \int_{\tau_0}^{\tau} d\tau_1\, \hat{H}_{TK}(\tau_1) + \frac{1}{2}\int_{\tau_0}^{\tau} d\tau_1 \int_{\tau_0}^{\tau} d\tau_2\, \mathcal{T}_\tau \left[\hat{H}_{TK}(\tau_1)\hat{H}_{TK}(\tau_2)\right] + \cdots \\
&= \mathcal{T}_\tau \exp\left[-\int_{\tau_0}^{\tau} d\tau_1\, \hat{H}_{TK}(\tau_1)\right].
\end{aligned} \tag{5.15}$$

Using the definition (5.4) and the relation

$$e^{-\beta\hat{H}} = e^{-\beta\hat{H}_0}\hat{U}(\beta,0) = e^{-\beta\hat{H}_0}\mathcal{T}_\tau \exp\left[-\int_0^{\beta} d\tau_1\, \hat{H}_{TK}(\tau_1)\right]. \tag{5.16}$$

one can write Eq. (5.12) using the average over non-interacting eigenstates [88],

$$G_{ij}(k,k';\tau,T) = -\frac{\left\langle \mathcal{T}_\tau \left[\hat{U}(\beta,0)\hat{a}_{k,i}(\tau)\hat{a}^\dagger_{k',j}(0)\right]\right\rangle_0}{\left\langle \hat{U}(\beta,0)\right\rangle_0}. \tag{5.17}$$

The Green's function may be evaluated using known diagrammatic methods developed for the Kondo problem; these differ somewhat from standard fermion Feynman diagram techniques due to the commutation properties of spin operators [89, 90]. Instead of using this modified diagram method, as we are interested only in low order perturbation theory, we will proceed by using Wick's theorem directly, which we found to be more straightforward.

Wick's theorem [88] states that the average of any string of equal number of annihilation and creations operators is

$$\left\langle \mathcal{T}_\tau \left[\hat{a}_{p_1}\cdots\hat{a}_{p_n}\hat{a}^\dagger_{q_1}\cdots\hat{a}^\dagger_{q_n}\right]\right\rangle_0 = \text{all possible full contractions}, \tag{5.18}$$

where a contraction is defined between an annihilation operator and a creation operator as

$$\underbrace{\hat{a}_p(\tau_1)\hat{a}^\dagger_q}(\tau_2) \equiv \left\langle \mathcal{T}_\tau \left[\hat{a}_p(\tau_1)\hat{a}^\dagger_q(\tau_2)\right]\right\rangle_0 = -G_0(p,q;\tau_1-\tau_2). \tag{5.19}$$

What is meant by "full contractions" here is that all operators are contracted, so that for $n = 2$ there is no term like $\underbrace{\hat{a}_{p_1}\hat{a}_{p_2}}\hat{a}^\dagger_{q_1}\hat{a}^\dagger_{q_2}$. Note that the contracted operators have to be brought to be adjacent with each other as in Eq. (5.18). Therefore, since we are dealing with fermions, there will be minus signs as the fermion operators are swapped.

Zeroth and first order

In the zeroth order, $\hat{U}^{(0)}(\beta,0) = 1$, so $\hat{G}_{ij}(k,k';\tau,T) = G_{0,ij}(k,k';\tau)$. Therefore, we obtain

$$G^{R,(0)}_{ij}(x,y;\omega,T) = G^R_{0,ij}(x,y;\omega), \tag{5.20}$$

which is simply the non-interacting retarded Green's function. In light of Eq. (5.5), this result is expected.

To first order in g_i, we have $\hat{U}^{(1)}(\beta,0) = -\int_0^\beta d\tau_1\, \hat{H}_{\rm TK}(\tau_1)$, where $\hat{H}_{\rm TK}$ takes the form

$$\hat{H}_{\rm TK} = \frac{iv_F}{2} \sum_{\alpha,a,b=1}^{3} \int_{-\infty}^{\infty}\int_{-\infty}^{\infty} dpdp'\, \lambda_\alpha \epsilon_{\alpha ba} \hat{a}^\dagger_{p,a}(\tau)\hat{a}_{p',b}(\tau)\hat{S}_\alpha, \tag{5.21}$$

and the dimensionless couplings λ_i are defined as

$$\lambda_i \equiv \frac{4g_i}{\pi v_F} \frac{\Pi_{j=1}^3 \cos(\theta_j/2)}{\cos(\theta_i/2)}. \tag{5.22}$$

Since the spin operator $\hat{S}_\alpha$ and the creation and the annihilation operators of the electron are in different Hilbert subspaces, the average over non-interacting eigenstates in Eq. (5.17) above must be performed in the corresponding subspaces. Specifically, the average of the creation and the annihilation operators must be performed over momentum eigenstates $\langle\ldots\rangle_0^k$, while the average of the spin operator must be performed over spin eigenstates $\langle\ldots\rangle_0^\sigma$. The vanishing of $\langle\hat{S}_\alpha\rangle_0^\sigma$ then implies $G_{ij}^{R,(1)}(k,k';\tau,T) = 0$. Therefore,

$$G_{ij}^{R,(1)}(x,y;\omega,T) = 0. \tag{5.23}$$

Second order

In this order, we have

$$\begin{aligned}
\hat{U}^{(2)}(\beta,0) &= \frac{1}{2}\int_0^\beta\int_0^\beta d\tau_1 d\tau_2\, \mathcal{T}_\tau\left[\hat{H}_{\rm TK}(\tau_1)\hat{H}_{\rm TK}(\tau_2)\right] \\
&= -\frac{v_F^2}{8}\int_0^\beta\int_0^\beta d\tau_1 d\tau_2 \int_{-\infty}^{\infty}\int_{-\infty}^{\infty}\int_{-\infty}^{\infty}\int_{-\infty}^{\infty} dpdp'dqdq' \sum_{\substack{\alpha,\alpha',\\ a,b,c,d=1}}^{3} \lambda_\alpha\lambda_{\alpha'}\epsilon_{\alpha ba}\epsilon_{\alpha' dc} \\
&\quad \mathcal{T}_\tau\left[\hat{a}^\dagger_{p,a}(\tau_1)\hat{a}_{p',b}(\tau_1)\hat{a}^\dagger_{q,c}(\tau_2)\hat{a}_{q',d}(\tau_2)\right]\hat{S}_\alpha\hat{S}_{\alpha'}.
\end{aligned} \tag{5.24}$$

Denote the numerator of Eq. (5.17) as $\widetilde{G}_{ij}(k,k';\tau,T) = -\left\langle \mathcal{T}_\tau\left[\hat{U}(\beta,0)\hat{a}_{k,i}(\tau)\hat{a}^\dagger_{k',j}(0)\right]\right\rangle_0$. Although the spin operator $\hat{S}_\alpha$ does not contain time dependence, it appears alongside

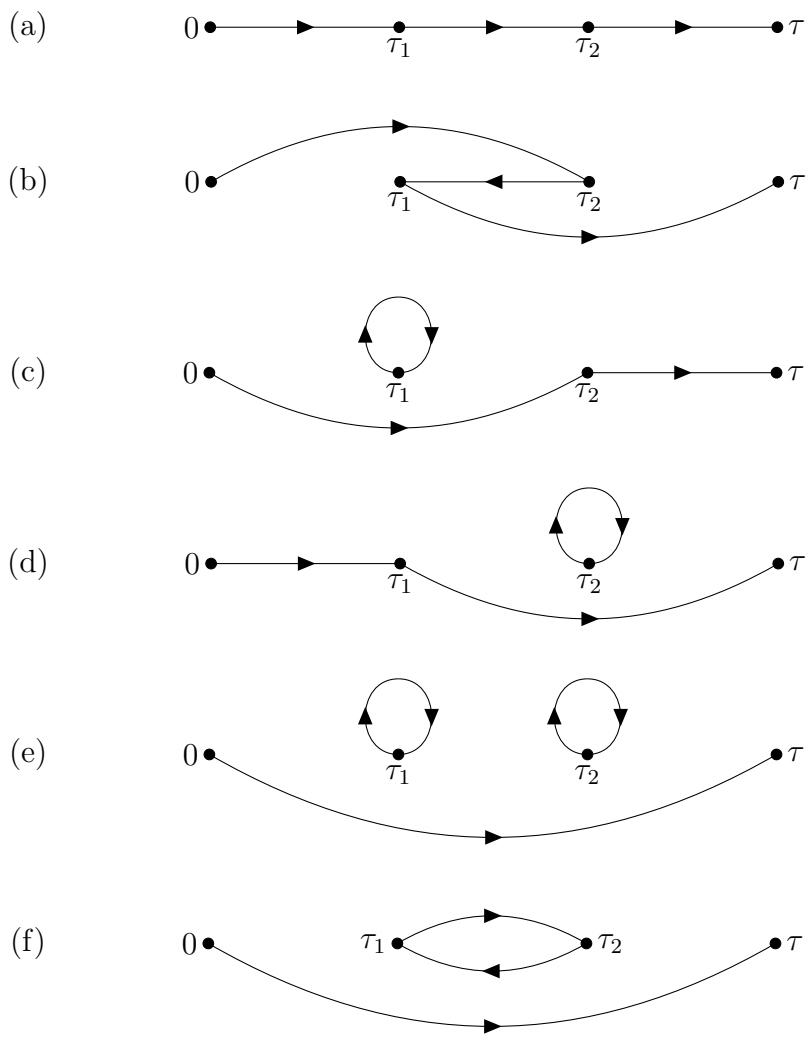

Figure 5.2: The diagrams representing the contractions of the numerator of the Matsubara Green's function in second order. Only the diagram (a) and (b) that are connected. All the disconnected diagrams will be cancelled by the denominator.

the creation and the annihilation operators that are time dependent. Therefore, we need to be careful when we perform the time ordering because the spin operator $\hat{S}_\alpha$ also has to follow this ordering [53]. However, since $\langle \hat{S}_{\alpha'} \hat{S}_\alpha \rangle_0^\sigma = \langle \hat{S}_\alpha \hat{S}_{\alpha'} \rangle_0^\sigma = \frac{1}{2}\delta_{\alpha\alpha'}$, we can focus only on the ordering of the creation and the annihilation operators.

Applying Wick's theorem to the quantity $\widetilde{G}_{ij}(k, k'; \tau, T)$ will give us a series of connected and disconnected terms (Fig. 5.2). The disconnected diagrams (Fig. 5.2c-f) will be cancelled by the denominator of Eq. (5.17) [88]. Therefore, we only need to calculate

the connected terms (Fig. 5.2a and b). Using $\left\langle \hat{S}_\alpha \hat{S}_{\alpha'} \right\rangle_0^\sigma = \frac{1}{2}\delta_{\alpha\alpha'}$, one finds

$$
\begin{aligned}
G_{ij}^{(2)}(k,k';\tau,T) &= \frac{v_F^2}{16}\sum_{\substack{\alpha,a,b,\\ c,d=1}}^{3}\int_{-\infty}^{\infty}\int_{-\infty}^{\infty}\int_{-\infty}^{\infty}\int_{-\infty}^{\infty} dpdp'dqdq' \int_0^\beta\int_0^\beta d\tau_1 d\tau_2\, \lambda_\alpha^2 \epsilon_{\alpha ba}\epsilon_{\alpha dc} \\
&\Big[\hat{a}^\dagger_{p,a}(\tau_1)\hat{a}_{p',b}(\tau_1)\hat{a}^\dagger_{q,c}(\tau_2)\hat{a}_{q',d}(\tau_2)\hat{a}_{k,i}(\tau)\hat{a}^\dagger_{k',j}(0) \\
&+ \hat{a}^\dagger_{p,a}(\tau_1)\hat{a}_{p',b}(\tau_1)\hat{a}^\dagger_{q,c}(\tau_2)\hat{a}_{q',d}(\tau_2)\hat{a}_{k,i}(\tau)\hat{a}^\dagger_{k',j}(0)\Big].
\end{aligned}
\tag{5.25}
$$

Employing the identity

$$
\sum_{\alpha,a,b,c,d=1}^{3}\lambda_\alpha^2\epsilon_{\alpha ba}\epsilon_{\alpha dc}\delta_{ad}\delta_{bj}\delta_{ci} = \sum_{\alpha,a=1}^{3}\lambda_\alpha^2\epsilon_{\alpha ja}\epsilon_{\alpha ai} = -\widetilde{\lambda}_i^2\delta_{ij}, \tag{5.26}
$$

where we have defined

$$
\widetilde{\lambda}_i^2 \equiv \sum_{j=1}^{3}\lambda_j^2 - \lambda_i^2, \tag{5.27}
$$

one gets

$$
\begin{aligned}
G_{ij}^{(2)}(k,k';\tau,T) &= \frac{v_F^2}{8}\widetilde{\lambda}_i^2\delta_{ij}\int_{-\infty}^{\infty}\int_{-\infty}^{\infty}\int_{-\infty}^{\infty}\int_{-\infty}^{\infty} dpdp'dqdq' \int_0^\beta\int_0^\beta d\tau_1 d\tau_2 \\
&\quad G_0(q',p;\tau_2-\tau_1)G_0(p',k';\tau_1)G_0(k,q;\tau-\tau_2).
\end{aligned}
\tag{5.28}
$$

Here we have applied the transformation $\tau_1 \longleftrightarrow \tau_2$, $p \longleftrightarrow q$, $p' \longleftrightarrow q'$ to the second term of Eq. (5.25).

Now the strategy is to transform the Matsubara Green's functions in the RHS of equation above from frequency domain to time domain using Eq. (B.10). We obtain

$$
\begin{aligned}
G_{ij}^{(2)}(k,k';\tau,T) &= \frac{v_F^2}{8\beta^3}\widetilde{\lambda}_i^2\delta_{ij}\sum_{l,n,s=-\infty}^{\infty}\int_{-\infty}^{\infty}\int_{-\infty}^{\infty}\int_{-\infty}^{\infty}\int_{-\infty}^{\infty} dpdp'dqdq' \int_0^\beta\int_0^\beta d\tau_1 d\tau_2 \\
&\quad e^{-i\omega_l\tau}e^{i(\omega_l-\omega_n)\tau_2}e^{i(\omega_n-\omega_s)\tau_1}G_0(k,q;i\omega_l)G_0(q',p;i\omega_n)G_0(p',k';i\omega_s).
\end{aligned}
\tag{5.29}
$$

The imaginary time integral can be performed using

$$\int_0^\beta d\tau\, e^{i(\omega_a-\omega_b)\tau} = \beta\delta_{ab}. \tag{5.30}$$

We then obtain

$$\begin{aligned} G^{(2)}_{ij}(k,k';\tau,T) &= \frac{v_F^2}{8\beta}\widetilde{\lambda}_i^2\delta_{ij}\sum_{l=-\infty}^{\infty}\int_{-\infty}^{\infty}\int_{-\infty}^{\infty}\int_{-\infty}^{\infty}\int_{-\infty}^{\infty} dpdp'dqdq'\, e^{-i\omega_l\tau} \\ &\quad G_0(k,q;i\omega_l)G_0(q',p;i\omega_l)G_0(p',k';i\omega_l). \end{aligned} \tag{5.31}$$

Transforming the Matsubara Green's function in the LHS to position space and frequency domain using Eqs. (B.9) and (B.11), followed by performing the analytic continuation $i\omega_l \to \omega + i\eta$, we get

$$\begin{aligned} G^{R,(2)}_{ij}(x,y;\omega,T) &= \frac{v_F^2}{8}\widetilde{\lambda}_i^2\delta_{ij}\frac{\sqrt{2\pi}}{1+r_i^*}\frac{\sqrt{2\pi}}{1+r_j}\left[\int_{-\infty}^{\infty}\int_{-\infty}^{\infty} dq'dp\, G_0^R(q',p;\omega)\right] \\ &\quad G_0^R(x,0;\omega)G_0^R(0,y;\omega). \end{aligned} \tag{5.32}$$

The integrals in the square bracket can be evaluated using the principal value method to get

$$G^{R,(2)}_{ij}(x,y;\omega,T) = -\frac{i\pi^2 v_F}{16\cos^2(\theta_i/2)}\widetilde{\lambda}_i^2\delta_{ij}G_0^R(x,0;\omega)G_0(0,y;\omega). \tag{5.33}$$

Finally, using Eq. (5.5) and (5.9), we conclude that the second order in g_i contribution to the function $\xi_i(\omega,T)$ is frequency and temperature independent,

$$\xi_i^{(2)}(\omega,T) = \frac{\pi^2}{4}\widetilde{\lambda}_i^2. \tag{5.34}$$

Third order

To third order in g_i, we have

$$\begin{aligned}\hat{U}^{(3)}(\beta,0) &= -\frac{1}{6}\int_0^\beta\int_0^\beta\int_0^\beta d\tau_1 d\tau_2 d\tau_3\,\mathcal{T}_\tau\left[\hat{H}_{\rm TK}(\tau_1)\hat{H}_{\rm TK}(\tau_2)\hat{H}_{\rm TK}(\tau_3)\right] \\ &= \frac{iv_F^3}{48}\sum_{\substack{\alpha,\beta,\gamma,a,\\ b,c,d,e,f=1}}^{3}\int_{-\infty}^{\infty}\int_{-\infty}^{\infty}\int_{-\infty}^{\infty}\int_{-\infty}^{\infty}\int_{-\infty}^{\infty}\int_{-\infty}^{\infty} dpdp'dqdq'drdr'\int_0^\beta\int_0^\beta\int_0^\beta d\tau_1 d\tau_2 d\tau_3 \\ &\quad \lambda_\alpha\lambda_\beta\lambda_\gamma\epsilon_{\alpha ba}\epsilon_{\beta dc}\epsilon_{\gamma fe}\mathcal{T}_\tau\left[\hat{a}^\dagger_{p,a}(\tau_1)\hat{a}_{p',b}(\tau_1)\hat{a}^\dagger_{q,c}(\tau_2)\hat{a}_{q',d}(\tau_2)\hat{a}^\dagger_{r,e}(\tau_3)\hat{a}_{r',f}(\tau_3)\right]\hat{S}_\alpha\hat{S}_\beta\hat{S}_\gamma.\end{aligned} \tag{5.35}$$

The situation now is different from the second order in which the time ordering does not affect anything due to $\langle\hat{S}_\alpha\hat{S}_\beta\rangle_0^\sigma = \langle\hat{S}_\beta\hat{S}_\alpha\rangle_0^\sigma$. However, in the third order, we note that the permutation of indices in the quantity $\langle\hat{S}_\alpha\hat{S}_\beta\hat{S}_\gamma\rangle_0^\sigma$ will affect the result. For example, $\langle\hat{S}_\alpha\hat{S}_\gamma\hat{S}_\beta\rangle_0^\sigma = -\langle\hat{S}_\alpha\hat{S}_\beta\hat{S}_\gamma\rangle_0^\sigma$. Since the order of spin operators is due to the time ordering, we have to keep track the ordering of the imaginary time τ_i using the Heaviside step

functions,

$$
\begin{aligned}
\widetilde{G}^{(3)}_{ij}(k,k';\tau,T) &= -\frac{iv_F^2}{48}\sum_{\substack{\alpha,\beta,\gamma,a,\\ b,c,d,e,f=1}}^{3}\int_{-\infty}^{\infty}\int_{-\infty}^{\infty}\int_{-\infty}^{\infty}\int_{-\infty}^{\infty}\int_{-\infty}^{\infty}\int_{-\infty}^{\infty} dpdp'dqdq'drdr' \\
&\int_0^\beta\int_0^\beta\int_0^\beta d\tau_1 d\tau_2 d\tau_3\,\lambda_\alpha\lambda_\beta\lambda_\gamma\epsilon_{\alpha ba}\epsilon_{\beta dc}\epsilon_{\gamma fe}\left\langle \hat{S}_\alpha\hat{S}_\beta\hat{S}_\gamma\right\rangle_0^\sigma \\
&\Bigg\{\Bigg\langle \mathcal{T}_\tau\Big[\hat{a}^\dagger_{p,a}(\tau_1)\hat{a}_{p',b}(\tau_1)\hat{a}^\dagger_{q,c}(\tau_2)\hat{a}_{q',d}(\tau_2)\hat{a}^\dagger_{r,e}(\tau_3)\hat{a}_{r',f}(\tau_3) \\
&\hat{a}_{k,i}(\tau)\hat{a}^\dagger_{k',j}(0)\Big]\Bigg\rangle_0^k \theta(\tau_1-\tau_2)\theta(\tau_2-\tau_3) \\
&-\Bigg\langle \mathcal{T}_\tau\Big[\hat{a}^\dagger_{p,a}(\tau_1)\hat{a}_{p',b}(\tau_1)\hat{a}^\dagger_{r,e}(\tau_3)\hat{a}_{r',f}(\tau_3)\hat{a}^\dagger_{q,c}(\tau_2)\hat{a}_{q',d}(\tau_2) \\
&\hat{a}_{k,i}(\tau)\hat{a}^\dagger_{k',j}(0)\Big]\Bigg\rangle_0^k \theta(\tau_1-\tau_3)\theta(\tau_3-\tau_2) \\
&-\Bigg\langle \mathcal{T}_\tau\Big[\hat{a}^\dagger_{q,c}(\tau_2)\hat{a}_{q',d}(\tau_2)\hat{a}^\dagger_{p,a}(\tau_1)\hat{a}_{p',b}(\tau_1)\hat{a}^\dagger_{r,e}(\tau_3)\hat{a}_{r',f}(\tau_3) \\
&\hat{a}_{k,i}(\tau)\hat{a}^\dagger_{k',j}(0)\Big]\Bigg\rangle_0^k \theta(\tau_2-\tau_1)\theta(\tau_1-\tau_3) \\
&+\Bigg\langle \mathcal{T}_\tau\Big[\hat{a}^\dagger_{q,c}(\tau_2)\hat{a}_{q',d}(\tau_2)\hat{a}^\dagger_{r,e}(\tau_3)\hat{a}_{r',f}(\tau_3)\hat{a}^\dagger_{p,a}(\tau_1)\hat{a}_{p',b}(\tau_1) \\
&\hat{a}_{k,i}(\tau)\hat{a}^\dagger_{k',j}(0)\Big]\Bigg\rangle_0^k \theta(\tau_2-\tau_3)\theta(\tau_3-\tau_1) \\
&+\Bigg\langle \mathcal{T}_\tau\Big[\hat{a}^\dagger_{r,e}(\tau_3)\hat{a}_{r',f}(\tau_3)\hat{a}^\dagger_{p,a}(\tau_1)\hat{a}_{p',b}(\tau_1)\hat{a}^\dagger_{q,c}(\tau_2)\hat{a}_{q',d}(\tau_2) \\
&\hat{a}_{k,i}(\tau)\hat{a}^\dagger_{k',j}(0)\Big]\Bigg\rangle_0^k \theta(\tau_3-\tau_1)\theta(\tau_1-\tau_2) \\
&-\Bigg\langle \mathcal{T}_\tau\Big[\hat{a}^\dagger_{r,e}(\tau_3)\hat{a}_{r',f}(\tau_3)\hat{a}^\dagger_{q,c}(\tau_2)\hat{a}_{q',d}(\tau_2)\hat{a}^\dagger_{p,a}(\tau_1)\hat{a}_{p',b}(\tau_1) \\
&\hat{a}_{k,i}(\tau)\hat{a}^\dagger_{k',j}(0)\Big]\Bigg\rangle_0^k \theta(\tau_3-\tau_2)\theta(\tau_2-\tau_1)\Bigg\}. \qquad (5.36)
\end{aligned}
$$

Each of these six terms are equivalent to each other. To see this point, let us perform the transformation $\{\tau_2 \longleftrightarrow \tau_3, q \longleftrightarrow r, q' \longleftrightarrow r', c \longleftrightarrow e, d \longleftrightarrow f, \beta \longleftrightarrow \gamma\}$ to the

second term. It will be identical to the first term except for the overall minus sign and the quantity $\langle \hat{S}_\alpha \hat{S}_\gamma \hat{S}_\beta \rangle_0^\sigma = -\langle \hat{S}_\alpha \hat{S}_\beta \hat{S}_\gamma \rangle_0^\sigma$. These two minus signs cancel each other. We can proceed similarly for the rest of the terms, so that we obtain

$$\begin{aligned}\widetilde{G}_{ij}^{(3)}(k,k';\tau,T) \;=\; & -\frac{iv_F^2}{8} \sum_{\substack{\alpha,\beta,\gamma,a,\\ b,c,d,e,f=1}}^{3} \int_{-\infty}^{\infty}\int_{-\infty}^{\infty}\int_{-\infty}^{\infty}\int_{-\infty}^{\infty}\int_{-\infty}^{\infty}\int_{-\infty}^{\infty} dp\,dp'\,dq\,dq'\,dr\,dr' \\ & \int_0^\beta\int_0^\beta\int_0^\beta d\tau_1 d\tau_2 d\tau_3\, \lambda_\alpha\lambda_\beta\lambda_\gamma \epsilon_{\alpha ba}\epsilon_{\beta dc}\epsilon_{\gamma fe} \left\langle \hat{S}_\alpha \hat{S}_\beta \hat{S}_\gamma \right\rangle_0^\sigma \theta(\tau_1-\tau_2)\theta(\tau_2-\tau_3) \\ & \left\langle \mathcal{T}_\tau \left[\hat{a}^\dagger_{p,a}(\tau_1)\hat{a}_{p',b}(\tau_1)\hat{a}^\dagger_{q,c}(\tau_2)\hat{a}_{q',d}(\tau_2)\hat{a}^\dagger_{r,e}(\tau_3)\hat{a}_{r',f}(\tau_3)\hat{a}_{k,i}(\tau)\hat{a}^\dagger_{k',j}(0)\right]\right\rangle .\end{aligned} \tag{5.37}$$

Applying Wick's theorem to the equation above, it will give us 24 possible terms. Out of these terms, there are only 6 connected terms (Fig. 5.3). This is because there are $3! = 6$ possibilities to start from time 0 and end at time τ while going through the permutation of $\{\tau_1, \tau_2, \tau_3\}$. Using $\langle \hat{S}_\alpha \hat{S}_\beta \hat{S}_\gamma \rangle_0^\sigma = \frac{i}{2}\epsilon_{\alpha\beta\gamma}$, these six terms are

$$\begin{aligned}G_{ij}^{(3)}(k,k';\tau,T) \;=\; & \frac{v_F^2}{16} \sum_{\substack{\alpha,\beta,\gamma,a,\\ b,c,d,e,f=1}}^{3} \int_{-\infty}^{\infty}\int_{-\infty}^{\infty}\int_{-\infty}^{\infty}\int_{-\infty}^{\infty}\int_{-\infty}^{\infty}\int_{-\infty}^{\infty} dp\,dp'\,dq\,dq'\,dr\,dr' \\ & \int_0^\beta\int_0^\beta\int_0^\beta d\tau_1 d\tau_2 d\tau_3\, \lambda_\alpha\lambda_\beta\lambda_\gamma \epsilon_{\alpha ba}\epsilon_{\beta dc}\epsilon_{\gamma fe}\epsilon_{\alpha\beta\gamma} \theta(\tau_1-\tau_2)\theta(\tau_2-\tau_3) \\ & \Big[\hat{a}^\dagger_{p,a}(\tau_1)\hat{a}_{p',b}(\tau_1)\hat{a}^\dagger_{q,c}(\tau_2)\hat{a}_{q',d}(\tau_2)\hat{a}^\dagger_{r,e}(\tau_3)\hat{a}_{r',f}(\tau_3)\hat{a}_{k,i}(\tau)\hat{a}^\dagger_{k',j}(0) \\ & + \hat{a}^\dagger_{p,a}(\tau_1)\hat{a}_{p',b}(\tau_1)\hat{a}^\dagger_{q,c}(\tau_2)\hat{a}_{q',d}(\tau_2)\hat{a}^\dagger_{r,e}(\tau_3)\hat{a}_{r',f}(\tau_3)\hat{a}_{k,i}(\tau)\hat{a}^\dagger_{k',j}(0) \\ & + \hat{a}^\dagger_{p,a}(\tau_1)\hat{a}_{p',b}(\tau_1)\hat{a}^\dagger_{q,c}(\tau_2)\hat{a}_{q',d}(\tau_2)\hat{a}^\dagger_{r,e}(\tau_3)\hat{a}_{r',f}(\tau_3)\hat{a}_{k,i}(\tau)\hat{a}^\dagger_{k',j}(0) \\ & + \hat{a}^\dagger_{p,a}(\tau_1)\hat{a}_{p',b}(\tau_1)\hat{a}^\dagger_{q,c}(\tau_2)\hat{a}_{q',d}(\tau_2)\hat{a}^\dagger_{r,e}(\tau_3)\hat{a}_{r',f}(\tau_3)\hat{a}_{k,i}(\tau)\hat{a}^\dagger_{k',j}(0) \\ & + \hat{a}^\dagger_{p,a}(\tau_1)\hat{a}_{p',b}(\tau_1)\hat{a}^\dagger_{q,c}(\tau_2)\hat{a}_{q',d}(\tau_2)\hat{a}^\dagger_{r,e}(\tau_3)\hat{a}_{r',f}(\tau_3)\hat{a}_{k,i}(\tau)\hat{a}^\dagger_{k',j}(0) \\ & + \hat{a}^\dagger_{p,a}(\tau_1)\hat{a}_{p',b}(\tau_1)\hat{a}^\dagger_{q,c}(\tau_2)\hat{a}_{q',d}(\tau_2)\hat{a}^\dagger_{r,e}(\tau_3)\hat{a}_{r',f}(\tau_3)\hat{a}_{k,i}(\tau)\hat{a}^\dagger_{k',j}(0) \Big].\end{aligned} \tag{5.38}$$

Using the identity

$$\sum_{\substack{\alpha,\beta,\gamma,a,\\ b,c,d,e,f=1}}^{3} \lambda_\alpha\lambda_\beta\lambda_\gamma\epsilon_{\alpha\beta\gamma}\epsilon_{\alpha ba}\epsilon_{\beta dc}\epsilon_{\gamma fe}\delta_{ad}\delta_{be}\delta_{ci}\delta_{fj} = 2\lambda_1\lambda_2\lambda_3\delta_{ij} \tag{5.39}$$

and writing the contractions in terms non-interacting Green's functions, we find

$$\begin{aligned}
G^{(3)}_{ij}(k,k';\tau,T) &= \frac{v_F^2}{8}\lambda_1\lambda_2\lambda_3\delta_{ij}\int_{-\infty}^{\infty}\int_{-\infty}^{\infty}\int_{-\infty}^{\infty}\int_{-\infty}^{\infty}\int_{-\infty}^{\infty}\int_{-\infty}^{\infty} dpdp'dqdq'drdr' \\
&\int_0^\beta\int_0^\beta\int_0^\beta d\tau_1 d\tau_2 d\tau_3\,\theta(\tau_1-\tau_2)\theta(\tau_2-\tau_3) \\
&\Big[G_0(q',p;\tau_2-\tau_1)G_0(p',r;\tau_1-\tau_3)G_0(k,q;\tau-\tau_2)G_0(r',k';\tau_3) \\
&+G_0(q',p;\tau_2-\tau_1)G_0(p',k';\tau_1)G_0(r',q;\tau_3-\tau_2)G_0(k,r;\tau-\tau_3) \\
&-G_0(r',p;\tau_3-\tau_1)G_0(p',q;\tau_1-\tau_2)G_0(q',k';\tau_2)G_0(k,r;\tau-\tau_3) \\
&-G_0(r',p;\tau_3-\tau_1)G_0(p',k';\tau_1)G_0(k,q;\tau-\tau_2)G_0(q',r;\tau_2-\tau_3) \\
&-G_0(k,p;\tau-\tau_1)G_0(p',q;\tau_1-\tau_2)G_0(q',r;\tau_2-\tau_3)G_0(r',k';\tau_3) \\
&+G_0(k,p;\tau-\tau_1)G_0(p',r;\tau_1-\tau_3)G_0(r',q;\tau_3-\tau_2)G_0(q',k';\tau_2)\Big].
\end{aligned} \tag{5.40}$$

We will define each of these six terms as $J_{a,ij}(k,k';\tau,T)$, where $1 \le a \le 6$.

The first term $J_{1,ij}(k,k';\tau,T)$ is given by

$$\begin{aligned}
J_{1,ij}(k,k';\tau,T) &= \frac{v_F^2}{8}\lambda_1\lambda_2\lambda_3\delta_{ij}\int_{-\infty}^{\infty}\int_{-\infty}^{\infty}\int_{-\infty}^{\infty}\int_{-\infty}^{\infty}\int_{-\infty}^{\infty}\int_{-\infty}^{\infty} dpdp'dqdq'drdr' \\
&\int_0^\beta\int_0^\beta\int_0^\beta d\tau_1 d\tau_2 d\tau_3\,\theta(\tau_1-\tau_2)\theta(\tau_2-\tau_3) \\
&G_0(q',p;\tau_2-\tau_1)G_0(p',r;\tau_1-\tau_3)G_0(k,q;\tau-\tau_2)G_0(r',k';\tau_3).
\end{aligned} \tag{5.41}$$

Transforming the non-interacting Matsubara Green's functions in the RHS from time domain to the frequency domain using Eq. (B.9), and remembering that $G_0(p,q;\tau) \propto$

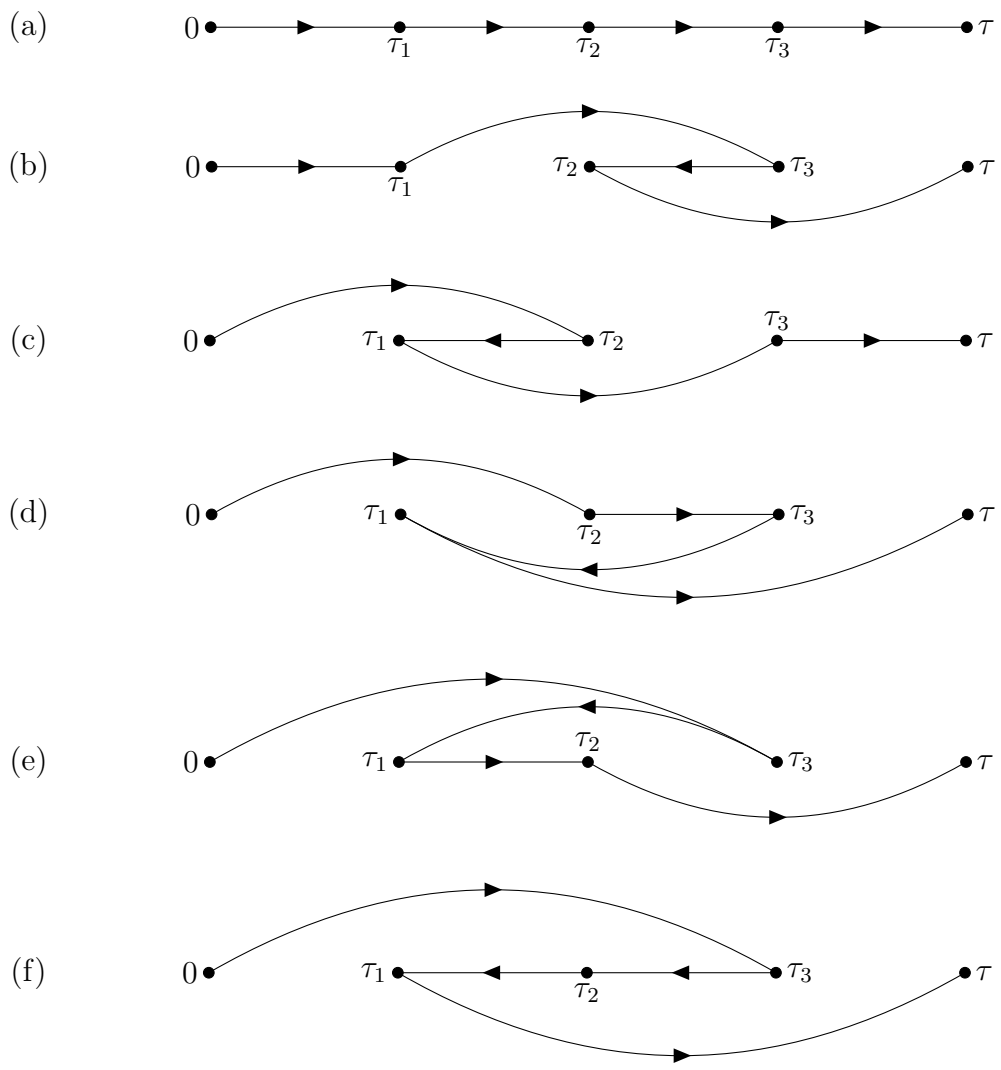

Figure 5.3: The connected diagrams representing the contractions of the numerator of the Matsubara Green's function in third order. All the disconnected diagrams (not shown here) will be cancelled by the denominator.

$\delta(p-q)$, we find

$$\begin{aligned} J_{1,ij}(k,k';\tau,T) &= \frac{v_F^2}{8\beta^4}\lambda_1\lambda_2\lambda_3\delta_{ij}\sum_{l,m,n,s=-\infty}^{\infty}\int_{-\infty}^{\infty}\int_{-\infty}^{\infty}dpdp'\int_0^\beta\int_0^\beta\int_0^\beta d\tau_1 d\tau_2 d\tau_3 \\ & e^{-i\omega_l\tau}e^{i(\omega_l-\omega_m)\tau_2}e^{i(\omega_m-\omega_n)\tau_1}e^{i(\omega_n-\omega_s)\tau_3}\theta(\tau_1-\tau_2)\theta(\tau_2-\tau_3) \\ & G_0(k;i\omega_l)G_0(p;i\omega_m)G_0(p';i\omega_n)G_0(k';i\omega_s). \end{aligned} \tag{5.42}$$

Now we have to be careful with the exponentials. Every exponential of the form $e^{i(\omega_a-\omega_b)\tau}$ has two possibilities, $a=b$ or $a\neq b$, which will give different results after the imaginary

time integration. Therefore, we can write

$$
\begin{aligned}
J_{1,ij}(k,k';\tau,T) &= \frac{v_F^2}{8\beta^4}\lambda_1\lambda_2\lambda_3\delta_{ij}\sum_{l,m,n,s=-\infty}^{\infty}\int_{-\infty}^{\infty}\int_{-\infty}^{\infty}dpdp'\int_0^\beta\int_0^\beta\int_0^\beta d\tau_1 d\tau_2 d\tau_3 \\
& e^{-i\omega_l\tau}\left[\delta_{lm}+e^{i(\omega_l-\omega_m)\tau_2}\eta_{lm}\right]\left[\delta_{mn}+e^{i(\omega_m-\omega_n)\tau_1}\eta_{mn}\right]\left[\delta_{ns}+e^{i(\omega_n-\omega_s)\tau_3}\eta_{ns}\right] \\
& \theta(\tau_1-\tau_2)\theta(\tau_2-\tau_3)G_0(k;i\omega_l)G_0(p;i\omega_m)G_0(p';i\omega_n)G_0(k';i\omega_s). \qquad (5.43)
\end{aligned}
$$

Using the list of integrals in App. D, we finally arrive at

$$
\begin{aligned}
J_{1,ij}(k,k';\tau,T) &= \frac{v_F^2}{8\beta^3}\lambda_1\lambda_2\lambda_3\delta_{ij}\sum_{l,m,n,s=-\infty}^{\infty}\int_{-\infty}^{\infty}\int_{-\infty}^{\infty}dpdp'\,e^{-i\omega_l\tau} \\
& \left\{\frac{\beta^2}{6}\delta_{mn}\delta_{lm}\delta_{ns}+\frac{1}{i(\omega_m-\omega_n)}\left[\frac{\beta}{2}-\frac{1}{i(\omega_m-\omega_n)}\right]\eta_{mn}\delta_{lm}\delta_{ns}\right. \\
& +\frac{1}{i(\omega_l-\omega_m)}\left[\frac{1}{i(\omega_l-\omega_m)}\delta_{mn}+\frac{\beta}{2}\delta_{ln}\eta_{mn}+\frac{1}{i(\omega_l-\omega_n)}\eta_{ln}\eta_{mn}\right]\eta_{lm}\delta_{ns} \\
& -\frac{1}{i(\omega_l-\omega_m)}\frac{1}{i(\omega_l-\omega_m)}\left[-\delta_{mn}+\delta_{ln}\eta_{mn}\right]\eta_{lm}\delta_{ns} \\
& +\frac{1}{i(\omega_n-\omega_s)}\frac{1}{i(\omega_n-\omega_s)}\left[-\delta_{mn}+\delta_{ms}\eta_{mn}\right]\delta_{lm}\eta_{ns} \\
& -\frac{1}{i(\omega_n-\omega_s)}\left[\frac{\beta}{2}\delta_{mn}+\frac{1}{i(\omega_m-\omega_n)}\eta_{mn}\right]\delta_{lm}\eta_{ns} \\
& +\frac{1}{i(\omega_n-\omega_s)}\left[\frac{\beta^2}{2}\delta_{mn}\delta_{0,(l-m+n-s)}+\frac{1}{i(\omega_m-\omega_n)}\eta_{mn}\delta_{0,(l-m+n-s)}\right]\eta_{lm}\eta_{ns} \\
& +\frac{1}{i(\omega_n-\omega_s)}\frac{1}{i(\omega_l-\omega_m+\omega_n-\omega_s)}\Big[-\delta_{mn}\eta_{0,(l-m+n-s)} \\
& +\delta_{ls}\eta_{mn}\eta_{0,(l-m+n-s)}\Big]\eta_{lm}\eta_{ns} \\
& \left.-\frac{1}{i(\omega_n-\omega_s)}\frac{1}{i(\omega_l-\omega_m)}\left[-\delta_{mn}+\delta_{ln}\eta_{mn}\right]\eta_{lm}\eta_{ns}\right\} \\
& G_0(k;i\omega_l)G_0(p;i\omega_m)G_0(p';i\omega_n)G_0(k';i\omega_s) \qquad (5.44)
\end{aligned}
$$

The calculations for $J_{a,ij}(k,k';\tau,T)$, for $2\leq a\leq 6$, are similar.

Combining all of these terms by exploiting the symmetry between their indices and

momenta under the transformation $\{l \longleftrightarrow s, m \longleftrightarrow n, k \longleftrightarrow k', p \longleftrightarrow p'\}$, we find

$$\begin{aligned} G_{ij}^{R,(3)}(k,k';\tau,T) &= \frac{v_F^2}{4\beta^2}\lambda_1\lambda_2\lambda_3\delta_{ij}\sum_{l,m=-\infty}^{\infty}\int_{-\infty}^{\infty}\int_{-\infty}^{\infty}dpdp'\,e^{-i\omega_l\tau}\frac{1}{i(\omega_l-\omega_m)}\eta_{lm} \\ &\Big[2G(p;i\omega_m)G(p';i\omega_l)-G(p;i\omega_m)G(p';i\omega_m)\Big]G(k;i\omega_l)G(k';i\omega_l). \end{aligned} \tag{5.45}$$

Transforming the Matsubara Green's function in the LHS to the frequency domain using Eq. (B.9), we then have

$$\begin{aligned} G_{ij}^{R,(3)}(k,k';i\omega_l,T) &= \frac{v_F^2}{4\beta}\lambda_1\lambda_2\lambda_3\delta_{ij}\sum_{m=-\infty}^{\infty}\int_{-\infty}^{\infty}\int_{-\infty}^{\infty}dpdp'\,\frac{1}{i(\omega_l-\omega_m)}\eta_{lm} \\ &\Big[2G(p;i\omega_m)G(p';i\omega_l)-G(p;i\omega_m)G(p';i\omega_m)\Big]G(k;i\omega_l)G(k';i\omega_l). \end{aligned} \tag{5.46}$$

The same result, apart from the second term in the square bracket which will be shown to vanish, could have been obtained also with Feynman diagrams [90].

Let us now define

$$S_1(p;i\omega_l) = \frac{1}{\beta}\sum_{m=-\infty}^{\infty}\frac{1}{i(\omega_l-\omega_m)}\eta_{lm}G_0(p;i\omega_m), \tag{5.47}$$

$$S_2(p,p';i\omega_l) = \frac{1}{\beta}\sum_{m=-\infty}^{\infty}\frac{1}{i(\omega_l-\omega_m)}\eta_{lm}G_0(p;i\omega_m)G_0(p';i\omega_m). \tag{5.48}$$

The sums of the Matsubara frequencies can be evaluated to give

$$S_1(p;i\omega_l) = -\frac{1}{2}\frac{\tanh(\beta v_F p/2)}{i\omega_l - v_F p} - \frac{1}{\beta}\frac{1}{(i\omega_l - v_F p)^2}, \tag{5.49}$$

$$\begin{aligned} S_2(p,p';i\omega_l) &= \frac{1}{v_F(p-p')}\Bigg[-\frac{1}{2}\frac{\tanh(\beta v_F p/2)}{i\omega_l - v_f p} + \frac{1}{2}\frac{\tanh(\beta v_F p'/2)}{i\omega_l - v_f p'} \\ &\quad -\frac{1}{\beta}\frac{1}{(i\omega_l - v_F p)^2} + \frac{1}{\beta}\frac{1}{(i\omega_l - v_F p')^2}\Bigg]. \end{aligned} \tag{5.50}$$

By introducing a momentum cutoff λ in the momentum integration, we will obtain

$$\begin{aligned}\int_{-\infty}^{\infty}\int_{-\infty}^{\infty} dpdp'\, S_2(p,p';i\omega_l) &= \frac{2}{v_F}\int_{-\Lambda}^{\Lambda} dp\left[-\frac{1}{2}\frac{\tanh\left(\beta v_F p/2\right)}{i\omega_l - v_F p} - \frac{1}{\beta}\frac{1}{(i\omega_l - v_F p)^2}\right]\log\left(\frac{\Lambda+p}{\Lambda-p}\right) \\ &\to 0, \qquad \text{as } \Lambda\to\infty. \end{aligned} \tag{5.51}$$

An exciting, non-trivial, result will come from the integration

$$\begin{aligned}&\int_{-\infty}^{\infty}\int_{-\infty}^{\infty} dpdp'\, S_1(p;i\omega_l)G_0(p';i\omega_l) \\ &\quad= \int_{-\infty}^{\infty} dp\left[-\frac{1}{2}\frac{\tanh\left(\beta v_F p/2\right)}{i\omega_l - v_F p} - \frac{1}{\beta}\frac{1}{(i\omega_l - v_F p)^2}\right]\int_{-\infty}^{\infty} dp'\,\frac{1}{i\omega_l - v_F p'}.\end{aligned} \tag{5.52}$$

Note that the integration of the second term in the square bracket above vanishes. After performing analytic continuation $i\omega_l \to \omega + i\eta$, one finds

$$\int_{-\infty}^{\infty}\int_{-\infty}^{\infty} dpdp'\, S_1(p;i\omega_l)G_0(p';i\omega_l) = -\frac{i\pi}{2v_F^2}\left[\fint_{-v_F\Lambda}^{v_F\Lambda} dq\,\frac{\tanh\left(\frac{q}{2T}\right)}{q-\omega} + i\pi\tanh\left(\frac{\omega}{2T}\right)\right], \tag{5.53}$$

where $\fint$ denotes principal value integration. For $v_F\Lambda \gg \omega, T$, the integral above can be approximated by [91]

$$\int_{-\infty}^{\infty}\int_{-\infty}^{\infty} dpdp'\, S_1(p;i\omega_l)G_0(p';i\omega_l) \approx -\frac{i\pi}{v_F^2}\log\left(\frac{v_F\Lambda}{\sqrt{\omega^2+4T^2}}\right) + \frac{\pi^2}{2v_F^2}\tanh\left(\frac{\omega}{2T}\right). \tag{5.54}$$

Since the magnitude of the second term in the RHS is much smaller than the logarithmic term, it can be neglected.

Therefore, the third order in g_i contribution to the retarded Green's function can be written as

$$G_{ij}^{R,(3)}(x,y;\omega) = -\frac{i\pi^2 v_F}{4\cos^2\left(\theta_i/2\right)}\lambda_1\lambda_2\lambda_3\delta_{ij}\log\left(\frac{v_F\Lambda}{\sqrt{\omega^2+4T^2}}\right)G_0^R(x,0;\omega)G_0^R(0,y;\omega), \tag{5.55}$$

such that

$$\xi_i^{(3)}(\omega,T) = \pi^2\lambda_1\lambda_2\lambda_3\log\left(\frac{v_F\Lambda}{\sqrt{\omega^2+4T^2}}\right). \tag{5.56}$$

Summation of the orders

Combining all of the calculations above, the function $\xi_i(\omega, T)$ is given by

$$\xi_i(\omega, T) = \frac{\pi^2}{4}\left[\widetilde{\lambda}_i^2 + 4\lambda_1\lambda_2\lambda_3 \log\left(\frac{v_F\Lambda}{\sqrt{\omega^2+4T^2}}\right)\right]. \tag{5.57}$$

In the isotropic case $\lambda_i \equiv \lambda_0$, it becomes

$$\xi(\omega, T) = \frac{\pi^2}{2}\left[\lambda_0^2 + 2\lambda_0^3 \log\left(\frac{v_F\Lambda}{\sqrt{\omega^2+4T^2}}\right)\right]. \tag{5.58}$$

Up to an overall factor, this result is the same as for ordinary single-channel Kondo systems [62].

5.1.2 Poor man's scaling

In this section we shall apply poor man's scaling to our system [80, 36]. We aim to calculate the following,

$$\delta\hat{H}_{\rm TK} = \delta\hat{H}^{ee}_{\rm TK} + \delta\hat{H}^{hh}_{\rm TK} + \delta\hat{H}^{eh}_{\rm TK} + \delta\hat{H}^{he}_{\rm TK}, \tag{5.59}$$

where

$$\delta\hat{H}^{ab}_{\rm TK} = (1-\hat{P})\hat{H}_{\rm TK}\hat{P}_a\frac{1}{\varepsilon-\hat{H}_0}\hat{P}_b\hat{H}_{\rm TK}(1-\hat{P}). \tag{5.60}$$

The projection operator $\hat{P}$ is given by $\hat{P} = \hat{P}_e + \hat{P}_h$, where $\hat{P}_{e(h)}$ projects onto states which have at least one electron (hole) with energy $D - \delta D < \varepsilon < D$ ($-D < \varepsilon < -D + \delta D$), with $D = v_F\Lambda$ the energy cutoff.

The term $\delta\hat{H}^{ee}_{\rm TK}$ has the form

$$\begin{aligned}\delta\hat{H}^{ee}_{\rm TK} &= \left[\frac{iv_F}{2}\sum_{\alpha,a,b=1}^{3}\int_m dp'\int_t dq'\,\lambda_\alpha\epsilon_{\alpha ba}\hat{a}^\dagger_{p',a}\hat{a}_{q',b}\hat{S}_\alpha\right]\frac{1}{\varepsilon-\hat{H}_0} \\ &\quad \left[\frac{iv_F}{2}\sum_{\beta,c,d=1}^{3}\int_t dq\int_m dp\,\lambda_\beta\epsilon_{\beta dc}\hat{a}^\dagger_{q,c}\hat{a}_{p,d}\hat{S}_\beta\right].\end{aligned} \tag{5.61}$$

The integral $\int_m dq$ stands for integration over the quantum states with energies in the range $|\varepsilon_q| = v_F|q| < D - \delta D$, while the integral $\int_t dq$ stands for those with energies in the range $D - \delta D < v_F|k| < D$.

We would like to bring all the operators from the right side of the operator $1/(\varepsilon - \hat{H}_0)$ to its left side. First of all, the spin operator $\hat{S}_\beta$ can be immediately moved since it commutes with $\hat{H}_0$. When the operator $1/(\varepsilon - \hat{H}_0)$ is applied to a state $|k\rangle$ with energy ε_k, it will not change the state except by multiplying it with the eigenvalue $1/(\varepsilon - \varepsilon_k)$. Therefore, as the operator $\hat{a}^\dagger_{q,c}\hat{a}_{p,d}$ when applied to a state $|\alpha\rangle$ will increase its energy by magnitude $\varepsilon_q - \varepsilon_p$, we need to transform the operator $1/(\varepsilon - \hat{H}_0)$ to $1/(\varepsilon - \hat{H}_0 - \varepsilon_q + \varepsilon_p)$ if we move $\hat{a}^\dagger_{q,c}\hat{a}_{p,d}$ to its left side. Since $\varepsilon_q \approx D$, one finds

$$\begin{aligned}\delta\hat{H}^{ee}_{\rm TK} &= -\frac{v_F^2}{4}\sum_{\substack{\alpha,\alpha'\\ a,b,c,d=1}}^{3}\int_m dp\int_t dq'\int_t dq\int_m dp\,\lambda_\alpha\lambda_\beta\epsilon_{\alpha ba}\epsilon_{\beta dc}\\ &\quad \hat{S}_\alpha\hat{S}_\beta\hat{a}^\dagger_{p',a}\hat{a}_{q',b}\hat{a}^\dagger_{q,c}\hat{a}_{p,d}\frac{1}{\varepsilon - \hat{H}_0 - D + \varepsilon_p}. \end{aligned} \tag{5.62}$$

Since the state with energy ε_q in the range $D - \delta D < \varepsilon_q < D$ is empty, we need to set $\hat{a}_{q',b}\hat{a}^\dagger_{q,c} = \delta_{bc}\delta(q - q')$. Substituting this into the expression of $\delta\hat{H}^{ee}_{\rm TK}$ above, the integral over q' disappears and so does any function of q and q'. Therefore, the integral $\int_t dq$ now simply counts the number of states that have energies $v_F|q|$ in the range between $D - \delta D$ and D. Since the wavevector q runs from $-\infty$ to ∞, the positive and negative sectors of q equally contribute to this energy range. Therefore, we have $\int_t dq = 2\delta\Lambda = \frac{2}{v_F}\delta D$. This also tells us that the density of states of the lead electrons is $\rho = 2/v_F$. Hence, we have

$$\delta\hat{H}^{ee}_{\rm TK} = -\frac{v_F}{2}\delta D\sum_{\substack{\alpha,\alpha'\\ a,b,d=1}}^{3}\int_m dp\int_m dp\,\lambda_\alpha\lambda_\beta\epsilon_{\alpha ba}\epsilon_{\beta db}\hat{S}_\alpha\hat{S}_\beta\hat{a}^\dagger_{p',a}\hat{a}_{p,d}\frac{1}{\varepsilon - \hat{H}_0 - D + \varepsilon_p}. \tag{5.63}$$

Now, let us use the identity $\sum_{k=1}^{3}\epsilon_{ijk}\epsilon_{imn} = \delta_{jm}\delta_{kn} - \delta_{jn}\delta_{km}$ and the relation satisfied by the multiplication of two spin operators $\hat{S}_\alpha\hat{S}_\beta = \frac{1}{4}\delta_{\alpha\beta} + \frac{i}{2}\sum_{\gamma=1}^{3}\epsilon_{\alpha\beta\gamma}\hat{S}_\gamma$. Since we are working with the states near the ground state, with energies much less than the energy

cutoff D, we can set $H_0 \approx 0$. So, we get

$$\begin{aligned}\delta\hat{H}^{ee}_{\rm TK} &= -\frac{iv_F}{4}\delta D\sum_{\alpha,\beta,\gamma=1}^{3}\int_m\int_m dpdp'\,\lambda_\alpha\lambda_\beta\epsilon_{\alpha\beta\gamma}\hat{S}_\gamma\hat{a}^\dagger_{p',\beta}\hat{a}_{p,\alpha}\frac{1}{\varepsilon - D + \varepsilon_p} \\ &\quad +\frac{v_F}{8}\delta D\sum_{\beta=1}^{3}\int_m\int_m dpdp'\,\widetilde{\lambda}^2_\beta\hat{a}^\dagger_{p',\beta}\hat{a}_{p,\beta}\frac{1}{\varepsilon - D + \varepsilon_p}. \end{aligned} \tag{5.64}$$

The term $\delta\hat{H}^{hh}_{\rm TK}$ is given by

$$\begin{aligned}\delta\hat{H}^{hh}_{\rm TK} &= \left[\frac{iv_F}{2}\sum_{\alpha,a,b=1}^{3}\int_m dp\int_b dq\,\lambda_\alpha\epsilon_{\alpha ba}\hat{a}^\dagger_{q,a}\hat{a}_{p,b}\hat{S}_\alpha\right]\frac{1}{\varepsilon - \hat{H}_0} \\ &\quad \left[\frac{iv_F}{2}\sum_{\beta,c,d=1}^{3}\int_b dq'\int_m dp'\,\lambda_\beta\epsilon_{\beta dc}\hat{a}^\dagger_{p',c}\hat{a}_{q',d}\hat{S}_\beta\right]. \end{aligned} \tag{5.65}$$

The integral $\int_b dq$ stands for integration over the quantum states with energies in the range $-D < v_F|q| < -D + \delta D$. The calculation is similar, except that now we have to remember that $\hat{a}^\dagger_{q,a}\hat{a}_{q',d} = \delta_{bc}\delta(q - q')$ because the state with energy ε_q in the range $-D < \varepsilon_q < -D + \delta D$ is filled. We also have to set $\varepsilon_q \approx -D$. Hence, we will obtain

$$\begin{aligned}\delta\hat{H}^{hh}_{\rm TK} &= -\frac{iv_F}{4}\delta D\sum_{\alpha,\beta,\gamma=1}^{3}\int_m\int_m dpdp'\,\lambda_\alpha\lambda_\beta\epsilon_{\alpha\beta\gamma}\hat{S}_\gamma\hat{a}^\dagger_{p',\beta}\hat{a}_{p,\alpha}\frac{1}{\varepsilon - \varepsilon_{p'} - D} \\ &\quad -\frac{v_F}{8}\delta D\sum_{\beta=1}^{3}\int_m\int_m dpdp'\,\widetilde{\lambda}^2_\beta\hat{a}^\dagger_{p',\beta}\hat{a}_{p,\beta}\frac{1}{\varepsilon - \varepsilon_{p'} - D} + \frac{v_F}{4}\delta D\int_m dp\sum_{\alpha=1}^{3}\lambda^2_\alpha\frac{1}{\varepsilon - \varepsilon_p - D}, \end{aligned} \tag{5.66}$$

where the last term is merely a constant, which then can be neglected.

The other terms of $\delta\hat{H}_{\rm TK}$, namely $\delta\hat{H}^{eh}_{TK}$ and $\delta\hat{H}^{he}_{TK}$, are vanishing. To see this point, let us note that the operator $(1-\hat{P})$ projects onto states which do not contain an electron in the energy interval $[D - \delta D, D]$ or a hole in the energy interval $[-D, -D + \delta D]$, while $\hat{P}_e\hat{P}_h = \hat{P}_h\hat{P}_e$ projects onto states which have at least both of them. The latter appears in term like $(1-\hat{P})\hat{H}_{\rm TK}\hat{P}_e\frac{1}{\varepsilon-\hat{H}_0}\hat{P}_h\hat{H}_{\rm TK}(1-\hat{P})$ because $\hat{P}_e$ and $\hat{P}_h$ commute with $1/(\varepsilon - \hat{H}_0)$. The Hamiltonian $\hat{H}_{\rm TK}$ only contains two operators: one to apply on the state that has

passed the projection operator $(1-\hat{P})$ and another one to send the resulting state into either a state which has at least one electron in the energy interval $[D-\delta D, D]$ or a state which has at least one hole in the energy interval $[-D, -D+\delta D]$, but not both. This explains the vanishing of $\delta\hat{H}^{eh}_{TK}$ and $\delta\hat{H}^{he}_{TK}$.

Since we are working with states which have energy much smaller than the energy cutoff D, we can set $\varepsilon, \varepsilon_p, \varepsilon_{p'} \ll D$. Therefore, we can write

$$\hat{H}_{\rm TK} + \delta\hat{H}_{\rm TK} = \frac{iv_F}{2}\sum_{\alpha,a,b=1}^{3}\int\int dpdp'\,\epsilon_{\alpha ba}\hat{a}^{\dagger}_{p,a}\hat{a}_{p',b}\hat{S}_{\alpha}\left[\lambda_{\alpha} + \lambda_a\lambda_b\frac{\delta D}{D}\right]. \tag{5.67}$$

This tells us that lowering the cutoff by δD will keep the structure of the Hamiltonian unchanged, but the couplings now change as a function of the cutoff D. The change of the coupling $\delta\lambda_{\alpha}$ is given by

$$|\epsilon_{\alpha ab}|\delta\lambda_{\alpha} = \lambda_a\lambda_b\frac{\delta D}{D}. \tag{5.68}$$

Since the cutoff D is decreased by δD, we have $dD = -\delta D$. Therefore, we can write

$$|\epsilon_{\alpha ab}|\frac{d\lambda_{\alpha}}{d(\log D)} = -\lambda_a\lambda_b. \tag{5.69}$$

In other words, we have [36]

$$\frac{d\lambda_1}{d(\log D)} = -\lambda_2\lambda_3, \qquad \frac{d\lambda_2}{d(\log D)} = -\lambda_3\lambda_1, \qquad \frac{d\lambda_3}{d(\log D)} = -\lambda_1\lambda_2. \tag{5.70}$$

In the isotropic case $\lambda_i = \lambda$, we have

$$\frac{d\lambda}{d(\log D)} = -\lambda^2. \tag{5.71}$$

This RG flow equation is identical to the one for the conventional, single-channel, Kondo model [62]. If the bare coupling is denoted by λ_0, then the solution of this equation is [62]

$$\lambda(E) = \frac{\lambda_0}{1-\lambda_0\log\left(v_F\Lambda/E\right)}. \tag{5.72}$$

The coupling λ diverges when the energy E approaches Kondo temperature T_K, which, to the accuracy of our RG equations, is given by [36, 39]

$$T_K = v_F \Lambda e^{-1/\lambda_0}. \tag{5.73}$$

Hence, from Eqs. (5.72) and (5.73), the coupling $\lambda(E)$ can be written in terms of T_K as [36]

$$\lambda(E) = \frac{1}{\log\left(E/T_K\right)}. \tag{5.74}$$

5.1.3 Kondo screening cloud

At high energies and focussing on the isotropic case for simplicity, we can write [60, 62]

$$\lambda^2(E) \approx \lambda_0^2 + 2\lambda_0^3 \log\left(\frac{v_F\Lambda}{E}\right), \tag{5.75}$$

which has the same structure as the function $\xi(\omega, T)$ in Eq. (5.58). Therefore, following Ref. [60] and [62], we can express $\xi(\omega, T)$ in Eq. (5.58) in terms of λ^2 as the following,

$$\xi(\omega, T) = \frac{\pi^2}{2}\lambda^2(\sqrt{\omega^2 + 4T^2}). \tag{5.76}$$

Finally, using Eq. (5.74), this equation can be written in terms of T_K as

$$\xi(\omega, T) = \frac{\pi^2/2}{\log^2\left(\frac{\sqrt{\omega^2+4T^2}}{T_K}\right)}. \tag{5.77}$$

Using the function $\xi(\omega, T)$ above and introducing the notation $y \equiv \omega/T$, we can obtain the expression for the Kondo screening cloud for isotropic couplings at zero bias,

$$\rho_{K,2k_F}(x, 0, T) \propto -\frac{1}{4}\int_{-\infty}^{\infty} dy\ \mathrm{sech}^2\left(\frac{y}{2}\right)\frac{(-\pi^2)}{v_F}\frac{1}{\log^2\left(\frac{2T}{T_K}\sqrt{\frac{y^2}{4}+1}\right)}\cos\left(2k_F|x| + 2y\frac{|x|}{L_T} + \theta\right). \tag{5.78}$$

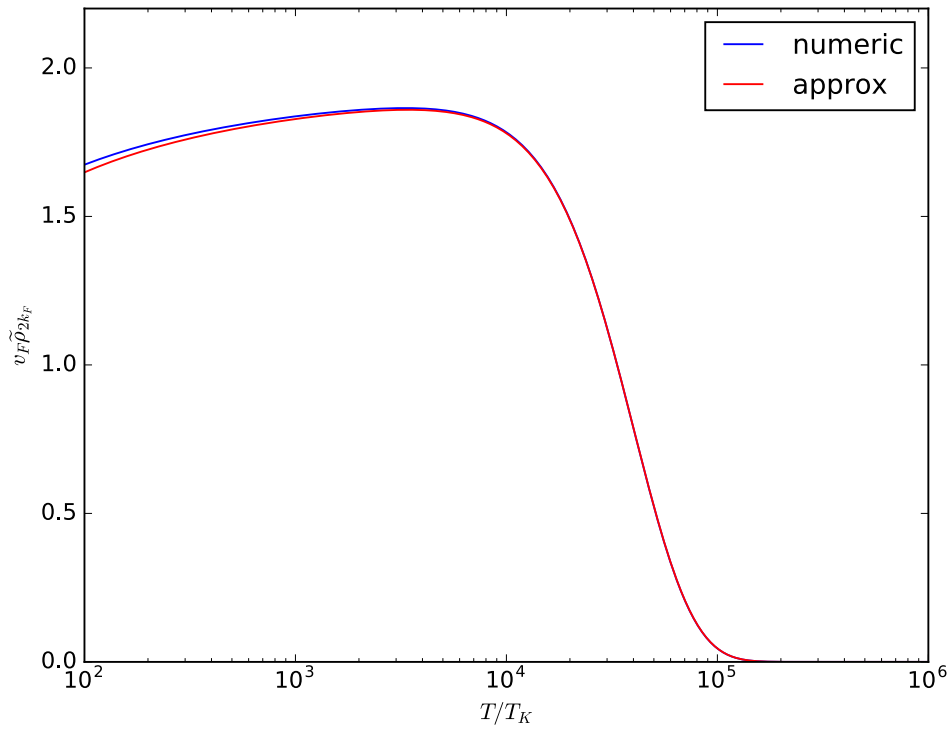

Figure 5.4: The numerical evaluation of the Kondo cloud in Eq. (5.78) is compared with its approximation in Eq. (5.81) by plotting the tDOS amplitude $\widetilde{\rho}_{2k_F} = \widetilde{\rho}_{0,2k_F} + \widetilde{\rho}_{K,2k_F}$ for $|x|/L_K = 10^{-5}$, which is the same value that is used to plot the $|x| \ll L_K$ graph in Fig. 5.1.

The logarithmic function in the integrand above can be written as

$$\frac{1}{\log^2\left(\frac{2T}{T_K}\sqrt{\frac{y^2}{4}+1}\right)} = \frac{1}{\left[\log\left(\frac{2T}{T_K}\right) + \log\left(\sqrt{\frac{y^2}{4}+1}\right)\right]^2}. \tag{5.79}$$

For temperature $T/T_K = 10^4$, the second logarithm in the denominator of the RHS is smaller than the first one by the ratio ~ 0.14 at $|y| = 8$, the width of the logistic distribution $\frac{1}{4}\,\mathrm{sech}^2\,(y/2)$, and this ratio continues to decrease as the temperature increases. Hence, we can expand the equation above in the form of a series,

$$\frac{1}{\log^2\left(\frac{2T}{T_K}\sqrt{\frac{y^2}{4}+1}\right)} = \frac{1}{\log^2\left(\frac{2T}{T_K}\right)} - 2\frac{\log\left(\sqrt{\frac{y^2}{4}+1}\right)}{\log^3\left(\frac{2T}{T_K}\right)} + \cdots. \tag{5.80}$$

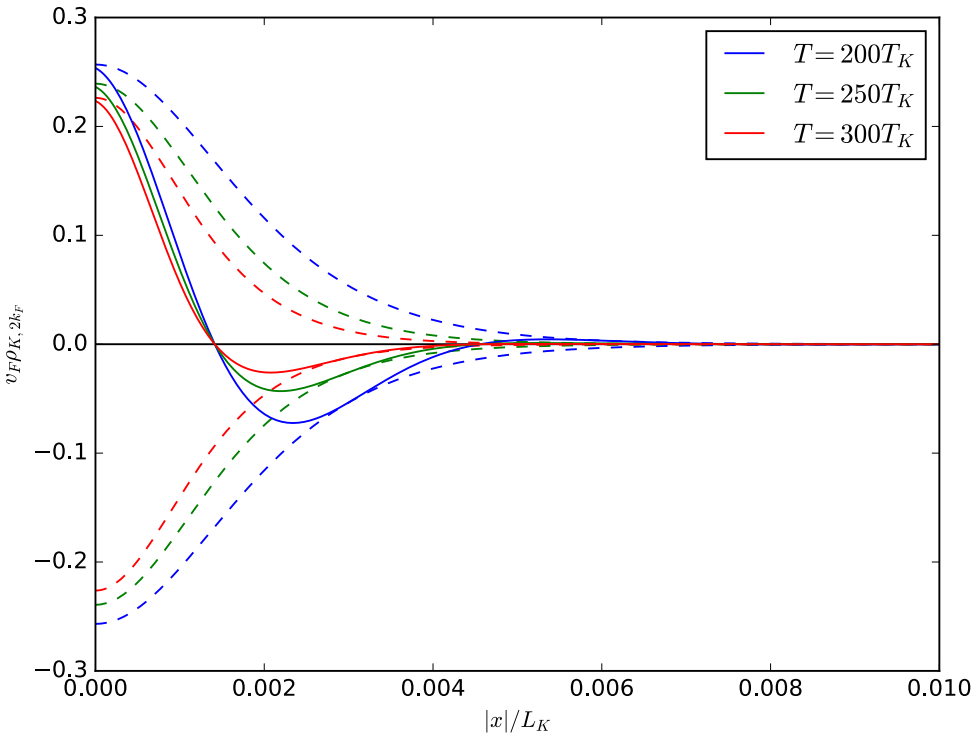

Figure 5.5: The Kondo cloud $\rho_{K,2k_F}$ (solid) and its amplitude $\widetilde{\rho}_{K,2k_F}$ (dashed) in the high energy regime, with $\theta = \pi/20$, $V = 0$, and $k_F L_K = 500$, where $L_K = v_F/T_K$ is the Kondo length. $\widetilde{\rho}_{K,2k_F}$ decays exponentially along x on the scale of L_T. This high energy Kondo cloud profile, up to an overall factor, is the same as for ordinary single channel Kondo systems represented by the lead-dot model (Fig. 5.7a). The figure is taken from Ref. [84].

Therefore, for temperatures higher than the aforementioned lower bound, we can approximate the LHS with the first term in the RHS. Multiplication with the logistic distribution $\frac{1}{4}\operatorname{sech}^2(y/2)$ makes this approximation still accurate even for a smaller temperature lower bound, $T/T_K \gtrsim 10^2$ (see Fig. 5.4), since as $|y|$ increases from 0 to ~ 8, the increasing difference between the LHS and the first term of the RHS is suppressed by the collapse in the logistic distribution. We then obtain

$$\rho_{K,2k_F}(x,0,T) \approx \frac{2\pi^3}{v_F}\frac{1}{\log^2(2T/T_K)}\frac{|x|}{L_T}\operatorname{cosech}\left(2\pi\frac{|x|}{L_T}\right)\cos(2k_F|x|+\theta). \tag{5.81}$$

The Kondo cloud evaluated numerically using Eq. (5.78) is depicted in Fig. 5.5 for various temperatures as a function of $|x|/L_K$, where $L_K \equiv v_F/T_K$ is the Kondo length.

Also shown is the amplitude of $\rho_{K,2k_F}$, denoted as $\widetilde{\rho}_{K,2k_F}$. (The temperatures used in Fig. 5.5 may strictly be slightly outside the domain where perturbation theory is accurate [39], but we believe that apart from a slight overestimation of the amplitude, the graph captures well the behaviour.) The exponential suppression of the function $(|x|/L_T)\,\mathrm{cosech}\,(2\pi|x|/L_T)$ in the limit $L_T \ll |x|$ is manifested in two complementary aspects: for fixed T, it shows that $\widetilde{\rho}_{K,2k_F}$ decays exponentially with increasing $|x|$ on the scale of L_T, and, for fixed x, given that $\rho_{0,2k_F}$ in Eq. (5.10) contains the same function, one sees that it governs the exponential decay of the high temperature tail of the tDOS amplitude $\widetilde{\rho}_{2k_F}$ shown in Fig. 5.1.

The temperature dependence of $\widetilde{\rho}_{K,2k_F}$ and $\widetilde{\rho}_{2k_F}$ is particularly interesting when there is a good scale separation so that $0 < |x| \ll L_K$. In this case, the high-energy regime $L_T \ll L_K$ displays a crossover upon lowering the temperature, from the exponential behaviour discussed above for $L_T \ll |x|$ to a $|x| \ll L_T \ll L_K$ regime where $\widetilde{\rho}_{K,2k_F} \sim 1/\log^2(2T/T_K)$ is governed by the Kondo logarithm. Extrapolating our results to $T \lesssim T_K$ beyond the perturbative regime we expect this logarithm-like increase of the Kondo cloud to develop into a contribution comparable to the free cloud and thus to govern the behaviour of $\widetilde{\rho}_{2k_F}$ itself. Conversely, for $|x| \gg L_K$, the Kondo cloud and $\widetilde{\rho}_{2k_F}$ remain exponentially suppressed even for $T \lesssim T_K$, thus the high-temperature regime crosses over to the low-temperature one without an intermediate logarithmic behaviour. The temperature dependence of $\widetilde{\rho}_{2k_F}$ in these two complementary regimes is shown in Fig. 5.1. The presence versus the suppression of the logarithmic contribution may be used to estimate L_K, that is, the extent of the Kondo screening cloud.

5.2 $2k_F$-tDOS at low energies

Now we turn to energies much below T_K. In this regime, weak g_α perturbation theory is inapplicable. Instead, we will work in the vicinity of the topological Kondo fixed point [36] and adapt the CFT results of Ref. [61] to obtain ξ_i. Let us start with the non-interacting

retarded Green's function in the position space and frequency domain,

$$G^R_{0,ij}(x,y;\omega) = \int\int dkdk'\, G^R_{0,ij}(k,k';\omega)\varphi_{k,i}(x)\varphi^*_{k',j}(y). \tag{5.82}$$

Since the function $\varphi_{k,i}(x)$ is a superposition of left and right movers (see Eq. (4.4)), one can write

$$\begin{aligned} G^R_{0,ij}(x,y;\omega) = \frac{1}{2\pi}\Big[& e^{ik_F(x-y)}G^R_{ij,RR}(x,y;\omega) + e^{-ik_F(x-y)}G^R_{ij,LL}(x,y;\omega) \\ & + e^{ik_F(x+y)}G^R_{ij,RL}(x,y;\omega) + e^{-ik_F(x+y)}G^R_{ij,LR}(x,y;\omega)\Big], \end{aligned} \tag{5.83}$$

where

$$\begin{aligned} G^R_{0,ij,RR}(x,y;\omega) &= \int\int dkdk'\, G^R_{0,ij}(k,k';\omega)\varphi^R_{k,i}(x)\varphi^{R*}_{k',j}(y) \\ &= -\frac{2\pi i}{v_F}\delta_{ij}e^{-i\frac{\omega}{v_F}(|x|-|y|)}\theta(|y|-|x|), && (5.84) \\ G^R_{0,ij,LL}(x,y;\omega) &= \int\int dkdk'\, G^R_{0,ij}(k,k';\omega)\varphi^L_{k,i}(x)\varphi^{L*}_{k',j}(y) \\ &= -\frac{2\pi i}{v_F}\delta_{ij}e^{i\frac{\omega}{v_F}(|x|-|y|)}\theta(|x|-|y|), && (5.85) \\ G^R_{0,ij,RL}(x,y;\omega) &= \int\int dkdk'\, G^R_{0,ij}(k,k';\omega)\varphi^R_{k,i}(x)\varphi^{L*}_{k',j}(y) \\ &= 0, && (5.86) \\ G^R_{0,ij,LR}(x,y;\omega) &= \int\int dkdk'\, G^R_{0,ij}(k,k';\omega)\varphi^L_{k,i}(x)\varphi^{R*}_{k',j}(y) \\ &= -\frac{2\pi i}{v_F}r_i\delta_{ij}e^{i\frac{\omega}{v_F}(|x|+|y|)}. && (5.87) \end{aligned}$$

Here $\theta(x)$ is the Heaviside step function.

On the other hand, the interacting retarded Green's function $G^R_{ij}(x,y;\omega,T)$ can be written as in Eq. (5.83). At the Kondo fixed point $T = 0$, the conformally invariant

boundary condition between left and right movers yields [61, 92]

$$G^R_{ij,RR}(x,y;\omega,0) = G^R_{0,ij,RR}(x,y;\omega), \tag{5.88}$$

$$G^R_{ij,LL}(x,y;\omega,0) = G^R_{0,ij,LL}(x,y;\omega), \tag{5.89}$$

$$G^R_{ij,RL}(x,y;\omega,0) = S_{(1)}G^R_{0,ij,RL}(x,y;\omega), \tag{5.90}$$

$$G^R_{ij,LR}(x,y;\omega,0) = S_{(1)}G^R_{0,ij,LR}(x,y;\omega), \tag{5.91}$$

where $S_{(1)}$ is the single-particle-to-single-particle scattering amplitude at the Fermi energy. It is given by

$$S_{(1)} = \frac{S^j_s/S^j_0}{S^0_s/S^0_0}, \tag{5.92}$$

with $S^j_s = \sqrt{\frac{2}{2+k}}\sin\left[\frac{\pi(2j+1)(2s+1)}{2+k}\right]$, where k is the level of the $\mathrm{SU}(2)_k$ current algebra, j is the spin of conduction electrons, and s is the impurity spin [61]. Therefore, using Eq. (5.83) and similar equation for G^R_{ij}, one obtains

$$\begin{aligned} G^R_{ij}(x,x;\omega,0) - G^R_{0,ij}(x,x;\omega) &= \frac{1}{2\pi}\left[S_{(1)}-1\right]\Big\{e^{2ik_Fx}G^R_{0,ij,RL}(x,x;\omega) \\ &\quad + e^{-2ik_Fx}G^R_{0,ij,LR}(x,x;\omega)\Big\} \\ &= \frac{i}{v_F}\left[1-S_{(1)}\right]\delta_{ij}e^{i\left(2k_F|x|+2\frac{\omega}{v_F}|x|+\theta_i\right)}. \end{aligned} \tag{5.93}$$

By comparing this equation with Eq. (5.5), one obtains the $\mathcal{T}$-matrix as

$$\mathcal{T}_{ij}(\omega,0) = \frac{iv_F}{4\cos^2(\theta_i/2)}\delta_{ij}\left[S_{(1)}-1\right]. \tag{5.94}$$

The function ξ_i at the Kondo fixed point, i.e., at zero energy where the RG-irrelevant perturbations near this fixed point completely decayed, can be obtained using Eq. (5.9), which yields

$$\xi_i(\omega\to 0, T\to 0) = 1 - S_{(1)}, \tag{5.95}$$

For our model, $s = 1/2$, $j = 1$, and $k = 4$, and therefore $S_{(1)} = 0$ [36, 39]. This remarkable

result signifies that, in stark contrast to Fermi liquid behaviour, there is no single-particle scattering in topological Kondo systems at the Kondo fixed point. In terms of ρ_{2k_F}, which measures the single electron interference of incoming and outgoing waves, the vanishing of $S_{(1)}$ at the Kondo fixed point translates into $\rho_{2k_F} \to 0$ as $T, V \to 0$. The $2k_F$-tDOS thus may be used to directly demonstrate the absence of single-particle scattering in the topological Kondo effect.

By comparing the $\mathcal{T}$-matrix in Eq. (5.94) above and the corresponding expression in Ref. [61] [see its Eq. (3.14)], we can identify the density of states ν in Ref. [61] in terms of the quantities in our setup, $\nu = \frac{2}{\pi v_F} \cos^2(\theta_i/2)$. With this identification, we can obtain the function $\xi_i(\omega, T)$ at low energies, but away from the Kondo fixed point, by using Eq. (3.50) in Ref. [61]. It yields

$$\xi_i(\omega, T) = 1 - N\delta\lambda\sqrt{3}\left(2\pi\frac{T}{T_K}\right)^{1/3} I(\omega, T), \tag{5.96}$$

with $\delta\lambda$ is the dimensionless coupling of the leading irrelevant perturbation to the Kondo fixed point, N is real satisfying $|N|^2 \approx 0.6$, and

$$I(\omega, T) \equiv \int_0^1 du \left[u^{-i\omega/2\pi T} u^{-1/2}(1-u)^{1/3} F(u) - \frac{\Gamma(5/3)}{\Gamma^2(4/3)} u^{-2/3}(1-u)^{-4/3}\right], \tag{5.97}$$

where Γ is the gamma function and $F(u) \equiv {}_2F_1(4/3, 4/3; 1; u)$ is the hypergeometric function. The power law $T^{\Delta_s - 1} = T^{1/3}$ in Eq. (5.96) directly informs on the scaling dimension $\Delta_s = 4/3$ of the leading irrelevant perturbation to the Kondo fixed point [36]. Note that in contrast to the description in the high-energy regime, the CFT does not determine T_K, but it rather enters as a microscopic parameter: it is the high-energy cutoff of the low-energy theory.

For low energies, it is useful to consider two complementary regimes: when $T = 0$ but $V \neq 0$, and when $V = 0$ with $T \geq 0$. Though as mentioned earlier, the $T = 0$ spatial correlations are due to the free Green's functions, there is useful information to

be obtained from ξ and the overall amplitude of ρ_{2k_F}. For ξ we find

$$\xi_i(\omega, 0) = 1 + N'\delta\lambda \left[\sqrt{3} - i\epsilon(\omega)\right] \left|\frac{\omega}{T_K}\right|^{1/3}, \tag{5.98}$$

where $N' \approx 3.98N$ and $\epsilon(\omega)$ is the step function. This expression, firstly, may be used to specify $N\delta\lambda$: while $\delta\lambda$ and the sign of N are free parameters for the CFT, the fact that the $\mathcal{T}$-matrix is a universal function [39] of ω/T_K implies that $N\delta\lambda$ also has a universal value. We can approximately obtain this by using Eq. (5.98) to fit to the numerically exact results of Ref. [39]; this gives $N\delta\lambda \approx -0.093$. It also follows that for $T \to 0$, ρ_{2k_F} is a simple expression set by the second term in Eq. (5.98):

$$\rho_{2k_F}(x, V, 0) \propto \frac{2}{v_F} N'\delta\lambda \left|\frac{eV}{T_K}\right|^{1/3} \left\{\sqrt{3}\cos\left[2K(eV, x)\right] + \epsilon(eV)\sin\left[2K(eV, x)\right]\right\}. \tag{5.99}$$

In the $V = 0$, $T \geq 0$ case, we plot the oscillating component of the tDOS of lead electrons for various temperatures (top panel of Fig. 5.6). As the function of temperature, ρ_{2k_F} is gradually suppressed for all x as T decreases. This is in contrast to the free cloud which gradually saturates upon lowering the temperature [see Eq. (5.10) and Fig. 5.1]. Note that at low energies, since L_K became the short-distance cutoff (as follows from T_K being the high-energy cutoff), the only length scale that can set long distance features is the thermal length L_T. This can be made manifest by noting that the tDOS amplitude $\widetilde{\rho}_{2k_F}$, as shown in Appendix E, admits the scaling from $\widetilde{\rho}_{2k_F} \propto (T/T_K)^{1/3} h(|x|/L_T)$ with the universal scaling function $h(|x|/L_T) = \widetilde{\rho}_{2k_F}/\widetilde{\rho}_{2k_F}(x \to 0)$. The corresponding scaling collapse, illustrated in the bottom panel of Fig. 5.6, may serve as a useful characteristic of the spatial organisation of conduction electrons near the topological Kondo fixed point, and as means to demonstrate the $T^{1/3}$ law (and thus the scaling dimension Δ_s) governing the suppression of the oscillations as the temperature is lowered (Fig. 5.1). [Extracting $\widetilde{\rho}_{2k_F}$ and thus the scaling function $h(|x|/L_T)$ from ρ_{2k_F} in practice may be facilitated by oscillation extrema much denser than L_T, including $k_F L_K > 1$. The latter is not inconsistent with L_K being the short distance cutoff of the CFT, since that only limits

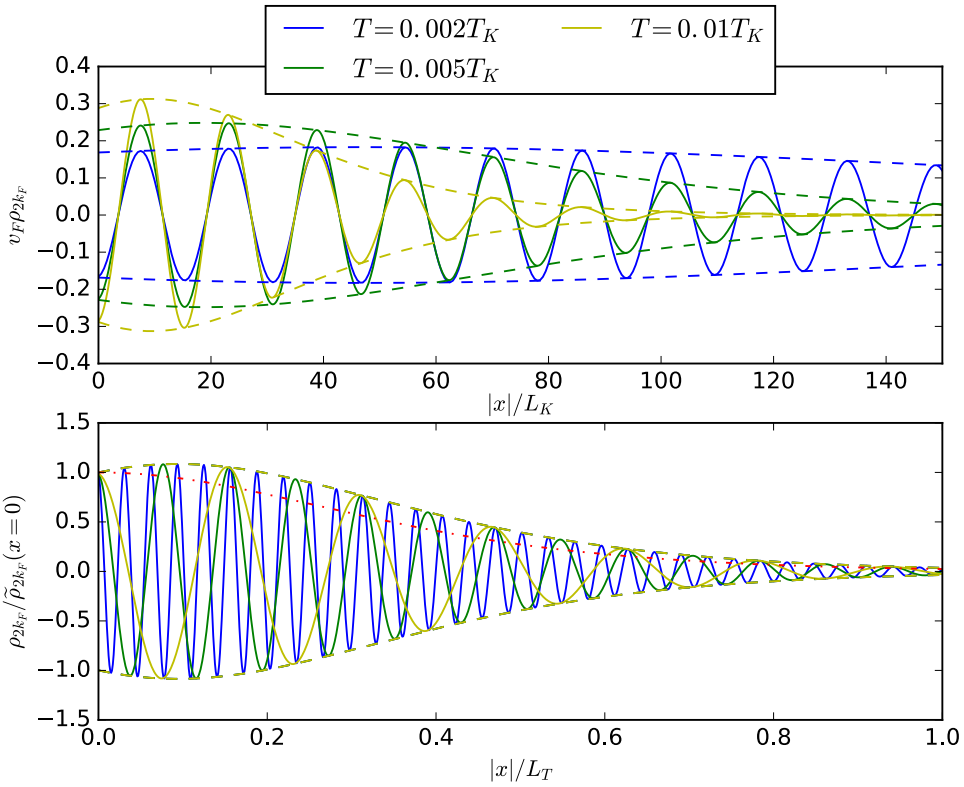

Figure 5.6: Top panel: The oscillating part of the tDOS ρ_{2k_F} (solid) and its amplitude $\widetilde{\rho}_{2k_F}$ (dashed) in the low energy regime, with $N\delta\lambda = -0.093$, $\theta = \pi/(20)$, $V = 0$ and $k_F L_K = 0.2$. Bottom panel: Rescaling ρ_{2k_F} and the corresponding scaling collapse of $\widetilde{\rho}_{2k_F}$, as follows from $\widetilde{\rho}_{2k_F} \propto (T/T_K)^{1/3} h(|x|/L_T)$. The universal scaling function (dashed) is also contrasted to that of free fermions (dash-dotted). The figure is taken from Ref. [84].

the spatial resolution for $\widetilde{\rho}_{2k_F}$, and not the wavelength of the $2k_F$ oscillations.] We note that a similar form, $\widetilde{\rho}_{2k_F} = f(T/T_K) h_{\rm high}(|x|/L_T)$, holds also in the high energy regime. The scaling function in that case, $h_{\rm high}(z = |x|/L_T) = 2\pi z \,\mathrm{cosech}\,(2\pi z)$, is however the same as for free fermions and thus unlike $h(|x|/L_T)$ for low energies, does not inform on Kondo features. The two curves are contrasted in the bottom panel of Fig. 5.6.

5.3 Discussion of the features and comparison to other systems

A common feature shared by our high- and low-temperature results is the thermal-length controlled large $|x|$ decay of the amplitude $\widetilde{\rho}_{2k_F}$ [see Eqs. (5.10) and (5.81) and Fig. 5.6].

In terms of the temperature dependence of $\widetilde{\rho}_{2k_F}(T, |x|)$ (illustrated in Fig. 5.1), the role of $|x|$ can thus be seen to be in controlling a competition between the thermal and Kondo lengths L_T and L_K, by setting the low temperature cutoff above which L_T dominates.

Considering that our high- and low-energy asymptotics are expected to hold [39] for $T \gtrsim 10^3 T_K$ and $T \lesssim 10^{-2} T_K$, respectively, one needs slightly exaggerated $|x|/L_K$ values to achieve good scale separation while staying within the domain of validity of our theory. (Fig. 5.1 uses $|x| = 10^{-5} L_K$ for $|x| \ll L_K$ and $|x| = 200 L_K$ for $|x| \gg L_K$.) It would be interesting to go beyond our method, e.g., using numerical renormalisation group calculations of the $\mathcal{T}$-matrix, to investigate the signatures of Kondo screening between these asymptotic regimes.

While in Subsection 5.1.3 we found that the high energy behaviour of $\widetilde{\rho}_{2k_F}$ and ρ_{2k_F} is similar to that in more conventional Kondo systems, there are important differences in the low energy regime. It is thus useful to contrast our results to such more conventional, single- and multi-channel Kondo systems. The simplest, single-channel Kondo effect arises in the lead-dot model shown Fig. 5.7a. Here $S_{(1)} = -1$ (see Appendix F.1), corresponding to a $\pi/2$ phase shift in single-particle scattering [83, 61]. This system is a local Fermi liquid at low energies. The low temperature $\widetilde{\rho}_{2k_F}$ thus is similar to the free cloud, increasing upon lowering temperature as the reduction of thermal smearing allows more and more single-particle interference.

Our findings are also in contrast to two-channel Kondo (2CK) systems proposed and later experimentally studied by Oreg and Goldhaber-Gordon [93, 94]. This is a two-lead 2CK model where there is a linear combination of modes without single-particle scattering at the Fermi energy [i.e., $S_{(1)} = 0$ for this linear combination], but there is another linear combination which still has single-particle scattering, translating into $\rho_{2k_F} \neq 0$ at the 2CK fixed point [95] (see Appendix F.3). It is interesting to note, however, that one may modify this model by removing one of the leads while maintaining the coupling symmetry between the remaining lead and the large dot (leading to the setup in Fig. 5.7b). Now there is only the $S_{(1)} = 0$ mode, which leads to $\rho_{2k_F} = 0$ at the 2CK fixed point. However,

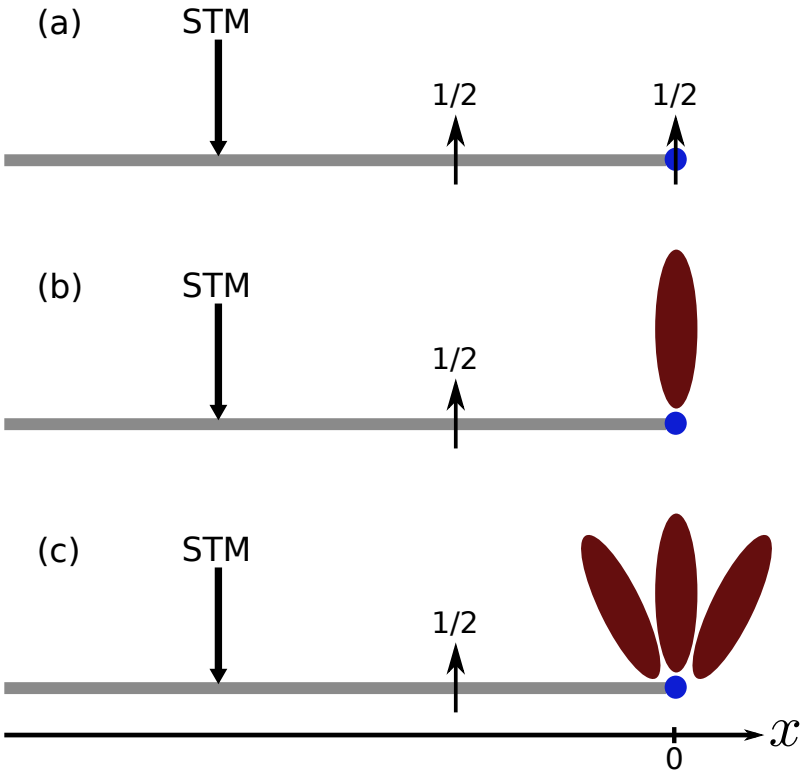

Figure 5.7: (a) The lead-dot model, with a small quantum dot forming a spin-$\frac{1}{2}$ "impurity" coupled to a lead of spin-$\frac{1}{2}$ conduction electrons. (b) The modified Oreg-Goldhaber-Gordon model [93], where now the small quantum dot is also coupled to a large quantum dot which acts as a reservoir of spin-$\frac{1}{2}$ electrons. This model is a modified version of the one confirmed experimentally to host the two-channel Kondo (2CK) effect [94]. (c) The generalised Oreg-Goldhaber-Gordon model, with a small dot and three large dots. In order for this model to host the four-channel Kondo (4CK) effect, the couplings to the large dots and the lead have to be symmetric. The figure is taken from Ref. [84].

as temperature is lowered, the power-law suppression is different: $\widetilde{\rho}_{2k_F}(x,0,T) \sim T^{1/2}$, as can be shown by adapting our considerations to this case (see Appendix F.3).

A system for which we do find the same power law (and $\mathrm{SU}(2)_4$ current algebra [86]) as for the topological Kondo effect is the 4CK model, corresponding to the generalised Oreg-Goldhaber-Gordon setup with three large dots [93, 96] (Fig. 5.7c). However, now the conduction electrons have $j = 1/2$, which results in $S_{(1)} = 1/\sqrt{3}$ and thus $\rho_{2k_F} \neq 0$ at the 4CK fixed point (see Appendix F.4).

5.4 Measuring $S_{(1)}$ in general situations

Generalising our considerations, it is also interesting to note that one may use ρ_{2k_F} at zero temperature and bias to measure $|S_{(1)}|$ in a range of Kondo and other quantum impurity systems, provided there is only one value of k_F to consider, as is the case for single-channel leads. (For N-channel leads, there will be N values of k_F because each channel has shifted energy spectrum due to the quantisation of transverse modes in the leads.) To this end, one takes the ratio between $\widetilde{\rho}_{2k_F} \propto 2|S_{(1)}|/v_F$ and the non-oscillating tDOS component $|\rho_{k=0}| = 2/v_F$. This is useful since the proportionality factor [originating from Eq. (5.1)] is the same in both cases and only depends on the density of states and physical characteristics of the STM tip [88, 97]. Therefore, $\widetilde{\rho}_{2k_F}/|\rho_{k=0}| = |S_{(1)}|$.

CHAPTER 6

CONCLUSIONS

This thesis discusses the influence of Majorana fermions on the scattering properties of metallic conduction electrons coupled to them in the context of the topological Kondo effect. Throughout this work, we have used the minimal setup of the topological Kondo model (TKM), which leads to the effective Kondo interaction between the spin-$\frac{1}{2}$ topological qubit generated by Majorana fermions and the effectively spin-1 conduction electrons. The effect of this Kondo coupling on the scattering properties of lead electrons is then studied using the oscillating component $\rho_{2k_F}(x)$ of the electron tunnelling density of states (tDOS), which can be measured in experiments using scanning tunnelling microscopy (STM).

Being governed by the finite-temperature retarded Green's function of lead electrons, the quantity ρ_{2k_F} can be calculated using perturbation theory in the Kondo coupling at energies much higher than the characteristic energy scale, the Kondo temperature T_K. We have performed the calculations up to third order using the method of perturbation expansion. At low energies, we have adapted results from conformal field theory calculations [61] to our model. We have discovered that the amplitude $\widetilde{\rho}_{2k_F}$ of the oscillating component of the tDOS displays a non-monotonic behaviour as a function of temperature. Starting from the exponential suppression at temperatures much larger than T_K, the behaviour of $\widetilde{\rho}_{2k_F}$ as the temperature is lowered strongly depends on the ratio of the position of the STM tip $|x|$ and the Kondo length $L_K = v_F/T_K$. When $|x| \gg L_K$, the

exponential suppression continues from high temperatures up to below the Kondo temperature before it crosses over to a power-law decay before the temperature reaches the topological Kondo fixed point. However, when $|x| \ll L_K$, there is an intermediate region in which the behaviour of $\widetilde{\rho}_{2k_F}$ is dominated by the Kondo logarithm. The existence or the suppression of this Kondo logarithmic peak therefore provides a way to estimate the extent of the Kondo screening cloud.

At energies much below the Kondo temperature, the $2k_F$-tDOS is described by a universal scaling function indicative of strong correlations. In this regime, non-Fermi liquid scattering occurs, which can be identified by the vanishing of single-particle scattering at topological Kondo fixed point that in turn manifests in the complete suppression of the $2k_F$-tDOS at zero temperature and bias. In this thesis, we have compared the low-energy behaviour of $\widetilde{\rho}_{2k_F}$ to three conventional Kondo systems: the conventional, single-channel, Kondo model which is represented by the lead-dot model, the modified Oreg-Goldhaber-Gordon 2CK model, and the generalised Oreg-Goldhaber-Gordon 4CK model. Although the TKM and all of these three systems share the same behaviour for $\widetilde{\rho}_{2k_F}$ at high energies, the first model has much different behaviour at low energies because it is governed by Fermi-liquid scattering. Like the topological Kondo model, the modified Oreg-Goldhaber-Gordon 2CK model also displays vanishing of single-particle scattering at zero temperature, although $\widetilde{\rho}_{2k_F}$ in this system decays according to a different power law. The situation is reversed for the last model; it decays according to the same power law but its $\widetilde{\rho}_{2k_F}$ is not completely suppressed at zero temperature and bias. Inspired by this comparison, in this thesis we also have provided a practical method to use $\widetilde{\rho}_{2k_F}$ to extract the information about the single-particle scattering matrix for more general quantum impurity systems.

There are several potential directions that need further investigation. Our current method cannot describe the behaviour of $\widetilde{\rho}_{2k_F}$ in the intermediate regime, when the energies are comparable to the Kondo temperature. As the exponential suppression may still dominate this regime when $|x| \gg L_K$, it is interesting to find out how $\widetilde{\rho}_{2k_F}$ evolves after

it displays the Kondo logarithm as the temperature is lowered and entering this regime when $|x| \ll L_K$. It is even more exciting to discover the behaviour when $|x| \sim L_K$. The numerical renormalisation group method is expected to be a suitable tool for this purpose. Also, since this thesis only focuses on the minimal setup of the TKM, working in a more general setup (e.g., with more leads, and/or including electron interactions in the leads) to discover how it affects the scattering properties of lead electrons is another open direction.

APPENDIX A

TUNNELLING SPECTROSCOPY

The purpose of this Appendix is to provide the derivation for the tunnelling density of states formula in Eq. (5.1). Here we will follow closely the derivation in Ref. [88]. Suppose an STM tip is located close to one of the metallic leads of the topological Kondo device (Fig. 5.1, inset), where a voltage bias V is applied between the lead and the tip. The electron wavefunctions from both of the lead and the tip may overlap with each other, such that electrons can now tunnel from the lead to the tip and vice versa [98, 99, 100]. The tunnelling Hamiltonian between the lead and the tip is given by

$$\hat{H}_{\text{tun}} = t_{\text{tun}} \hat{\psi}_1^\dagger(x) \hat{\psi}_T(y_0) + \text{h.c.}, \tag{A.1}$$

where $\hat{\psi}_1(x)$ is the annihilation operator for the electron at coordinate x of the lead under the STM, $\hat{\psi}_T(y_0)$ is the annihilation operator for the electron at a coordinate y_0 of the tip endpoint in a tip coordinate system, and t_{tun} is the tunnelling amplitude. Note that the electronic leads are single channel and effectively spinless, consistent with the effectively spinless nature of the nanowires for Majorana fermion realisations. We are also working with one species of tip electrons, e.g., as in spin-polarised STM [101, 99], hence it is also considered spinless. Since the tunnelling takes place between the tip end and the point in the lead that is closest to the tip [98, 99], x therefore is the position of the tip measured in the lead coordinate. The Hamiltonian above is regarded as a perturbation to the composite system of the topological Kondo device and the STM tip,

each in thermodynamic equilibrium, corresponding to $\hat{H}_{t_{\rm tun}=0} = \hat{H}_T + \hat{H}_{TK+\rm leads}$, where $\hat{H}_T$ is the Hamiltonian of the tip and $\hat{H}_{TK+\rm leads}$ is the Hamiltonian of the full topological Kondo system.

The particle current operator $\hat{\mathcal{I}}$ between the lead and the tip is $\hat{\mathcal{I}} = \dot{\hat{N}}_T$, where $\hat{N}_T$ is the tip electron number operator. Therefore, the electric current from the tip to the lead can be written as $I = e\langle\hat{\mathcal{I}}\rangle$, where $-e$ is the electron charge and $\langle\hat{\mathcal{I}}\rangle$ is the expectation value of $\hat{\mathcal{I}}$ with respect to the state that arises from the initial separate equilibrium states after turning on the tunnelling perturbation in the distant past.

For weak tunnelling, we can use the Kubo formula to calculate the quantity $\langle\hat{\mathcal{I}}\rangle$ [88],

$$\langle\hat{\mathcal{I}}\rangle(t) = \int_{-\infty}^{\infty} dt'\, C^R(t,t'), \tag{A.2}$$

$$C^R(t,t') = -i\theta(t-t')\left\langle\left[\hat{\mathcal{I}}(t), \hat{H}_{\rm tun}(t')\right]\right\rangle_0, \tag{A.3}$$

where the subscript 0 indicates that the expectation value is taken with respect to the eigenstates of $\hat{H}_{t_{\rm tun}=0}$. Given that the tunnelling was turned on in the distant past, we may set $t = 0$ without loss of generality. Since the number operator is given by $\hat{N}_T = \int dy\, \hat{\psi}_T^\dagger(y)\hat{\psi}_T(y)$, the particle current operator $\hat{\mathcal{I}} = \dot{\hat{N}}_T = i[\hat{H}_{\rm tun}, \hat{N}_T]$ takes the form

$$\hat{\mathcal{I}} = i\left[t_{\rm tun}\hat{\psi}_1^\dagger(x)\hat{\psi}_T(y_0) - t_{\rm tun}^*\hat{\psi}_T^\dagger(y_0)\hat{\psi}_1(x)\right]. \tag{A.4}$$

Using this result, we can show that $C^R(0,t')$ contains four terms. Two of these have the form $\left\langle\left[\hat{\psi}_1^\dagger(x)\hat{\psi}_T(y_0), \hat{\psi}_1^\dagger(x)\hat{\psi}_T(y_0)\right]\right\rangle_0$ and $\left\langle\left[\hat{\psi}_T^\dagger(y_0)\hat{\psi}_1(x), \hat{\psi}_T^\dagger(y_0)\hat{\psi}_1(x)\right]\right\rangle_0$. These two terms give vanishing contribution because they do not conserve the subsystem particle

numbers, while the unperturbed Hamiltonian does. Therefore, we obtain

$$\begin{aligned} C^R(0,t') &= \theta(-t')|t_{\rm tun}|^2\Big\{ \Big\langle \Big[\hat{\psi}_1^\dagger(x,0)\hat{\psi}_T(y_0,0), \hat{\psi}_T^\dagger(y_0,t')\hat{\psi}_1(x,t')\Big]\Big\rangle_0 \\ &\quad - \Big\langle \Big[\hat{\psi}_T^\dagger(y_0,0)\hat{\psi}_1(x,0), \hat{\psi}_1^\dagger(x,t')\hat{\psi}_T(y_0,t')\Big]\Big\rangle_0 \Big\} \\ &= \theta(-t')|t_{\rm tun}|^2\, 2{\rm Re}\Big\{ \Big\langle \hat{\psi}_1^\dagger(x,t')\hat{\psi}_T(y_0,t')\hat{\psi}_T^\dagger(y_0,0)\hat{\psi}_1(x,0)\Big\rangle_0 \\ &\quad - \Big\langle \hat{\psi}_T^\dagger(y_0,0)\hat{\psi}_1(x,0)\hat{\psi}_1^\dagger(x,t')\hat{\psi}_T(y_0,t')\Big\rangle_0 \Big\}. \end{aligned} \tag{A.5}$$

Since the expectation values above are taken with respect to the eigenstates of $\hat{H}_{t_{\rm tun}=0}$, we can factorise them into the topological Kondo and the tip parts,

$$\begin{aligned} C^R(0,t') &= \theta(-t')|t_{\rm tun}|^2\, 2{\rm Re}\Big\{ \Big\langle \hat{\psi}_1^\dagger(x,t')\hat{\psi}_1(x,0)\Big\rangle_0 \Big\langle \hat{\psi}_T(y_0,t')\hat{\psi}_T^\dagger(y_0,0)\Big\rangle_0 \\ &\quad - \Big\langle \hat{\psi}_1(x,0)\hat{\psi}_1^\dagger(x,t')\Big\rangle_0 \Big\langle \hat{\psi}_T^\dagger(y_0,0)\hat{\psi}_T(y_0,t')\Big\rangle_0 \Big\}. \end{aligned} \tag{A.6}$$

In our setup, a voltage bias is applied, so the operator $\hat{\psi}_1^\dagger(x,t')$ above has an additional time dependence $e^{i(-eV)t'}$. Extracting this factor explicitly from $\hat{\psi}_1^\dagger(x,t')$ and writing the correlation function $C^R(0,t')$ above in terms of the lesser and greater Green's functions defined respectively by [88]

$$G_{1,T}^<(x;t-t') = i\Big\langle \hat{\psi}_{1,T}^\dagger(x,t')\hat{\psi}_{1,T}(x,t)\Big\rangle_0, \tag{A.7}$$

$$G_{1,T}^>(x;t-t') = -i\Big\langle \hat{\psi}_{1,T}(x,t)\hat{\psi}_{1,T}^\dagger(x,t')\Big\rangle_0, \tag{A.8}$$

we obtain

$$C^R(0,t') = \theta(-t')|t_{\rm tun}|^2\, 2\,{\rm Re}\Big\{ G_1^<(x;-t')G_T^>(y_0;t') - G_1^>(x;-t')G_T^<(y_0;t')\Big\}e^{-ieVt'}, \tag{A.9}$$

After performing the Fourier transformations,

$$G^{\gtrless}_{1,T}(x;t) = \int_{-\infty}^{\infty} \frac{d\omega}{2\pi}\, G^{\gtrless}_{1,T}(x;\omega)e^{-i\omega t}, \tag{A.10}$$

the quantity $\langle\hat{\mathcal{I}}\rangle(0)$ takes the form

$$\langle\hat{\mathcal{I}}\rangle(0) = \int_{-\infty}^{\infty} \frac{d\omega}{2\pi}\, |t_{\rm tun}|^2 \Big\{ G^{<}_{1}(x;\omega)G^{>}_{T}(y_0;\omega - eV) - G^{>}_{1}(x;\omega)G^{<}_{T}(y_0;\omega - eV) \Big\}. \tag{A.11}$$

Now we would like to express the lesser and greater Green's functions above in terms of the spectral function $A_{1,T}(x;\omega) \equiv -2\,\mathrm{Im}[G^R_{1,T}(x;\omega)]$ using the Lehmann representation [88]. Starting from the definition of $G^{>}_1(x;t-t')$ in Eq. (A.8) and the definition of the expectation value in Eq. (5.4), we can write

$$G^{>}_{1}(x;t-t') = -\frac{i}{Z_1}\sum_{n_1}\langle n_1|e^{-\beta\hat{H}_{TK+\rm leads}}\hat{\psi}_1(x,t)\hat{\psi}^{\dagger}_1(x,t')|n_1\rangle, \tag{A.12}$$

where $|n_1\rangle$ is the eigenstate of $\hat{H}_{TK+\rm leads}$ and $Z_1 = \mathrm{Tr}[e^{-\beta\hat{H}_{TK+\rm leads}}]$. Inserting the identity $1 = \sum_{n_1'} |n_1'\rangle\langle n_1'|$, we get

$$G^{>}_{1}(x;t-t') = -\frac{i}{Z_1}\sum_{n_1,n_1'} e^{-\beta E_{n_1}}\langle n_1|\hat{\psi}_1(x)|n_1'\rangle\langle n_1'|\hat{\psi}^{\dagger}_1(x)|n_1\rangle e^{i(E_{n_1}-E_{n_1'})(t-t')}, \tag{A.13}$$

which, after Fourier transformation, leads to

$$G^{>}_{1}(x;\omega) = -\frac{2\pi i}{Z_1}\sum_{n_1,n_1'} e^{-\beta E_{n_1}}\langle n_1|\hat{\psi}_1(x)|n_1'\rangle\langle n_1'|\hat{\psi}^{\dagger}_1(x)|n_1\rangle\delta(\omega + E_{n_1} - E_{n_1'}). \tag{A.14}$$

Similar calculations for $G^{<}_1(x;\omega)$ give

$$G^{<}_{1}(x;\omega) = \frac{2\pi i}{Z_1}\sum_{n_1,n_1'} e^{-\beta E_{n_1}}\langle n_1|\hat{\psi}^{\dagger}_1(x)|n_1'\rangle\langle n_1'|\hat{\psi}_1(x)|n_1\rangle\delta(\omega - E_{n_1} + E_{n_1'}). \tag{A.15}$$

Swapping the indices $n_1 \longleftrightarrow n_1'$ and writing the resulting exponential as $e^{-\beta(E_{n_1}+\omega)}$, which

is guaranteed by the delta function, we arrive at

$$G_1^<(x;\omega) = -G_1^>(x;\omega)e^{-\beta\omega}. \tag{A.16}$$

The retarded Green's function $G_1^R(x;t-t')$ can be expressed in terms of the lesser and greater Green's functions as [88]

$$G_1^R(x;t-t') = \theta(t-t')\Big[G_1^>(x;t-t') - G_1^<(x;t-t')\Big]. \tag{A.17}$$

Using the previous results for $G_1^{\gtrless}(x;t-t')$ and performing the Fourier transformation $G_1^R(x;\omega) = \int_{-\infty}^{\infty} dt\, G_1^R(x;t)e^{i(\omega+i\eta)t}$, with $\eta \to 0^+$, we get

$$G_1^R(x;\omega) = \frac{1}{Z_1}\sum_{n_1,n_1'} e^{-\beta E_{n_1}}\left[\frac{\langle n_1|\hat{\psi}_1(x)|n_1'\rangle\langle n_1'|\hat{\psi}_1^\dagger(x)|n_1\rangle}{\omega + E_{n_1} - E_{n_1'} + i\eta} + \frac{\langle n_1|\hat{\psi}_1^\dagger(x)|n_1'\rangle\langle n_1'|\hat{\psi}_1(x)|n_1\rangle}{\omega - E_{n_1} + E_{n_1'} + i\eta}\right], \tag{A.18}$$

which, upon swapping again the indices $n_1 \longleftrightarrow n_1'$ on the second term in the square bracket above and taking the imaginary component of $G_1^R(x;\omega)$ by using the relation $(\omega + i\eta)^{-1} = \mathcal{P}\frac{1}{\omega} - i\pi\delta(\omega)$, yields

$$2\,\mathrm{Im}[G_1^R(x;\omega)] = -iG_1^>(x;\omega)(1 + e^{-\beta\omega}). \tag{A.19}$$

From Eqs. (A.16) and (A.19), and using $A_1(x;\omega) = 2\,\mathrm{Im}[G_1^R(x;\omega)]$ and $n_F(\omega) = (1 + e^{\beta\omega})^{-1}$, we obtain

$$iG_1^>(x;\omega) = A_1(x;\omega)[1 - n_F(\omega)], \tag{A.20}$$

$$-iG_1^<(x;\omega) = A_1(x;\omega)n_F(\omega). \tag{A.21}$$

Similar expressions for $G_T^{\gtrless}(y_0;\omega)$ are straightforward.

Using these results, the electric current $I = e\langle\hat{\mathcal{I}}\rangle$ can be calculated from Eq. (A.11) to

obtain

$$I = e \int_{-\infty}^{\infty} \frac{d\omega}{2\pi} \, |t_{\rm tun}|^2 A_T(y_0; \omega - eV) A_1(x; \omega) \left[n_F(\omega) - n_F(\omega - eV) \right]. \tag{A.22}$$

We will assume that the tip is made of material with nearly constant density of states, $A_T(y_0; \omega - eV) \approx$ constant, in which case the differential conductance dI/dV can be expressed as

$$\frac{dI}{dV} \propto \int_{-\infty}^{\infty} d\omega \, \frac{\partial n_F(\omega - eV)}{\partial \omega} A_1(x; \omega). \tag{A.23}$$

Our tDOS in Eq. (5.1), in which the temperature dependence has been made explicit in its notation, is proportional to this differential conductance.

APPENDIX B

THE MATSUBARA GREEN'S FUNCTION

The Matsubara Green's function is defined as the Green's function with imaginary time argument [88],

$$G(\tau - \tau') \equiv - \left\langle \mathcal{T}_\tau \left[\hat{c}(\tau) \hat{c}^\dagger(\tau') \right] \right\rangle . \tag{B.1}$$

Let us now introduce two Matsubara Green's functions: the one in position space,

$$G_{ij}(x, y; \tau) = - \left\langle \mathcal{T}_\tau \left[\hat{\psi}_i(x, \tau) \hat{\psi}_j^\dagger(y, 0) \right] \right\rangle , \tag{B.2}$$

and the one in momentum space,

$$G_{ij}(k, k'; \tau) = - \left\langle \mathcal{T}_\tau \left[\hat{a}_{k,i}(\tau) \hat{a}_{k',j}^\dagger(0) \right] \right\rangle . \tag{B.3}$$

Note that the relation between the operators $\hat{\psi}_i(x, \tau)$ and $\hat{a}_{k,i}(\tau)$ is given in Eq. (4.3). Therefore, the relation between $G_{ij}(x, y; \tau)$ and $G_{ij}(k, k'; \tau)$ is given by

$$G_{ij}(x, y; \tau) = \int \int dk dk' \, G_{ij}(k, k'; \tau) \varphi_{k,i}(x) \varphi_{k',j}^*(y), \tag{B.4}$$

$$G_{ij}(k, k'; \tau) = \int \int dx dy \, G_{ij}(x, y; \tau) \varphi_{k,i}^*(x) \varphi_{k',j}(y). \tag{B.5}$$

We can also Fourier transform the Matsubara Green's function (B.2) from time domain

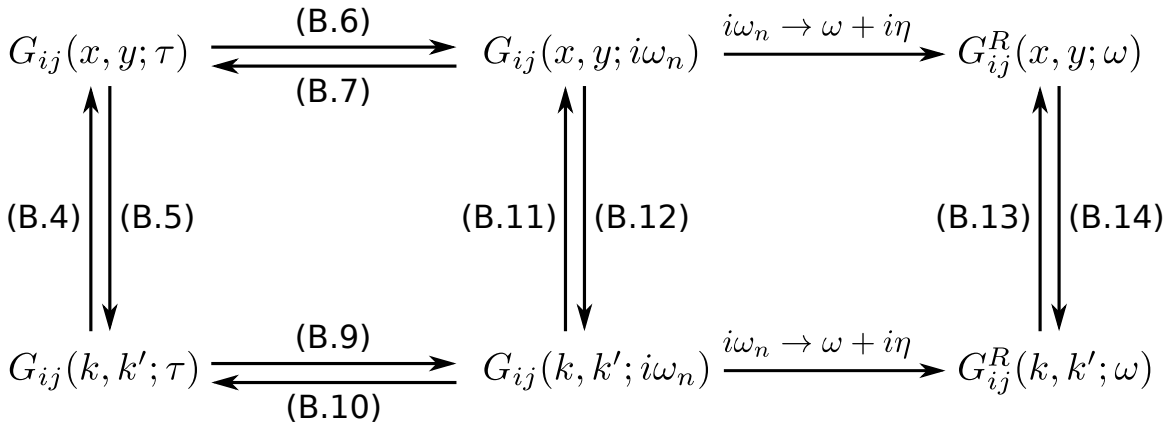

Figure B.1: Fourier transformations of Matsubara and retarded Green's functions between position and momentum spaces and between time and frequency domains.

to frequency domain [88],

$$G_{ij}(x,y;i\omega_n) = \int_0^\beta d\tau\, e^{i\omega_n\tau} G_{ij}(x,y;\tau), \tag{B.6}$$

$$G_{ij}(x,y;\tau) = \frac{1}{\beta}\sum_{n=-\infty}^{\infty} e^{-i\omega_n\tau} G_{ij}(x,y;i\omega_n), \tag{B.7}$$

where ω_n is the Matsubara frequency. For fermions, it has the form

$$\omega_n = \frac{(2n+1)\pi}{\beta}, \qquad n = 0, \pm 1, \pm 2, \ldots. \tag{B.8}$$

Similarly, the Matsubara Green's function (B.3) can also be transformed to the frequency domain,

$$G_{ij}(k,k';i\omega_n) = \int_0^\beta d\tau\, e^{i\omega_n\tau} G_{ij}(k,k';\tau), \tag{B.9}$$

$$G_{ij}(k,k';\tau) = \frac{1}{\beta}\sum_{n=-\infty}^{\infty} e^{-i\omega_n\tau} G_{ij}(k,k';i\omega_n). \tag{B.10}$$

Now, in frequency domain, the relations between $G_{ij}(x,y;i\omega_n)$ and $G_{ij}(k,k';i\omega_n)$ are given

by

$$G_{ij}(x,y;i\omega_n) = \int\int dkdk'\, G_{ij}(k,k';i\omega_n)\varphi_{k,i}(x)\varphi^*_{k',j}(y), \tag{B.11}$$

$$G_{ij}(k,k';i\omega_n) = \int\int dxdy\, G_{ij}(x,y;i\omega_n)\varphi^*_{k,i}(x)\varphi_{k',j}(y). \tag{B.12}$$

Finally, the Matsubara Green's functions $G_{ij}(x,y;i\omega_n)$ and $G_{ij}(k,k';i\omega_n)$ can be transformed into the retarded Green's functions $G^R_{ij}(x,y;\omega)$ and $G^R_{ij}(k,k';\omega)$ using analytic continuation $i\omega_n \to \omega + i\eta$ [88]. The last two objects then can be transformed into each other in a way similar to Eqs. (B.4) and (B.5),

$$G^R_{ij}(x,y;\omega) = \int\int dkdk'\, G^R_{ij}(k,k';\omega)\varphi_{k,i}(x)\varphi^*_{k',j}(y), \tag{B.13}$$

$$G^R_{ij}(k,k';\omega) = \int\int dxdy\, G^R_{ij}(x,y;\omega)\varphi^*_{k,i}(x)\varphi_{k',j}(y). \tag{B.14}$$

All of these transformations are summarised in Fig. B.1.

APPENDIX C

THE NON-INTERACTING RETARDED GREEN'S FUNCTION

The non-interacting Matsubara Green's function can be calculated from [88]

$$G_{0,ij}(k,k';\tau) = -\left\langle \mathcal{T}_\tau \left[\hat{a}_{k,i}(\tau)\hat{a}^\dagger_{k',j}(0)\right]\right\rangle_0 . \tag{C.1}$$

Since $\mathcal{T}_\tau$ is a time ordering operator, one can write

$$G_{0,ij}(k,k';\tau) = -\theta(\tau)\left\langle \hat{a}_{k,i}(\tau)\hat{a}^\dagger_{k',j}(0)\right\rangle_0 + \theta(-\tau)\left\langle \hat{a}^\dagger_{k',j}(0)\hat{a}_{k,i}(\tau)\right\rangle_0 , \tag{C.2}$$

where the sign of the second term is flipped due to the interchange of the operators. Since $\hat{a}_{k,i}(\tau)$ is a Heisenberg operator which evolves according to $\hat{a}_{k,i}(\tau) = e^{\hat{H}_0\tau}\hat{a}_{k,i}(0)e^{-\hat{H}_0\tau}$, one gets

$$G_{0,ij}(k,k';\tau) = -\left[\theta(\tau)\left(1-n_F(\varepsilon_k)\right) - \theta(-\tau)n_F(\varepsilon_k)\right]\delta_{ij}\delta(k-k')e^{-\varepsilon_k\tau}, \tag{C.3}$$

where ε_k is the kinetic energy of non-interacting lead electrons. Here we also have used the relation

$$\left\langle \hat{a}^\dagger_{k',j}\hat{a}_{k,i}\right\rangle_0 = n_F(\varepsilon_k)\delta_{ij}\delta(k-k'), \tag{C.4}$$

where $n_F(\varepsilon_k) = (1+e^{\beta\varepsilon_k})^{-1}$ is the Fermi function. We can transform the Matsubara Green's function above into the frequency domain by using Eq. (B.9). Using the fact that

$e^{i\omega_n\beta} = -1$ for all values of n, we arrive at

$$G_{0,ij}(k,k';i\omega_n) = \frac{1}{i\omega_n - \varepsilon_k}\delta_{ij}\delta(k-k'). \tag{C.5}$$

We then can perform analytic continuation $i\omega_n \to \omega + i\eta$ such that we get

$$G^R_{0,ij}(k,k';\omega) = \frac{1}{\omega - \varepsilon_k + i\eta}\delta_{ij}\delta(k-k'). \tag{C.6}$$

Since our aim in the main text is to obtain the expression for the non-interacting tDOS or the free cloud, we now have to calculate $G^R_{0,ij}(x,y;\omega)$ from $G^R_{0,ij}(k,k';\omega)$ using Eq. (B.13). Assuming the linearised dispersion relation $\varepsilon_k = v_F k$ and remembering that the eigenfunction $\varphi_{k,i}(x)$ has right and left movers,

$$\varphi_{k,i}(x) = \frac{1}{\sqrt{2\pi}}\left[e^{ik_F x}\varphi^R_{k,i}(x) + e^{-ik_F x}\varphi^L_{k,i}(x)\right], \tag{C.7}$$

one can calculate the Green's function for each combination of these two movers. We then obtain

$$\begin{aligned}
G^R_{0,ij,RR}(x,y;\omega) &= -\frac{i}{v_F}\delta_{ij}e^{-ik_F(|x|-|y|)}e^{-i\frac{\omega}{v_F}(|x|-|y|)}\theta(|y|-|x|), && \text{(C.8)}\\
G^R_{0,ij,LL}(x,y;\omega) &= -\frac{i}{v_F}\delta_{ij}e^{ik_F(|x|-|y|)}e^{i\frac{\omega}{v_F}(|x|-|y|)}\theta(|x|-|y|), && \text{(C.9)}\\
G^R_{0,ij,RL}(x,y;\omega) &= 0, && \text{(C.10)}\\
G^R_{0,ij,LR}(x,y;\omega) &= -\frac{i}{v_F}r_i\delta_{ij}e^{ik_F(|x|+|y|)}e^{i\frac{\omega}{v_F}(|x|+|y|)}. && \text{(C.11)}
\end{aligned}$$

If we define

$$g_{ij}(x;\omega) \equiv -\frac{i}{v_F}\delta_{ij}e^{ik_F x}e^{i\frac{\omega}{v_F}x}\theta(x), \tag{C.12}$$

then we can write

$$G^R_{0,ij,RR}(x,y;\omega) = g_{ij}(|y|-|x|;\omega), \tag{C.13}$$

$$G^R_{0,ij,LL}(x,y;\omega) = g_{ij}(|x|-|y|;\omega), \tag{C.14}$$

$$G^R_{0,ij,RL}(x,y;\omega) = r^*_i g_{ij}(-|x|-|y|;\omega), \tag{C.15}$$

$$G^R_{0,ij,LR}(x,y;\omega) = r_i g_{ij}(|x|+|y|;\omega). \tag{C.16}$$

Since the coordinates x and y are always non-positive, one gets $G^R_{0,ij,RL}(x,y;\omega) = 0$ as before.

In the main text we will need the non-interacting retarded Green's functions $G^R_{0,ij}(x,x;\omega)$, $G^R_{0,ij}(x,0;\omega)$, and $G^R_{0,ij}(0,x;\omega)$. Therefore, we can write

$$G^R_{0,ij}(x,x;\omega) = -\frac{i}{v_F}\delta_{ij} - \frac{i}{v_F}\delta_{ij}e^{i2K_i(\omega,x)}, \tag{C.17}$$

$$G^R_{0,ij}(x,0;\omega) = -\frac{2i}{v_F}\cos\left(\frac{\theta_i}{2}\right)\delta_{ij}e^{iK_i(\omega,x)}, \tag{C.18}$$

where we have defined

$$2K_i(\omega,x) \equiv 2k_F|x| + 2\frac{\omega}{v_F}|x| + \theta_i. \tag{C.19}$$

Note that by using Eqs. (C.13)-(C.16) above, we have

$$G^R_{0,ij}(0,x;\omega) = G^R_{0,ij}(x,0;\omega). \tag{C.20}$$

This is due to the relation satisfied by the left and right movers, $\varphi^R_{k,i}(x) = r^*_i\varphi^L_{k,i}(-x)$.

APPENDIX D

SOME USEFUL INTEGRALS

Let us define $\eta_{ab} \equiv 1 - \delta_{ab}$, where δ_{ab} is the Kronecker delta and the indices a and b are integers between $-\infty$ to ∞. We also define

$$f(\omega_a - \omega_b; \tau)\eta_{ab} \equiv \frac{1}{i(\omega_a - \omega_b)} \left[e^{i(\omega_a - \omega_b)\tau} - 1\right] \eta_{ab}, \tag{D.1}$$

so that $f(\omega_a - \omega_b; \beta)\eta_{ab} = 0$. Here is a list of integrals that are useful to calculate the third order retarded Green's function.

$$\int_0^{\tau'} d\tau \left[\delta_{ab} + e^{i(\omega_a - \omega_b)\tau}\eta_{ab}\right] = \tau'\delta_{ab} + f(\omega_a - \omega_b; \tau')\eta_{ab}, \tag{D.2}$$

$$\int_0^{\beta} d\tau \left[\delta_{ab} + e^{i(\omega_a - \omega_b)\tau}\eta_{ab}\right] = \beta\delta_{ab}, \tag{D.3}$$

$$\begin{aligned}\int_0^{\tau'} d\tau \left[\delta_{ab} + e^{i(\omega_a - \omega_b)\tau}\eta_{ab}\right]\tau &= \frac{\tau'^2}{2}\delta_{ab} \\ &+ \frac{1}{i(\omega_a - \omega_b)} \left[\tau' e^{i(\omega_a - \omega_b)\tau'} - f(\omega_a - \omega_b; \tau')\right] \eta_{ab}\end{aligned} \tag{D.4}$$

$$\int_0^{\beta} d\tau \left[\delta_{ab} + e^{i(\omega_a - \omega_b)\tau}\eta_{ab}\right]\tau = \frac{\beta^2}{2}\delta_{ab} + \frac{1}{i(\omega_a - \omega_b)}\beta\eta_{ab}, \tag{D.5}$$

$$\int_0^{\tau'} d\tau \left[\delta_{ab} + e^{i(\omega_a-\omega_b)\tau}\eta_{ab}\right] \tau e^{i(\omega_c-\omega_d)\tau}\eta_{cd} = \frac{1}{i(\omega_c-\omega_d)}\left[\tau' e^{i(\omega_c-\omega_d)\tau'} - f(\omega_c-\omega_d;\tau')\right]\delta_{ab}\eta_{cd} + \frac{\tau'^2}{2}\delta_{0,(a-b+c-d)}\eta_{ab}\eta_{cd} + \frac{1}{i(\omega_a-\omega_b+\omega_c-\omega_d)}\Big[\tau' e^{i(\omega_a-\omega_b+\omega_c-\omega_d)\tau'} - f(\omega_a-\omega_b+\omega_c-\omega_d;\tau')\Big]\eta_{0,(a-b+c-d)}\eta_{ab}\eta_{cd}, \tag{D.6}$$

$$\int_0^{\beta} d\tau \left[\delta_{ab} + e^{i(\omega_a-\omega_b)\tau}\eta_{ab}\right] \tau e^{i(\omega_c-\omega_d)\tau}\eta_{cd} = \frac{1}{i(\omega_c-\omega_d)}\beta\delta_{ab}\eta_{cd} + \frac{\beta^2}{2}\delta_{0,(a-b+c-d)}\eta_{ab}\eta_{cd} + \frac{1}{i(\omega_a-\omega_b+\omega_c-\omega_d)}\beta\eta_{0,(a-b+c-d)}\eta_{ab}\eta_{cd}, \tag{D.7}$$

$$\int_0^{\tau'} d\tau \left[\delta_{ab} + e^{i(\omega_a-\omega_b)\tau}\eta_{ab}\right] \frac{\tau^2}{2} = \frac{\tau'^3}{6}\delta_{ab} + \frac{1}{i(\omega_a-\omega_b)}\left\{\frac{\tau'^2}{2}e^{i(\omega_a-\omega_b)\tau'} - \frac{1}{i(\omega_a-\omega_b)}\left[\tau' e^{i(\omega_a-\omega_b)\tau'} - f(\omega_a-\omega_b;\tau')\right]\right\}\eta_{ab}, \tag{D.8}$$

$$\int_0^{\beta} d\tau \left[\delta_{ab} + e^{i(\omega_a-\omega_b)\tau}\eta_{ab}\right] \frac{\tau^2}{2} = \frac{\beta^3}{6}\delta_{ab} + \frac{1}{i(\omega_a-\omega_b)}\left[\frac{\beta^2}{2} - \frac{1}{i(\omega_a-\omega_b)}\beta\right]\eta_{ab}, \tag{D.9}$$

$$\int_0^{\tau'} d\tau \left[\delta_{ab} + e^{i(\omega_a-\omega_b)\tau}\eta_{ab}\right] f(\omega_c-\omega_d;\tau)\eta_{cd} = \frac{1}{i(\omega_c-\omega_d)}\left[f(\omega_c-\omega_d;\tau') - \tau'\right]\delta_{ab}\eta_{cd} + \frac{1}{i(\omega_c-\omega_d)}\Bigg[\tau'\delta_{0,(a-b+c-d)} + f(\omega_a-\omega_b+\omega_c-\omega_d;\tau')\eta_{0,(a-b+c-d)} - f(\omega_a-\omega_b;\tau')\Bigg]\eta_{ab}\eta_{cd}, \tag{D.10}$$

$$\int_0^{\beta} d\tau \left[\delta_{ab} + e^{i(\omega_a-\omega_b)\tau}\eta_{ab}\right] f(\omega_c-\omega_d;\tau)\eta_{cd} = \frac{1}{i(\omega_c-\omega_d)}\beta\left[-\delta_{ab} + \delta_{0,(a-b+c-d)}\eta_{ab}\right]\eta_{cd}. \tag{D.11}$$

APPENDIX E

THE SCALING FORM OF THE AMPLITUDE OF THE OSCILLATING PART OF THE TDOS AT LOW ENERGIES

Following closely the Appendix of our preprint [84], here we will demonstrate the scaling form of the amplitude $\widetilde{\rho}_{2k_F}$ of the oscillating component of the tDOS at low energies in the zero bias regime. If we define $y \equiv \omega/T$, the envelope of the oscillating part of the spectral function is given by

$$\widetilde{A}_{2k_F}\left(\frac{|x|}{L_T}, y, T\right) = \frac{2}{v_F} N\delta\lambda\sqrt{3}\left(2\pi\frac{T}{T_K}\right)^{1/3} \mathrm{Re}\left[I(y)e^{\left(i2y\frac{|x|}{L_T}\right)}\right]. \tag{E.1}$$

Therefore, the amplitude of the $2k_F$-tDOS is

$$\widetilde{\rho}_{2k_F}\left(\frac{|x|}{L_T}, 0, T\right) = -\frac{2}{v_F} N\delta\lambda\sqrt{3}\left(2\pi\frac{T}{T_K}\right)^{1/3} h\left(\frac{|x|}{L_T}\right), \tag{E.2}$$

for some scaling function h. To extract the $T \to 0$ asymptotic power law, we may take $L_T \gg |x|$, and thus substitute $h(|x|/L_T) \sim h(0)$. This gives the $T^{1/3}$ decay.

APPENDIX F

DISCUSSIONS ON SEVERAL CONVENTIONAL KONDO MODELS

F.1 The lead-dot model

In this section we aim to discuss the conventional, single-channel, Kondo model exemplified by the lead-dot model (Fig. 5.7a). It consists of a spin-$\frac{1}{2}$ quantum dot that is coupled with 1D lead of spin-$\frac{1}{2}$ electrons. This model is described by the Hamiltonian

$$\hat{H} = \sum_{i=1}^{2} \int dk\, v_F k\, \hat{a}^{\dagger}_{k,i} \hat{a}_{k,i} + \sum_{\alpha=1}^{3} g_\alpha \hat{I}_\alpha \hat{S}_\alpha, \tag{F.1}$$

where the first term is the kinetic energy for the conduction electrons and the second term is the Kondo interaction between the spin of the quantum dot $\hat{\boldsymbol{S}}$ and the spin of the conduction electrons $\hat{\boldsymbol{I}}$.

It is important to note that the conduction electrons in the lead are now spinful, unlike our discussions in Chapter 4 and 5 where the lead electrons are spinless. Therefore, here the index i in the electron operator $\hat{a}_{k,i}$ denotes the spin of the conduction electrons. The operator $\hat{I}_\alpha$ is given by

$$\hat{I}_\alpha = \sum_{i,j}^{2} \hat{\psi}^{\dagger}_i \frac{\sigma^{\alpha}_{ij}}{2} \hat{\psi}_j, \tag{F.2}$$

where the operator $\hat{\psi}_i$ is the annihilation operator of the electron with spin component

$i = 1, 2$ in the position space and $\{\sigma^\alpha\}$ are the Pauli matrices. $\hat{\psi}_i$ has the same form as Eq. (4.3), but $r_i = e^{i\theta_i}$ is now the reflection amplitude for the electron with spin i.

Since our aim is to study the tDOS of the lead electrons in this system, we will perform similar calculations to those for the topological Kondo model. Our aim is to find the retarded Green's function (5.5) for our model, which in turn is described by the function $\xi(\omega, T)$ in Eq. (5.9). We also note that the non-interacting retarded Green's function $G^{(}_{ij}x, y; \omega)$ has the same expression as the one for the topological Kondo model (Appendix C), but again the index i and j now refer to the spin of the lead electrons.

For simplicity, we will consider the isotropic case where $g_\alpha \equiv g$. The function $\xi(\omega, T)$ for the lead-dot model at high energies is given by

$$\xi(\omega, T) = \frac{3\pi^2}{16}\left[\lambda_0^2 + 2\lambda_0^3 \log\left(\frac{v_F\Lambda}{\sqrt{\omega^2 + 4T^2}}\right)\right], \tag{F.3}$$

where we have defined

$$\lambda_0 \equiv \frac{4}{\pi v_F} g \cos^2\left(\frac{\theta}{2}\right). \tag{F.4}$$

Up to an overall constant, this result is the same as for the topological Kondo model, Eq. (5.58).

For the lead-dot model, we have $s = 1/2$, $j = 1/2$, and $k = 1$, such that $S_{(1)} = -1$. Therefore, $\widetilde{\rho}_{2k_F}$ does not vanish at $T = 0$.

F.2 The original Oreg-Goldhaber-Gordon 2CK model

Before we discuss the modified Oreg-Goldhaber-Gordon (Fig. 5.7b), let us first discuss the original Oreg-Goldhaber-Gordon model [93].

This system consists of a small quantum dot that is connected to two leads of conduction electrons and a large quantum dot (Fig. F.1). The system is described by the

Hamiltonian

$$\begin{aligned}\hat{H} &= \sum_{s=1}^{2}\sum_{k}\varepsilon_{m,k,s}\hat{m}^{\dagger}_{k,s}\hat{m}_{k,s}+\sum_{s=1}^{2}\varepsilon_{d,s}\hat{d}^{\dagger}_{s}\hat{d}_{s}+E^{n_m}_{n_d} \\ &+\sum_{s=1}^{2}\int_{0}^{\infty}dk\,\varepsilon_{L,k,s}\hat{L}^{\dagger}_{k,s}\hat{L}_{k,s}+\sum_{s=1}^{2}\int_{0}^{\infty}dk\,\varepsilon_{R,k,s}\hat{R}^{\dagger}_{k,s}\hat{R}_{k,s} \\ &+\left(V_m\sum_{s=1}^{2}\sum_{k}\hat{m}^{\dagger}_{k,s}\hat{d}_{s}+V_L\sum_{s=1}^{2}\xi^{\dagger}_{L,s}(0)\hat{d}_{s}+V_R\sum_{s=1}^{2}\xi^{\dagger}_{R,s}(0)\hat{d}_{s}+\text{h.c.}\right), \quad \text{(F.5)}\end{aligned}$$

where $\hat{d}_s$ ($\hat{m}_{k,s}$) is the electron operator in the small (large) dot, $\hat{L}_{k,s}$ ($\hat{R}_{k,s}$) is the electron operator in the left (right) lead in the momentum space, and $\hat{\xi}_{L,s}$ ($\hat{\xi}_{R,s}$) is the electron operator in the left (right) lead in the position space. $E^{n_m}_{n_d}$ denotes the charging energy when the small dot has n_d electrons and the large dot has n_m electrons. Note that we have

$$\hat{\xi}_{L,i}(x) \equiv \int_{0}^{\infty}dk\,\hat{L}_{k,i}\varphi_{L,k}(x), \quad \text{(F.6)}$$

$$\hat{\xi}_{R,i}(x) \equiv \int_{0}^{\infty}dk\,\hat{R}_{k,i}\varphi_{R,k}(x), \quad \text{(F.7)}$$

where $\varphi_{L,k}(x)$ and $\varphi_{R,k}(x)$ are eigenfunctions of the conduction electrons in the left and right leads, respectively,

$$\varphi_{L,k}(x) \equiv \frac{1}{\sqrt{2\pi}}\left(e^{ikx}+r_L e^{-ikx}\right), \quad \text{(F.8)}$$

$$\varphi_{R,k}(x) \equiv \frac{1}{\sqrt{2\pi}}\left(e^{ikx}+r_R e^{-ikx}\right), \quad \text{(F.9)}$$

and $r_{L,R} \equiv e^{i\theta_{L,R}}$ are the reflection amplitudes.

Let us rotate the electron operators in the left and right leads as the following,

$$\begin{pmatrix}\hat{\psi}_{k,s}\\ \hat{\phi}_{k,s}\end{pmatrix} = \begin{pmatrix}\cos\alpha & \sin\alpha\\ -\sin\alpha & \cos\alpha\end{pmatrix}\begin{pmatrix}e^{i\theta_L/2}\hat{L}_{k,s}\\ e^{i\theta_R/2}\hat{R}_{k,s}\end{pmatrix}, \quad \text{(F.10)}$$

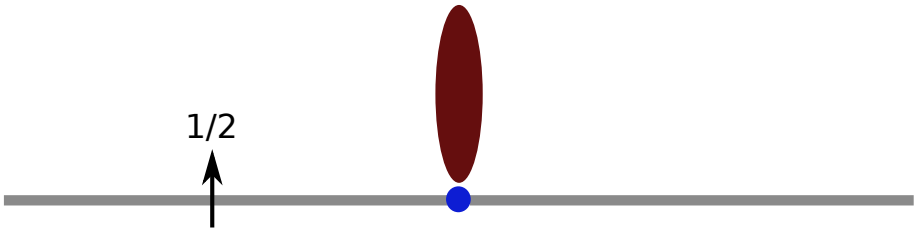

Figure F.1: The small quantum dot d is connected through tunnelling to the large quantum dot m and two metallic leads called the left and right leads. Different from the setup of topological Kondo model discussed in the main text, here the conduction electrons are spinful. This system displays 2CK effect if the couplings between the small dot and the leads are symmetric [93].

where the rotation angle α is given by

$$\tan\alpha \equiv \frac{\cos\left(\theta_R/2\right)}{\cos\left(\theta_L/2\right)}\frac{V_R}{V_L}, \qquad V_\psi \equiv \sqrt{\frac{2}{\pi}\cos^2\left(\frac{\theta_L}{2}\right)V_L^2 + \frac{2}{\pi}\cos^2\left(\frac{\theta_R}{2}\right)V_R^2}. \tag{F.11}$$

Using this rotation, we can rewrite the Hamiltonian above as

$$\begin{aligned}\hat{H} \;=\; & \sum_{s=1}^{2}\sum_{k}\varepsilon_{m,k,s}\hat{m}^\dagger_{k,s}\hat{m}_{k,s} + \sum_{s=1}^{2}\varepsilon_{d,s}\hat{d}^\dagger_s\hat{d}_s + E^{n_m}_{n_d} \\ & + \sum_{s=1}^{2}\int_0^\infty dk\,\varepsilon_{\psi,k,s}\hat{\psi}^\dagger_{k,s}\hat{\psi}_{k,s} + \sum_{s=1}^{2}\int_0^\infty dk\,\varepsilon_{\phi,k,s}\hat{\phi}^\dagger_{k,s}\hat{\phi}_{k,s} \\ & + \left(V_m\sum_{s=1}^{2}\sum_{k}\hat{m}^\dagger_{k,s}\hat{d}_s + V_\psi\sum_{s=1}^{2}\int_0^\infty dk\,\hat{\psi}^\dagger_{k,s}\hat{d}_s + \text{h.c.}\right).\end{aligned} \tag{F.12}$$

Now the left- and right-lead electron operators are effectively replaced by $\hat{\psi}_{k,s}$ and $\hat{\phi}_{k,s}$. However, the only tunnelling term that survives the rotation is $\hat{\psi}^\dagger_{k,s}\hat{d}_s$, so there is no tunnelling between the small dot and the effective lead ϕ.

Since we are working at energies much smaller than the charging energy of the large dot m, we will perform the Schrieffer-Wolff transformation to obtain the effective low-energy Hamiltonian. Note that due to the Coulomb blockade, the charge fluctuation in the large dot m is suppressed. Therefore, we focus only on the following virtual second-order tunnelling processes,

1. An electron hops off the small dot d onto the large dot m, then an electron hops off the large dot m onto the small dot d.

2. An electron hops off the small dot d onto the effective lead ψ, then an electron hops off the effective lead ψ onto the small dot d.

The resulting low-energy Hamiltonian takes the form

$$\begin{aligned}\hat{H} &= \sum_{s=1}^{2}\sum_{k}\varepsilon_{m,k,s}\hat{m}^{\dagger}_{k,s}\hat{m}_{k,s}+\sum_{s=1}^{2}\varepsilon_{d,s}\hat{d}^{\dagger}_{s}\hat{d}_{s} \\ &\quad+\sum_{s=1}^{2}\int_{0}^{\infty}dk\,\varepsilon_{\psi,k,s}\hat{\psi}^{\dagger}_{k,s}\hat{\psi}_{k,s}+\sum_{s=1}^{2}\int_{0}^{\infty}dk\,\varepsilon_{\phi,k,s}\hat{\phi}^{\dagger}_{k,s}\hat{\phi}_{k,s} \\ &\quad+2J_{m}\hat{\boldsymbol{S}}_{d}\cdot\hat{\boldsymbol{S}}_{m}+2J_{\psi}\hat{\boldsymbol{S}}_{d}\cdot\hat{\boldsymbol{S}}_{\psi}, \end{aligned} \tag{F.13}$$

where the first two lines are the kinetic energies of electrons in the large dot m, small dot d, and effective leads ψ and ϕ. The last line contains Kondo interaction between small dot d and large dot m with coupling J_m and between small dot d and effective lead ψ with coupling J_ψ. The spin operators are defined as

$$\hat{\boldsymbol{S}}_{d} \equiv \sum_{s,s'}\hat{d}^{\dagger}_{s}\frac{1}{2}\boldsymbol{\sigma}_{ss'}\hat{d}_{s'}, \tag{F.14}$$

$$\hat{\boldsymbol{S}}_{m} \equiv \sum_{s,s'=1}^{2}\hat{\xi}^{\dagger}_{m,s}(0)\frac{1}{2}\boldsymbol{\sigma}_{ss'}\hat{\xi}_{m,s'}(0), \tag{F.15}$$

$$\hat{\boldsymbol{S}}_{\psi} \equiv \sum_{s,s'=1}^{2}\hat{\xi}^{\dagger}_{\psi,s}(0)\frac{1}{2}\boldsymbol{\sigma}_{ss'}\hat{\xi}_{\psi,s'}(0), \tag{F.16}$$

while the Kondo couplings are defined as

$$J_{m} \equiv \left[\frac{1}{E^{1}_{0}-E^{0}_{1}}+\frac{1}{E^{-1}_{2}-E^{0}_{1}}\right]V^{2}_{m}, \tag{F.17}$$

$$J_{\psi} \equiv \left[\frac{1}{E^{0}_{0}-E^{0}_{1}}+\frac{1}{E^{0}_{2}-E^{0}_{1}}\right]V^{2}_{\psi}. \tag{F.18}$$

For the 2CK effect to occur, we need to set $J_m = J_\psi \equiv J$.

Using the lead rotation (F.10), the Matsubara Green's function for the conduction

electrons in the left lead is a linear combination of the ones for the effective leads ψ and ϕ,

$$G_{ij}^{(L)}(k,k';\tau,T) = \cos^2(\alpha) G_{ij^{(\psi)}}(k,k';\tau,T) + \sin^2(\alpha) G_{ij^{(\phi)}}(k,k';\tau,T). \tag{F.19}$$

This then immediately translates to

$$G_{ij}^{R,(L)}(x,y;\omega,T) = \cos^2(\alpha) G_{ij^{R,(\psi)}}(x,y;\omega,T) + \sin^2(\alpha) G_{ij^{R,(\phi)}}(x,y;\omega,T). \tag{F.20}$$

The retarded Green's function for the effective lead ϕ, $G_{ij^{(\phi)}}(x,y;\omega,T)$, is simply the non-interacting one,

$$G_{ij^{(\phi)}}(x,y;\omega,T) = G_{0,ij}(x,y;\omega,T), \tag{F.21}$$

since the operator $\hat{\phi}$ is effectively non-interacting in the Hamiltonian (F.13) above. The function $\xi^{(\psi)}(\omega,T)$ for the effective lead ψ at high energies is given by

$$\xi(\omega,T) = \frac{3\pi^2}{16}\left[\lambda_0^2 + 2\lambda_0^3 \log\left(\frac{v_F\Lambda}{\sqrt{\omega^2+4T^2}}\right)\right], \tag{F.22}$$

where the dimensionless coupling λ_0 is defined as

$$\lambda_0 \equiv \frac{4}{v_F} J. \tag{F.23}$$

Finally, the retarded Green's function $G_{ij}^{R,(L)}(x,x;\omega,T)$ for the left lead is given by

$$G_{ij}^{R,(L)}(x,x;\omega,T) = -\frac{i}{v_F}\delta_{ij} - \frac{i}{v_F}\delta_{ij}\left[1-\cos^2(\alpha)\xi^{(\psi)}(\omega,T)\right] e^{i2K(\omega,x)}. \tag{F.24}$$

For an overscreened Kondo model with general $S_{(1)}$ [see Eq. (5.92)] and $\Delta \equiv \Delta_s - 1 = 2/(2+k)$, where Δ_s is the scaling dimension of the leading irrelevant perturbation to the Kondo fixed point, the function $\xi(\omega,T)$ for finite temperature T takes the form [61]

$$\xi(\omega,T) = 1 - S_{(1)} - N\delta\lambda\left(2\pi\frac{T}{T_K}\right)^{\Delta} 2\sin(\pi\Delta) I(\omega,T,\Delta), \tag{F.25}$$

where

$$I(\omega,T,\Delta)=\int_0^1 du\left[u^{-i\omega/2\pi T}u^{-1/2}(1-u)^{\Delta}F(u)-\frac{\Gamma(1+2\Delta)}{\Gamma^2(1+\Delta)}u^{\Delta-1}(1-u)^{-(1+\Delta)}\right]. \tag{F.26}$$

For $T=0$ the function $\xi(\omega,0)$ takes the form [61]

$$\begin{aligned}\xi(\omega,0) &= 1-S_{(1)} \\ &\quad +2N\delta\lambda\frac{\sin(\pi\Delta)\Gamma(1+2\Delta)\Gamma(1-\Delta)}{\Delta\Gamma^2(1+\Delta)}\left[\cos\left(\frac{\pi\Delta}{2}\right)-i\epsilon(\omega)\sin\left(\frac{\pi\Delta}{2}\right)\right]|\omega|^{\Delta},\end{aligned} \tag{F.27}$$

where $\epsilon(\omega)$ is the step potential. Hence, the amplitude of the oscillating part of the tDOS $\widetilde{\rho}_{2k_F}$ at zero temperature and bias is given by

$$\widetilde{\rho}_{2k_F}(x,0,0)\propto-\frac{2}{v_F}S_{(1)}. \tag{F.28}$$

Since $s=1/2$, $j=1/2$, and $k=2$ for the effective lead ψ in the Oreg-Goldhaber-Gordon 2CK model, we have $S_{(1)}=0$. This is the same as the topological Kondo model. However, the amplitude of the oscillating part of the tDOS $\widetilde{\rho}_{2k_F}$ at zero temperature and bias will not vanish, since there is still a contribution from the effective lead ϕ that we need to count too. This contributes a free cloud $\widetilde{\rho}_{0,2k_F}$ to the total $\widetilde{\rho}_{2k_F}$, hence $\widetilde{\rho}_{2k_F}\neq 0$ at the 2CK fixed point.

F.3 The modified Oreg-Goldhaber-Gordon 2CK model

Let us modify the original Oreg-Goldhaber-Gordon 2CK model discussed in the previous section by removing the right lead (Fig. 5.7b). Hence, the Hamiltonian becomes

$$\begin{aligned}\hat{H} &= \sum_{s=1}^{2}\sum_{k}\varepsilon_{m,k,s}\hat{m}^{\dagger}_{k,s}\hat{m}_{k,s}+\sum_{s=1}^{2}\varepsilon_{d,s}\hat{d}^{\dagger}_{s}\hat{d}_{s}+E^{n_m}_{n_d}+\sum_{s=1}^{2}\int_{0}^{\infty}dk\,\varepsilon_{L,k,s}\hat{L}^{\dagger}_{k,s}\hat{L}_{k,s}\\ &+\left(V_m\sum_{s=1}^{2}\sum_{k}\hat{m}^{\dagger}_{k,s}\hat{d}_{s}+V_L\sum_{s=1}^{2}\xi^{\dagger}_{L,s}(0)\hat{d}_{s}+\text{h.c.}\right).\end{aligned} \tag{F.29}$$

This is essentially the same as the Hamiltonian (F.12), but the effective lead ψ is now replaced by the left lead and the kinetic energy term for the effective lead ϕ is now eliminated. Therefore, after performing Schrieffer-Wolff transformation [49], the Hamiltonian should take the form

$$\begin{aligned}\hat{H} &= \sum_{s=1}^{2}\sum_{k}\varepsilon_{m,k,s}\hat{m}^{\dagger}_{k,s}\hat{m}_{k,s}+\sum_{s=1}^{2}\varepsilon_{d,s}\hat{d}^{\dagger}_{s}\hat{d}_{s}+\sum_{s=1}^{2}\int_{0}^{\infty}dk\,\varepsilon_{L,k,s}\hat{L}^{\dagger}_{k,s}\hat{L}_{k,s}\\ &+2J\hat{\boldsymbol{S}}_d\cdot\hat{\boldsymbol{S}}_m+2J\hat{\boldsymbol{S}}_d\cdot\hat{\boldsymbol{S}}_\psi.\end{aligned} \tag{F.30}$$

The function $\xi(\omega,T)$ at high energies for this model is the same as the function $\xi^{(\psi)}(\omega,T)$ for the original 2CK model,

$$\xi(\omega,T)=\frac{3\pi^2}{16}\left[\lambda_0^2+2\lambda_0^3\log\left(\frac{v_F\Lambda}{\sqrt{\omega^2+4T^2}}\right)\right], \tag{F.31}$$

where again the dimensionless coupling λ_0 is defined as

$$\lambda_0\equiv\frac{4}{v_F}J. \tag{F.32}$$

Up to an overall constant, this result is the same as for the topological Kondo model, Eq. (5.58).

As the effective lead ϕ now has been amputated, the values $s=1/2$, $j=1/2$, and $k=2$ will give us $S_{(1)}=0$ for the left (i.e., the only) lead. This is now the same as the

topological Kondo model, so that the amplitude of the oscillating part of the tDOS $\widetilde{\rho}_{2k_F}$ at zero temperature and bias will also vanish (see Eq. (F.28)). However, as can be seen by adapting the derivation in Appendix E, the decay of $\widetilde{\rho}_{2k_F}$ as the temperature is lowered now takes the form $T^{1/2}$.

F.4 The generalised Oreg-Goldhaber-Gordon 4CK model

The Hamiltonian of this system (Fig. 5.7c) is given by

$$\begin{aligned}\hat{H} &= \sum_{i=1}^{3}\sum_{s=1}^{2}\sum_{k}\varepsilon_{m_i,k,s}\hat{m}^{\dagger}_{i,k,s}\hat{m}_{i,k,s} + \sum_{s=1}^{2}\varepsilon_{d,s}\hat{d}^{\dagger}_{s}\hat{d}_{s} + E_{n_d}^{n_{m_1},n_{m_2},n_{m_3}} \\ &\quad + \sum_{s=1}^{2}\int_{0}^{\infty} dk\,\varepsilon_{L,k,s}\hat{L}^{\dagger}_{k,s}\hat{L}_{k,s} + \left(\sum_{i=1}^{3}\sum_{s=1}^{2}\sum_{k}V_{m_i}\hat{m}^{\dagger}_{i,k,s}\hat{d}_{s} + V_L\sum_{s=1}^{2}\xi^{\dagger}_{L,s}(0)\hat{d}_{s} + \text{h.c.}\right),\end{aligned} \tag{F.33}$$

where $\hat{m}_{i,k,s}$ is the annihilation operator for the electron in the large dot m_i, with $1 \leq i \leq 3$.

The retarded Green's function for this model at high energies is identical to that of the modified Oreg-Goldhaber-Gordon 2CK model discussed in the previous section.

Since we have $s = 1/2$, $j = 1/2$, and $k = 4$, we have $S_{(1)} = 1/\sqrt{3}$ and $\Delta = 1/3$. Therefore, $\widetilde{\rho}_{2k_F}$ at zero temperature and bias does not vanish. However, it has the same power-law decay as the topological Kondo model.

LIST OF REFERENCES

[1] Ettore Majorana. Teoria simmetrica dell'elettrone e del positrone. *Il Nuovo Cimento*, 14:171–184, 1937.

[2] A. Yu. Kitaev. Fault–tolerant quantum computation by anyons. *Ann. Phys. (Berlin)*, 303(1):2–30, 2003.

[3] Chetan Nayak, Steven H. Simon, Ady Stern, Michael Freedman, and Sankar Das Sarma. Non–Abelian anyons and topological quantum computation. *Rev. Mod. Phys.*, 80:1083–1159, Sep 2008.

[4] Ady Stern. Non–Abelian states of matter. *Nature*, 464:187–193, 03 2010.

[5] Jason Alicea. Majorana fermions in a tunable semiconductor device. *Phys. Rev. B*, 81:125318, Mar 2010.

[6] Yuval Oreg, Gil Refael, and Felix von Oppen. Helical liquids and Majorana bound states in quantum wires. *Phys. Rev. Lett.*, 105:177002, Oct 2010.

[7] F. Duncan M. Haldane. Nobel lecture: Topological quantum matter. *Rev. Mod. Phys.*, 89:040502, Oct 2017.

[8] Frank Wilczek. Majorana returns. *Nat. Phys.*, 5(9):614–618, 09 2009.

[9] Jason Alicea. New directions in the pursuit of Majorana fermions in solid state systems. *Rep. Prog. Phys.*, 75(7):076501, 2012.

[10] C.W.J. Beenakker. Search for Majorana fermions in superconductors. *Ann. Rev. Cond. Mat. Phys.*, 4(1):113–136, 2013.

[11] A. Yu. Kitaev. Unpaired Majorana fermions in quantum wires. *Physics-Uspekhi*, 44(10S):131, 2001.

[12] Martin Leijnse and Karsten Flensberg. Introduction to topological superconductivity and Majorana fermions. *Semiconductor Science and Technology*, 27(12):124003, 2012.

[13] Liang Fu and C. L. Kane. Superconducting proximity effect and Majorana fermions at the surface of a topological insulator. *Phys. Rev. Lett.*, 100:096407, Mar 2008.

[14] Roman M. Lutchyn, Jay D. Sau, and S. Das Sarma. Majorana fermions and a topological phase transition in semiconductor–superconductor heterostructures. *Phys. Rev. Lett.*, 105:077001, Aug 2010.

[15] B. D. Josephson. Coupled superconductors. *Rev. Mod. Phys.*, 36:216–220, Jan 1964.

[16] Yong-Joo Doh, Jorden A. van Dam, Aarnoud L. Roest, Erik P. A. M. Bakkers, Leo P. Kouwenhoven, and Silvano De Franceschi. Tunable supercurrent through semiconductor nanowires. *Science*, 309(5732):272–275, 2005.

[17] Jorden A. van Dam, Yuli V. Nazarov, Erik P. A. M. Bakkers, Silvano De Franceschi, and Leo P. Kouwenhoven. Supercurrent reversal in quantum dots. *Nature*, 442:667, 2006.

[18] K. T. Law, Patrick A. Lee, and T. K. Ng. Majorana fermion induced resonant Andreev reflection. *Phys. Rev. Lett.*, 103:237001, Dec 2009.

[19] Karsten Flensberg. Tunneling characteristics of a chain of Majorana bound states. *Phys. Rev. B*, 82:180516, Nov 2010.

[20] Jay D. Sau, Sumanta Tewari, Roman M. Lutchyn, Tudor D. Stanescu, and S. Das Sarma. Non–Abelian quantum order in spin–orbit–coupled semiconductors: Search for topological Majorana particles in solid–state systems. *Phys. Rev. B*, 82:214509, Dec 2010.

[21] M Wimmer, A R Akhmerov, J P Dahlhaus, and C W J Beenakker. Quantum point contact as a probe of a topological superconductor. *New Journal of Physics*, 13(5):053016, 2011.

[22] Alex Zazunov, Alexander Altland, and Reinhold Egger. Transport properties of the Coulomb-Majorana junction. *New Journal of Physics*, 16(1):015010, 2014.

[23] V. Mourik, K. Zuo, S. M. Frolov, S. R. Plissard, E. P. A. M. Bakkers, and L. P. Kouwenhoven. Signatures of Majorana fermions in hybrid superconductor–semiconductor nanowire devices. *Science*, 336(6084):1003–1007, 2012.

[24] Anindya Das, Yuval Ronen, Yunatan Most, Yuval Oreg, Moty Heiblum, and Hadas Shtrikman. Zero–bias peaks and splitting in an Al-InAs nanowire topological superconductor as a signature of Majorana fermions. *Nat. Phys.*, 8:887895, 2012.

[25] M. T. Deng, C. L. Yu, G. Y. Huang, M. Larsson, P. Caroff, and H. Q. Xu. Anomalous zero–bias conductance peak in a NbInSb nanowire-Nb hybrid device. *Nano Letters*, 12(12):6414–6419, 2012. PMID: 23181691.

[26] A. D. K. Finck, D. J. Van Harlingen, P. K. Mohseni, K. Jung, and X. Li. Anomalous modulation of a zero–bias peak in a hybrid nanowire–superconductor device. *Phys. Rev. Lett.*, 110:126406, Mar 2013.

[27] Fabrizio Nichele, Asbjørn C. C. Drachmann, Alexander M. Whiticar, Eoin C. T. O'Farrell, Henri J. Suominen, Antonio Fornieri, Tian Wang, Geoffrey C. Gardner, Candice Thomas, Anthony T. Hatke, Peter Krogstrup, Michael J. Manfra, Karsten Flensberg, and Charles M. Marcus. Scaling of Majorana zero–bias conductance peaks. *Phys. Rev. Lett.*, 119:136803, Sep 2017.

[28] Hao Zhang, Chun-Xiao Liu, Sasa Gazibegovic, Di Xu, John A. Logan, Guanzhong Wang, Nick van Loo, Jouri D. S. Bommer, Michiel W. A. de Moor, Diana Car, Roy L. M. Op het Veld, Petrus J. van Veldhoven, Sebastian Koelling, Marcel A. Verheijen, Mihir Pendharkar, Daniel J. Pennachio, Borzoyeh Shojaei, Joon Sue Lee, Chris J. Palmstrm, Erik P. A. M. Bakkers, S. Das Sarma, and Leo P. Kouwenhoven. Quantized Majorana conductance. *Nature*, 556:74–79, 2018.

[29] Dmitry Bagrets and Alexander Altland. Class *D* spectral peak in Majorana quantum wires. *Phys. Rev. Lett.*, 109:227005, Nov 2012.

[30] D I Pikulin, J P Dahlhaus, M Wimmer, H Schomerus, and C W J Beenakker. A zero–voltage conductance peak from weak antilocalization in a Majorana nanowire. *New Journal of Physics*, 14(12):125011, 2012.

[31] Jie Liu, Andrew C. Potter, K. T. Law, and Patrick A. Lee. Zero–bias peaks in the tunneling conductance of spin–orbit–coupled superconducting wires with and without Majorana end–states. *Phys. Rev. Lett.*, 109:267002, Dec 2012.

[32] G. Kells, D. Meidan, and P. W. Brouwer. Near–zero–energy end states in topologically trivial spin–orbit coupled superconducting nanowires with a smooth confinement. *Phys. Rev. B*, 86:100503, Sep 2012.

[33] Diego Rainis, Luka Trifunovic, Jelena Klinovaja, and Daniel Loss. Towards a realistic transport modeling in a superconducting nanowire with Majorana fermions. *Phys. Rev. B*, 87:024515, Jan 2013.

[34] Liang Fu. Electron teleportation via Majorana bound states in a mesoscopic superconductor. *Phys. Rev. Lett.*, 104:056402, 02 2010.

[35] S. M. Albrecht, A. P. Higginbotham, M. Madsen, F. Kuemmeth, T. S. Jespersen, J. Nygrd, P. Krogstrup, and C. M. Marcus. Exponential protection of zero modes in Majorana islands. *Nature*, 531:206–209, 2016.

[36] B. Béri and N. R. Cooper. Topological Kondo effect with Majorana fermions. *Phys. Rev. Lett.*, 109:156803, 10 2012.

[37] Alexander Altland and Reinhold Egger. Multiterminal Coulomb–Majorana junction. *Phys. Rev. Lett.*, 110:196401, 05 2013.

[38] Benjamin Béri. Majorana–Klein hybridization in topological superconductor junctions. *Phys. Rev. Lett.*, 110:216803, May 2013.

[39] Martin R. Galpin, Andrew K. Mitchell, Jesada Temaismithi, David E. Logan, Benjamin Béri, and Nigel R. Cooper. Conductance fingerprint of Majorana fermions in the topological Kondo effect. *Phys. Rev. B*, 89:045143, Jan 2014.

[40] A Altland, B Bri, R Egger, and A M Tsvelik. Bethe ansatz solution of the topological Kondo model. *Journal of Physics A: Mathematical and Theoretical*, 47(26):265001, 2014.

[41] A. Altland, B. Béri, R. Egger, and A. M. Tsvelik. Multichannel Kondo impurity dynamics in a Majorana device. *Phys. Rev. Lett.*, 113:076401, Aug 2014.

[42] Erik Eriksson, Christophe Mora, Alex Zazunov, and Reinhold Egger. Non–Fermi–liquid manifold in a Majorana device. *Phys. Rev. Lett.*, 113:076404, Aug 2014.

[43] Erik Eriksson, Andrea Nava, Christophe Mora, and Reinhold Egger. Tunneling spectroscopy of Majorana–Kondo devices. *Phys. Rev. B*, 90:245417, Dec 2014.

[44] S. Plugge, A. Zazunov, E. Eriksson, A. M. Tsvelik, and R. Egger. Kondo physics from quasiparticle poisoning in Majorana devices. *Phys. Rev. B*, 93:104524, 03 2016.

[45] A. Zazunov, F. Buccheri, P. Sodano, and R. Egger. 6π Josephson effect in Majorana box devices. *Phys. Rev. Lett.*, 118:057001, Feb 2017.

[46] B. Béri. Exact nonequilibrium transport in the topological Kondo effect. *Phys. Rev. Lett.*, 119:027701, Jul 2017.

[47] Karen Michaeli, L. Aviad Landau, Eran Sela, and Liang Fu. Electron teleportation and statistical transmutation in multiterminal Majorana islands. *Phys. Rev. B*, 96:205403, Nov 2017.

[48] Matthias Gau, Stephan Plugge, and Reinhold Egger. Quantum transport in coupled Majorana box systems. *Phys. Rev. B*, 97:184506, May 2018.

[49] A. C. Hewson. *The Kondo Problem to Heavy Fermions*. Cambridge University Press, first edition edition, 1997.

[50] Ph. Nozières and A. Blandin. Kondo effect in real metals. *J. Phys. France*, 41(3):193–211, 1980.

[51] Ian Affleck. A current algebra approach to the Kondo effect. *Nuclear Physics B*, 336:517, 1990.

[52] Ian Affleck and Andreas W. W. Ludwig. The Kondo effect, conformal field theory and fusion rules. *Nuclear Physics B*, 352:849, 1991.

[53] Ian Affleck and Andreas W.W. Ludwig. Critical theory of overscreened Kondo fixed points. *Nuclear Physics B*, 360(2):641–696, 1991.

[54] Ian Affleck, Andreas W. W. Ludwig, H.-B. Pang, and D. L. Cox. Relevance of anisotropy in the multichannel Kondo effect: Comparison of conformal field theory and numerical renormalization–group results. *Phys. Rev. B*, 45:7918–7935, Apr 1992.

[55] Erik S. Sørensen and Ian Affleck. Scaling theory of the Kondo screening cloud. *Phys. Rev. B*, 53:9153–9167, Apr 1996.

[56] Victor Barzykin and Ian Affleck. Screening cloud in the k–channel Kondo model: Perturbative and large–k results. *Phys. Rev. B*, 57:432–448, 01 1998.

[57] Ian Affleck and Pascal Simon. Detecting the Kondo screening cloud around a quantum dot. *Phys. Rev. Lett.*, 86:2854–2857, Mar 2001.

[58] Pascal Simon and Ian Affleck. Kondo screening cloud effects in mesoscopic devices. *Phys. Rev. B*, 68:115304, Sep 2003.

[59] László Borda. Kondo screening cloud in a one–dimensional wire: Numerical renormalization group study. *Phys. Rev. B*, 75:041307, Jan 2007.

[60] Ian Affleck, László Borda, and Hubert Saleur. Friedel oscillations and the Kondo screening cloud. *Phys. Rev. B*, 77:180404, 05 2008.

[61] Ian Affleck and Andreas W. W. Ludwig. Exact conformal–field–theory results on the multichannel Kondo effect: Single–fermion Green's function, self-energy, and resistivity. *Phys. Rev. B*, 48:7297–7321, Sep 1993.

[62] Ian Affleck. The Kondo screening cloud: What it is and how to observe it. In Amnon Aharony and Ora Entin-Wohlman, editors, *Perspective of Mesoscopic Physics: Dedicated to Yoseph Imry's 70th Birthday*, chapter 1. World Scientific, 2010.

[63] Andriy Nevidomskyy. The Kondo model and poor man's scaling. In Eva Pavarini, Erik Koch, and Piers Coleman, editors, *Many–Body Physics: From Kondo to Hubbard*, chapter 4, page 123. Institute of Advanced Simulation, 2015.

[64] D. A. Ivanov. Non–Abelian statistics of half–quantum vortices in p–wave superconductors. *Phys. Rev. Lett.*, 86:268–271, Jan 2001.

[65] Michael E. Peskin and Daniel V. Schroeder, editors. *An Introduction to Quantum Field Theory*. Perseus Books, 1995.

[66] Palash B. Pal. Dirac, Majorana, and Weyl fermions. *American Journal of Physics*, 79(5):485–498, 2011.

[67] Steven R. Elliott and Marcel Franz. Colloquium: Majorana fermions in nuclear, particle, and solid–state physics. *Rev. Mod. Phys.*, 87:137–163, Feb 2015.

[68] Charles Kane and Joel Moore. Topological insulators. *Physics World*, 24(02):32, 2011.

[69] Michel Fruchart and David Carpentier. An introduction to topological insulators. *Comptes Rendus Physique*, 14(9):779–815, 2013. Topological insulators / Isolants topologiques.

[70] Mikio Nakahara. *Geometry, Topology, and Physics*. Institute of Physics Publishing, second edition edition, 2003.

[71] M. Wimmer, A. R. Akhmerov, M. V. Medvedyeva, J. Tworzydło, and C. W. J. Beenakker. Majorana bound states without vortices in topological superconductors with electrostatic defects. *Phys. Rev. Lett.*, 105:046803, Jul 2010.

[72] Jay D. Sau, Roman M. Lutchyn, Sumanta Tewari, and S. Das Sarma. Generic new platform for topological quantum computation using semiconductor heterostructures. *Phys. Rev. Lett.*, 104:040502, Jan 2010.

[73] T D Stanescu and S Tewari. Majorana fermions in semiconductor nanowires: Fundamentals, modeling, and experiment. *Journal of Physics: Condensed Matter*, 25(23):233201, 2013.

[74] Jason Alicea, Yuval Oreg, Gil Refael, Felix von Oppen, and Matthew P. A. Fisher. Non–Abelian statistics and topological quantum information processing in 1D wire networks. *Nature*, 7:412, 2011.

[75] Sankar Das Sarma, Michael Freedman, and Chetan Nayak. Topological quantum computation. *Physics Today*, 59:32, July 2006.

[76] Jun Kondo. Resistance minimum in dilute magnetic alloys. *Progress of Theoretical Physics*, 32(1):37–49, 1964.

[77] Kenneth G. Wilson. The renormalization group: Critical phenomena and the Kondo problem. *Rev. Mod. Phys.*, 47:773–840, Oct 1975.

[78] P B Wiegmann. Exact solution of the s–d exchange model (Kondo problem). *Journal of Physics C: Solid State Physics*, 14(10):1463, 1981.

[79] Andreas W.W. Ludwig and Ian Affleck. Exact conformal–field–theory results on the multi–channel Kondo effect: Asymptotic three–dimensional space– and time–dependent multi–point and many–particle Green's functions. *Nuclear Physics B*, 428(3):545–611, 1994.

[80] P W Anderson. A poor man's derivation of scaling laws for the Kondo problem. *Journal of Physics C: Solid State Physics*, 3(12):2436, 1970.

[81] P. W. Anderson. Localized magnetic states in metals. *Phys. Rev.*, 124:41–53, Oct 1961.

[82] Leo Kouwenhoven and Leonid Glazman. Revival of the Kondo effect. *Physics World*, 14(1):33, 2001.

[83] P. Nozières. A "Fermi–liquid" description of the Kondo problem at low temperatures. *Journal of Low Temperature Physics*, 17(1):31–42, Oct 1974.

[84] Andy Latief and Benjamin Béri. Screening cloud and non–Fermi–liquid scattering in topological kondo devices. *arXiv:1803.10565*, 03 2018.

[85] Yuli V. Nazarov and Yaroslav M. Blanter. *Quantum Transport: Introduction to Nanoscience*. Cambridge University Press, 2009.

[86] M. Fabrizio and Alexander O. Gogolin. Toulouse limit for the overscreened four–channel Kondo problem. *Phys. Rev. B*, 50:17732–17735, Dec 1994.

[87] Amit Agarwal, Sourin Das, Sumathi Rao, and Diptiman Sen. Enhancement of tunneling density of states at a junction of three Luttinger liquid wires. *Phys. Rev. Lett.*, 103:026401, Jul 2009.

[88] Henrik Bruus and Karsten Flensberg. *Many–Body Quantum Theory in Condensed Matter Physics*. Oxford University Press, 2004.

[89] A. A. Abrikosov. Electron scattering on magnetic impurities in metals and anomalous resistivity effects. *Physics Physique Fizika*, 2:5–20, Sep 1965.

[90] Richard D. Mattuck. *A Guide to Feynman Diagrams in the Many–Body Problem*. Dover Publications, Inc., second edition edition, 1992.

[91] C. Y. Cheung and R. D. Mattuck. Removing the divergence at the Kondo temperature by means of self–consistent perturbation theory. *Phys. Rev. B*, 2:2735–2745, Oct 1970.

[92] Ian Affleck. Conformal field theory approach to the Kondo effect. *Acta Physica Polonica B*, 26(12):1869, Dec 1995.

[93] Yuval Oreg and David Goldhaber-Gordon. Two–channel Kondo effect in a modified single electron transistor. *Phys. Rev. Lett.*, 90:136602, 04 2003.

[94] R. M. Potok, I. G. Rau, Hadas Shtrikman, Yuval Oreg, and D. Goldhaber-Gordon. Observation of the two–channel Kondo effect. *Nature*, 446:167–171, 2007.

[95] Assaf Carmi, Yuval Oreg, Micha Berkooz, and David Goldhaber-Gordon. Transmission phase shifts of Kondo impurities. *Phys. Rev. B*, 86:115129, 09 2012.

[96] S. Florens and A. Rosch. Climbing the entropy barrier: Driving the single– towards the multichannel Kondo effect by a weak Coulomb blockade of the leads. *Phys. Rev. Lett.*, 92:216601, May 2004.

[97] Alex D Gottlieb and Lisa Wesoloski. Bardeen's tunnelling theory as applied to scanning tunnelling microscopy: A technical guide to the traditional interpretation. *Nanotechnology*, 17(8):R57, 2006.

[98] C. Julian Chen. *Introduction to Scanning Tunneling Microscopy*. Oxford University Press, 1993.

[99] Samir Lounis. Theory of scanning tunneling microscopy. *arXiv:1404.0961*, Apr 2014.

[100] Piers Coleman. *Introduction to Many–Body Physics*. Cambridge University Press, 2015.

[101] M. Bode. Spin-polarized scanning tunnelling microscopy. *Reports on Progress in Physics*, 66(4):523, 2003.